STRUCTURAL DYNAMIC PROPERTIES OF TACTICAL MISSILE JOINTS

- PHASE I -

FINAL REPORT
(MAY 1969 to JUNE 1970)

JUNE 1970

PREPARED UNDER CONTRACT N00019-69-C-0319

FOR THE

NAVAL AIR SYSTEMS COMMAND

UNCLASSIFIED
Security Classification

DOCUMENT CONTROL DATA - R & D

(Security classification of title, body of abstract and indexing annotation must be entered when the overall report is classified)

ORIGINATING ACTIVITY (Corporate author) Electro Dynamic Division of General Dynamics Inc. 1675 W. Mission Boulevard Pomona, California 91766	2a. REPORT SECURITY CLASSIFICATION UNCLASSIFIED 2b. GROUP

3. REPORT TITLE

STRUCTURAL DYNAMIC PROPERTIES OF TACTICAL MISSILE JOINTS - PHASE I

4. DESCRIPTIVE NOTES (Type of report and inclusive dates)
Final (May 1969 thru June 1970)

5. AUTHOR(S) (First name, middle initial, last name)

John G. Maloney, Michael T. Shelton, David A. Underhill

6. REPORT DATE June 1970	7a. TOTAL NO. OF P 127	7b. NO. OF REFS 8
8a. CONTRACT OR GRANT NO. N00019-69-C-0319 b. PROJECT NO. c. d.	9a. ORIGINATOR'S REPORT NUMBER(S) CR-6-348-945-001 9b. OTHER REPORT NO(S) (Any other numbers that may be assigned this report)	

10. DISTRIBUTION STATEMENT
Approved for public release, distribution unlimited.

11. SUPPLEMENTARY NOTES	12. SPONSORING MILITARY ACTIVITY Naval Air Systems Command Department of the Navy Washington, D. C. 20360

13. ABSTRACT

This report covers the first phase in a general study of the structural dynamic properties of tactical missile joints. The nature of the basic problem - sizeable and of en unpredictable joint effects on airframe dynamic response - is traced in a brief aerospace industry and literature survey and explored in a parametric study designed to identify and illustrate controlling mechanisms and relationships. The importance of the number and spacing of load paths through a joint interface is developed in a conceptual analysis and clearly demonstrated in the results of a limited test program using simple idealized test specimens. Two analysis procedures for determining joint properties are briefly evaluated. The first involves a method for extracting multiple joint properties from missile dynamic test data. The second is based on direct application of finite element modeling of one of the test specimens. Both approaches show considerable promise and are concluded to merit further investigation.

DD FORM 1 NOV 68 1473 (PAGE 1)

S/N 0101-807-6801

UNCLASSIFIED
Security Classification

14 KEY WORDS	LINK A		LINK B		LINK C	
	ROLE	WT	ROLE	WT	ROLE	WT
Tactical Missile Joints						
Dynamics of Joints						
Joint Compliance						
Joint Damping						
Joint Coupling						
Joint Stiffness						
Elastic Modes						

GENERAL DYNAMICS
Electro Dynamic Division

STRUCTURAL DYNAMIC PROPERTIES OF TACTICAL MISSILE JOINTS - PHASE I

Final Report

(May 1969 to June 1970)

June 1970

CR-6-348-945-001

By

J. G. Maloney
M. T. Shelton
D. A. Underhill

Prepared Under Contract N00019-69-C-0319

for the

Naval Air Systems Command

by

Electro Dynamic Division

Pomona Operation of the General Dynamics, Inc.

1675 W. Mission Blvd,
Pomona, California 91766

FOREWORD

This study has been conducted by the Pomona Operation of General Dynamics Corporation for the Naval Air Systems Command under Contract N00019-69-C-0319.

The principal investigator for the study has been Mr. John G. Maloney. The experimental work and much of the analytical work was carried out by Mr. Michael T. Shelton. Dr. George Lasker served as a staff consultant and provided the finite element analysis for the correlation analysis. Mr. Kenneth L. McIntyre developed the joint compliance extraction technique and the joint spring coupling analysis. The direct technical supervisor has been Mr. David A. Underhill, Structural Dynamics Section Head.

The Naval Air Systems Command technical monitor has been Mr. George P. Maggos.

TABLE OF CONTENTS

Section	Title	Page
1.0	SUMMARY	1
2.0	INTRODUCTION	2
3.0	THE STRUCTURAL DYNAMIC ROLE OF TACTICAL MISSILE JOINTS	4
	3.1 COMPLIANCE	4
	3.2 ENERGY DISSIPATION	6
	3.3 ENERGY TRANSFER	7
4.0	STRUCTURAL DYNAMIC MODELING OF AIRFRAME JOINTS	14
	4.1 AIRFRAME REPRESENTATION	14
	4.2 DETERMINATION OF JOINT COMPLIANCE	16
	4.3 JOINT COMPLIANCE COMPARISONS	17
5.0	PARAMETRIC STUDIES	22
	5.1 JOINT STIFFNESS AND LOCATION	22
	5.1.1 Method of Analyses	22
	5.1.2 Joint Location Effects	23
	5.1.3 Joint Compliance Effects	24
	5.1.4 Non-dimensional Presentation	24
	5.1.5 Multiple Joint Applications	25
	5.1.6 Tactical Missile Application	26
	5.2 CROSS PLANE SPRING COUPLING OF AIRFRAME JOINTS	27
	5.2.1 Introduction	27
	5.2.2 Conceptual Model for Joint Elastic Coupling	27
	5.2.3 Joint Spring Coupling Parametric Study	30
	5.2.4 Spring Coupling Studies for an Actual Tactical Missile	34

TABLE OF CONTENTS
(Cont'd.)

Section	Title	Page
6.0	EXTRACTION OF JOINT COMPLIANCES FROM MEASURED MODAL DATA	54
	6.1 METHOD OF ANALYSIS	54
	6.2 TEST CASE	61
	6.3 SENSITIVITY ANALYSIS	62
	6.4 CURRENT RESTRICTIONS	63
7.0	EXPERIMENTAL VERIFICATION	69
	7.1 TEST MODEL	69
	7.2 TEST SETUP	70
	7.3 RESULTS	70
	7.4 CORRELATION ANALYSIS	71
8.0	CONCLUSIONS	81
REFERENCES		83
APPENDIX I	AEROSPACE INDUSTRY SURVEY	84
APPENDIX II	BIBLIOGRAPHY	119

LIST OF FIGURES

Figure No.	Title	Page
3-1	Typical Missile Airframe Joints	9
3-2	STANDARD ARM Mechanical Joint Data	10
3-3	Effect of Joints on STANDARD ARM Bending Modes	11
3-4	Example of Cross Plane Response	12
3-5a	Example of Harmonic Distortion Due to Airframe Joint	13
3-5b	Example of Noise Generation Due to Airframe Joint	13
4-1	Joint Rating System From Alley and Leadbetter	18
4-2	Tactical Missile Joint Compliance Vs. Diameter Comparison with "NASA" Criteria	19
4-3	Comparison of STANDARD ARM Joints with "NASA" Criteria	20
4-4	Missile Joint Classification Comparison	21
5-1	"Nominal" Uniform Beam Without Joints Bending Moment Distribution	36
5-2	"Nominal" Uniform Beam First Bending Mode Shape for Various Locations of a Joint of "Moderate" Compliance	37
5-3	"Nominal" Uniform Beam First Mode Normalized Bending Moment Distribution for Various Locations of a Joint of "Moderate" Compliance	38
5-4	"Nominal" Uniform Beam Effect of Joint Location on First Bending Mode Frequency	39
5-5	"Nominal" Uniform Beam First Bending Mode Shape for Various Joints at Midspan	40
5-6	"Nominal" Uniform Beam First Mode Bending Moment Distribution for Joints at 50% Span of Various Compliance	41

LIST OF FIGURES
(Cont'd.)

Figure No.	Title	Page
5-7	"Nominal" Uniform Beam Effect of Joint Stiffness and Location on First Bending Mode Frequency	42
5-8	Uniform Beam Frequency Ratio Vs. Joint Compliance Ratio for Various Locations of the Joint	43
5-9	Uniform Beam With a Fineness Ratio of 13 - Frequency Ratio Vs. Joint Stiffness Ratio for Various Locations of the Joint	44
5-10	Actual Tactical Missile Stiffness Distribution	45
5-11	Measured Frequency Response at the Missile Nose Due to Force Excitation at the Tail Station	46
5-12	Mechanical Joint Elastic Coupling Introduced by Load Path Dissymmetry - 3 Spring Idealization	47
5-13	"Nominal" Uniform Beam "Good" Joint at 50% Span Effect of Joint Spring Coupling Magnitude on Response at 0% Span for Excitation at 100% Span	48
5-14	"Nominal" Uniform Beam "Moderate" Joint at 50% Span Effect of Joint Spring Coupling Magnitude on Response at 0% Span for Excitation at 100% Span	49
5-15	"Nominal" Uniform Beam Total First Mode Frequency Shift Vs. Joint Spring Coupling	50
5-16	Computed Frequency Response at the Missile Nose Due to Force Excitation at the Tail Station	51
6-1	Joint Compliance Extraction Technique Test Case Stiffness and Weight Distributions	65
6-2	Joint Compliance Extraction Technique Convergence Results	66
7-1	Joint Simulation Models	73
7-2	Test Setup of Joint Simulation Models	74

LIST OF FIGURES
(Cont'd.)

Figure No.	Title	Page
7-3	Effective Length of Stiffness Reduction Vs. Stiffness Ratio and Number of Remaining Segments Using Test Results	75
7-4	EI Discontinuity Test Data - Stiffness Ratio Vs. Frequency Ratio	76
7-5	Description of Shell, Shell Loading and Shell Segment Used in Finite Element Analysis	77
7-6	Distribution of Shell Segment Finite Elements	78
I-1 thru I-31	Diagrams of Tactical Missile Joints	88-118

LIST OF TABLES

Table No.	Title	Page
3-1	Joint Effects on STANDARD ARM Modes	5
3-2	Estimated Joint Effects - Missile First Mode Characteristics	6
5-1	First Mode Frequency Ratio Variation With Joint Location and Rating	52
5-2	Modal Frequency Ratio Variation With Midspan Joint Rating	52
5-3	Modal Frequency Ratio Variation With "Moderate" Joint Location	52
5-4	Uniform Beam With Multiple Joints Calculated and Estimated Frequency Ratios	53
6-1	Sensitivity of Joint Compliance to Input Frequency Errors	67
6-2	Sensitivity of Joint Compliance to Number of Modes Used	68
7-1	Vibration Test Results Free-Free Joint Simulation Models	79
7-2A	Compliance and Compliance Ratio Results for Joint Simulation Models	80
7-2B	Test Specimen Effective Compliance Comparison With Joint Rating Classification	80
I-1	Aerospace Industry Survey Results	86-87

Section 1.0

SUMMARY

The initial results of a study of the structural dynamic properties of tactical missile joints are presented. The scope of this phase of the investigation has included:

1. A review of the types of mechanical joints in common usage and the methods employed in estimating and representing joint load/deflection characteristics in structural dynamic response studies.

2. A parametric study to identify and illustrate the controlling mechanisms and relative importance of joint and airframe structural properties and geometries.

3. The preliminary evaluation of a method for extracting joint compliances from measured modal data.

4. A simplified test series using idealized models to explore and illustrate the effects of load path discontinuities and dissymmetries.

Based on comments and replies received in an industry survey (included as an appendix to this report), tactical missile joints are generally represented in dynamic analysis by equivalent rotational springs selected by trial and error to match measured response characteristics. Most respondents cited significant reductions in airframe flexural mode frequencies due to joint deflections, indicating substantial losses in local airframe stiffness. Using a classification basis proposed in a NASA study, a joint considered to be "moderate" in compliance, for example, is shown to result typically in a ninety-five percent loss in effective airframe stiffness for a reference span of half a body diameter.

Parametric analysis and test results illustrate the effects of joint location and rating on airframe dynamic response characteristics and show the sensitivity of joint compliance to load path dissymmetry. Load path discontinuities and dissymmetries are concluded to be a major contributor to joint compliance.

A method of steepest ascent applied to the problem of extracting joint compliance from measured modal data is developed and shown to have considerable promise. Direct analysis of joint characteristics using finite element modeling techniques, applied in a test case for correlation purposes, similarly shows significant potential as an analytical tool. The status of the study at the completion of the first phase is reviewed and the objectives of the second phase outlined.

Section 2.0

INTRODUCTION

The trend with high performance missiles as with aircraft is toward structural design requirements in which airframe stiffness plays an increasingly important role. The source of airframe stiffness requirements can stem from a variety of system design considerations including static and dynamic aeroelastic stability margins, airframe aeroelastic coupling with guidance and control systems, and structural dynamic loads and response induced by logistic and flight environments.

Experience has shown that many of the mechanical joints commonly employed in tactical missiles to serve modular design requirements can result in substantial and often unpredictable reductions in the stiffness of the primary structure. In the absence of reliable analysis methods for estimating joint effects on airframe stiffness, common practice is to rely on experimental data for definition of joint properties. The shortcoming of this approach, however, is that data obtained for a particular joint design on a given missile often cannot be extrapolated with any confidence to a different airframe design or even, in many cases, to a different location on the same airframe. The lack of reliable methods for predicting the load/deflection behavior of mechanical joints is a limitation of increasing concern in the development of efficient structures for advanced tactical missile airframes and in the early assurance of structural integrity in the design development phase.

The study described in this report represents the first phase in a basic investigation of the structural dynamic properties of tactical missile joints being undertaken by the Pomona Division of General Dynamics for the Naval Air Systems Command.

One of the initial tasks has been a compilation of the types of mechanical joints in common usage together with a review of the current methods employed in estimating and representing joint load/deflection characteristics in structural dynamic response studies. This effort has included a literature search as well as an aerospace industry survey and is summarized in Sections 3.0 and 4.0.

Following this, a parametric study was undertaken to investigate the controlling mechanisms and relative importance of joint structural properties by examining their effects on the structural dynamic response of representative missile structures. The results of this study are presented and discussed in Section 5.0 with the first part, Section 5.1, devoted to the effects of variations in joint compliance, location and number, and the second part, Section 5.2 concerned with joint dissymmetry and elastic coupling behavior.

Section 6.0 presents a preliminary evaluation of an analysis procedure for extracting joint compliances from measured modal response data. The assumption is made that in most cases the basic airframe stiffness and weight distributions are adequately defined, with the primary unknown being the airframe joint compliances. Given a set of measured mode shapes and frequencies, the objective is to devise a rapid means for converging on the effective joint compliances. The accuracy and limitations in the current form of the analysis are reviewed.

A limited test program described in Section 7.0 has been accomplished using highly simplified models to illustrate and verify some of the parametric analysis results. The models employ section property discontinuities and dissymmetries intended to simulate mechanical joint behavior.

Section 8.0 presents a status review for the first phase of this investigation and outlines the scope of the study planned for the second phase.

Section 3.0

THE STRUCTURAL DYNAMIC ROLE OF TACTICAL MISSILE JOINTS

Mechanical joints are a common feature of tactical missile structures used to join major airframe sections such as guidance, control, ordnance, autopilot, and propulsion. The great variety in the types of joints used for these purposes is illustrated in the results of an aerospace industry survey presented in the Appendix to this report. Sketches of some typical joints in common usage in tactical missile airframe design are shown in Figure 3-1.

Although both separable and non-separable joints are included in the survey, the ones of primary interest to this study are of the separable design. Non-separable joints designed for permanent attachment of sections tend to be stiffer, stronger, consistent and more predictable in their properties by virtue of being welded, bonded and/or riveted with many fasteners. Separable joints, however, especially those designed for ease of assembly and disassembly under field and depot conditions, exhibit behavior under dynamic loading which is often difficult to predict and sensitive to many parameters which cannot readily be specified or controlled. Torque values, for example, are frequently specified for joint fasteners in an attempt to control interface preloads. Measurements made with instrumented bolts, however, have shown that the axial load in bolts torqued to the same value can vary significantly due to dimensional, frictional, and thermal variations.

The characteristics of airframe joints that influence the structural dynamic behavior of tactical missiles can be categorized as follows:

1. Compliance
2. Energy dissipation
3. Energy transfer

3.1 COMPLIANCE

The most pronounced characteristic of the typical airframe joint in a tactical missile is its local compliance. A joint constitutes a disturbance in load path which can result in substantial losses in effective stiffness in the vicinity of the joint. The consequences of joint stiffness losses are well illustrated by examining the bending modes for an actual tactical missile. The missile used in this example is the Standard ARM. The type, location, and estimated compliance of the six principal airframe joints are shown in Figure 3-2. The bending modes for the airframe were computed using a conventional lumped parameter beam representation in a modified Holzer-Myklestad modal analysis method (Reference 7). Values for the joint compliances were derived by a trial

and error matching of the airframe modes measured in ground vibration testing. The first three bending mode frequencies for this airframe with and without joint compliance are tabulated below and the corresponding mode shapes shown in Figure 3-3. In this example, the influence of internal appendages and the control surfaces is purposely omitted in order to show the direct effect of the airframe joint compliance.

Table 3-1

JOINT EFFECTS ON STANDARD ARM MODES

Mode No.	Mode Frequency (Hz)		Freq. Loss %	Stiffness Loss %
	Without Joints	With Joints		
1	62	51	18	32
2	159	115	28	48
3	302	206	32	53

The estimated equivalent loss in airframe generalized stiffness for each mode is based on the approximate assumption of no change in generalized mass:

$$\left(\frac{f_1}{f_2}\right)^2 = \frac{K_1}{M_1} \cdot \frac{M_2}{K_2} = \frac{K_1}{K_2}$$

This assumption is not strictly speaking true since changes in mode shape are obvious, but it does give a fair indication of the powerful influence that the joints have on the airframe stiffness.

Table 3-2 presents for comparison purposes similar information obtained in the Industry Survey (Appendix I) for several other tactical missiles. In this case, data only on the first mode are shown. The equivalent stiffness loss for the airframe has again been estimated on the same basis as previously discussed.

The significant point is that substantial joint compliance effects are evident on many representative tactical missile airframes. In view of this, it is clear that accurate estimates of joint compliance are likely to be of critical importance in predicting airframe response characteristics.

Table 3-2

ESTIMATED JOINT EFFECTS - MISSILE FIRST MODE CHARACTERISTICS

Missile	Number of Joints	1st Mode Freq. Loss %	Stiffness Loss %
Sidewinder	4	7	13
SRAM	6	17	31
Standard (MR)	7	17	31
Standard (ER)	7	18	33
Phoenix	10	29	49

3.2 ENERGY DISSIPATION

Tactical missile joints clearly play a major role in dissipating vibratory energy. This conclusion is unavoidable considering the nature of tactical missile structures and the fact that a substantial portion of the total potential energy in the lower modes of interest is stored in the joint load/deflection characteristics. Missile airframe structure between joints typically consists of a simple single element cylindrical section (as opposed to built up structure) in which the only source of damping is that inherent in the material properties. Connections associated with internal appendage mountings of course constitute another source of energy dissipation, but are not believed to be a major contributor to airframe damping in the lower modes.

The precise nature of energy dissipation in mechanical joints is not well understood but is believed to involve two basic mechanisms:

1. Sliding friction
2. Gas pumping

Sliding friction is suspected to be the dominant source in the low to moderate frequency range with gas pumping effects becoming important at higher frequencies (Ref. 6).

It is interesting to note that the modal damping of missile structures is generally in the same domain as aircraft structures (at least in the lower modes, typically ranging from 1 to 3 percent of critical) although their structural configurations are considerably different.

Aircraft structural damping, however, tends to be distributed more uniformly over the structure rather than localized at a few major joints as in the case of missile structures. Missile structural dynamic response in consequence often exhibits abrupt and sizable phase shifts across joints.

3.3 ENERGY TRANSFER

Missile airframe joints, in addition to their compliance and damping characteristics, are responsible for two important forms of energy transfer:

1. Elastic coupling of missile response coordinates.

2. Energy transfer in the frequency domain through joint interface non-linearities and impact.

The elastic coupling behavior of joints is believed to result from a non-axially symmetric distribution of load paths through a joint interface. A conceptual model of this is developed and applied in Section 5.2 of this report. A representative example of cross plane response attributed to joint elastic coupling on an actual tactical missile is presented in Figure 3-4. The data describes the angular response in pitch (in-plane) and yaw (cross-plane) at the autopilot rate gyro station for a unit force at the control surface station driving the pitch plane. In this example, the cross-plane response is within 2 dB of the in-plane response in both of the first two dominant modes.

The transfer of energy in the frequency domain attributable to airframe joints, is a result of joint stiffness non-linearities. This characteristic manifests itself in two forms: as harmonic distortion of the response with certain forms of stiffness non-linearities, and as a high frequency noise source when free play results in impact of the contacting surfaces of the joint.

An example of the harmonic distortion response which an airframe joint can produce is taken from Reference 5. These results were obtained during an investigation of the effect of out-of-tolerance thread lead on the coupling nut used in the airframe joint shown in Figure I-15. The tests were conducted using a dummy forward section attached to a vibration fixture via the coupling nut joint. The assembly was excited with 4g peak sinusoidal vibration in a lateral direction at 30 Hz, which was approximately two octaves in frequency below the first lateral resonance of the assembly. It was found that the presence of a set screw in the coupling nut (used to lock the assembly) had a profound influence on the assembly response characteristics. The lateral response acceleration time history was monitored at a joint in the dummy guidance section well removed from the joint. The acceleration traces are presented in Figure 3-5a for one of the coupling nut specimens with the set screw removed and

with the set screw properly installed. It can be seen that the acceleration response is a very clean sinusoid when the set screw is properly installed but that harmonic distortion of the response occurs when the set screw is not installed.

An example of the generation of high frequency noise due apparently to free play in a joint can be seen in Figure 3-5b. The test conditions are exactly the same as those described above. The coupling nut has been replaced with a second sample. The absence of the set screw results in an acceleration response with considerable high frequency energy content. In this instance the harmonic distortion and high frequency noise occurred only when the joints were improperly installed, that is when the set screws were not in place. These examples have been cited only to show in a qualitative sense the phenomena of airframe joint energy transfer characteristics in the frequency domain.

FIGURE 3-1

TYPICAL MISSILE AIRFRAME JOINTS

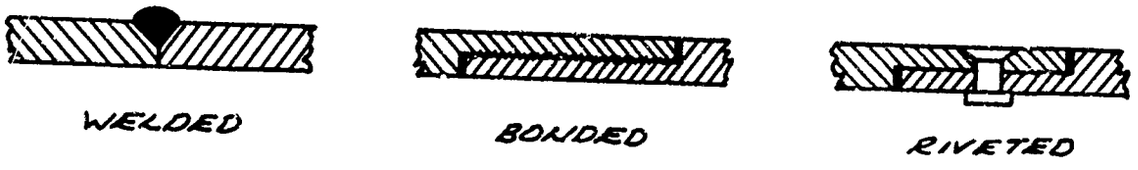

NON-SEPARABLE JOINTS

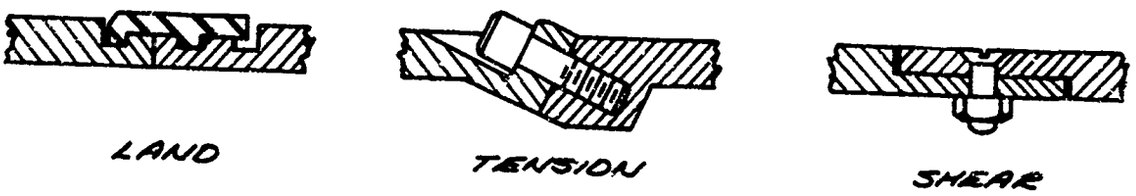

SEPARABLE JOINTS

FIGURE 3-2

STANDARD ARM MECHANICAL JOINT DATA

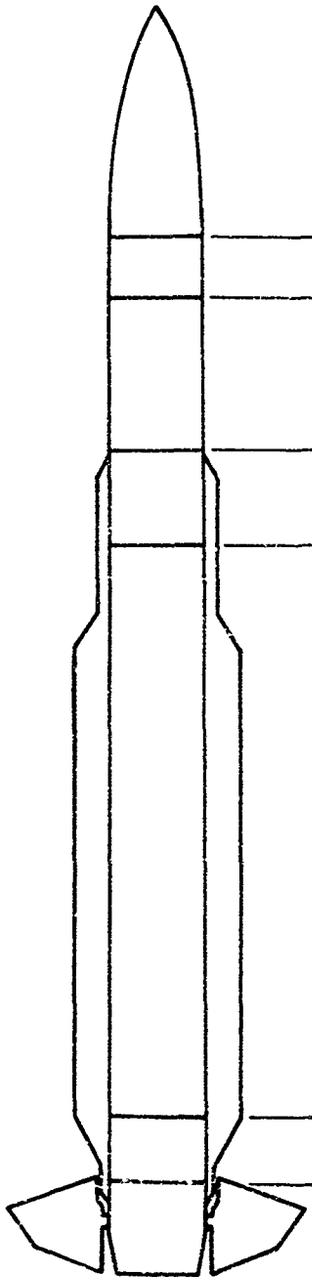

TYPE	FIGURE NO. (APPENDIX)	COMPLIANCE $C_\theta \times (10)^8 \frac{RAD}{IN-LB}$
RING	I-19	0.75
"TENSION" CLAMP	I-20	5.0
RING	I-21	2.0
TENSION	I-22	0.1
SHEAR	I-23	1.0
TENSION	I-24	1.0

FIGURE 3-3

EFFECT OF JOINTS ON
STANDARD ARM BENDING MODES

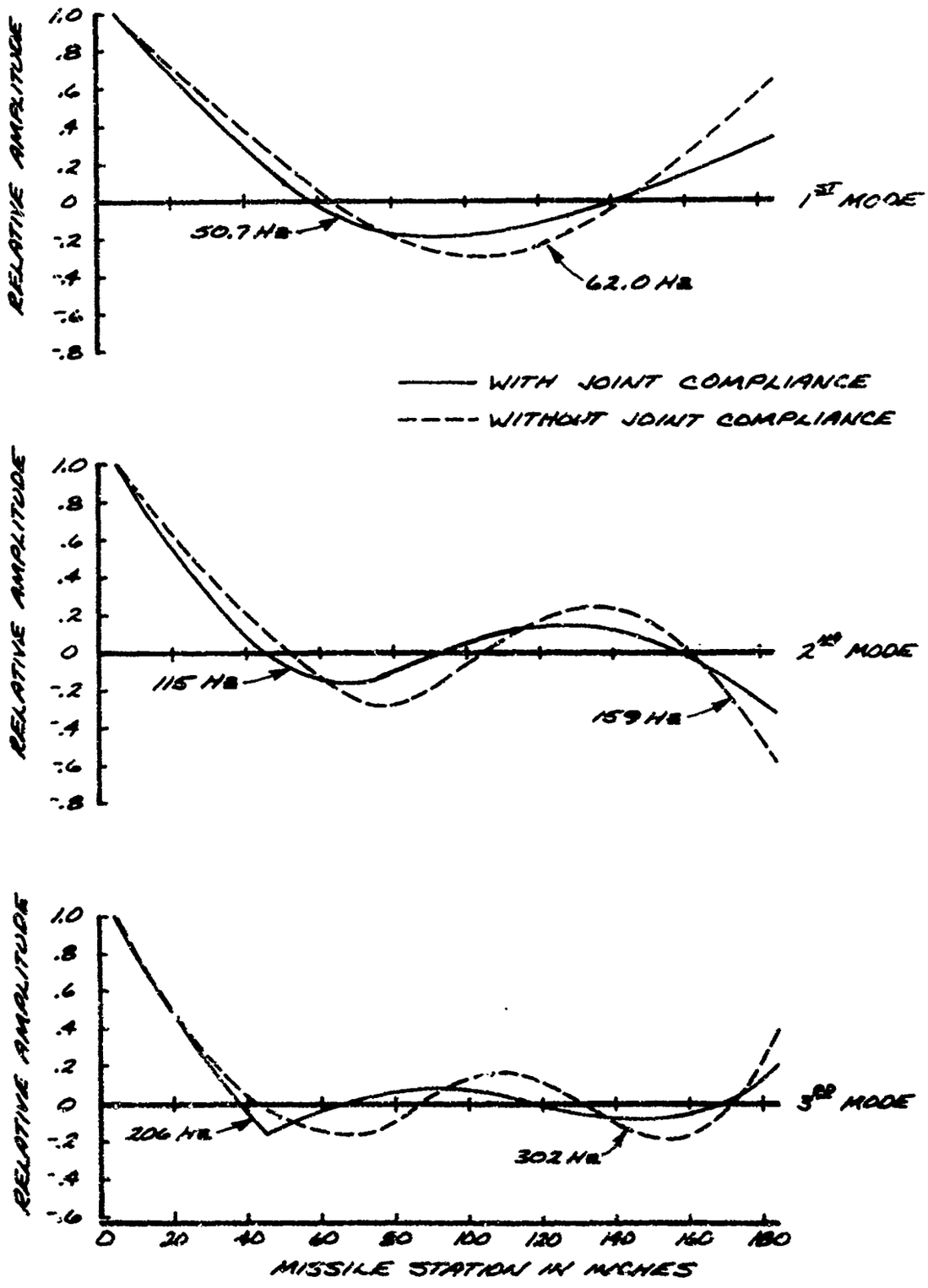

FIGURE 3-4

EXAMPLE OF CROSS PLANE RESPONSE

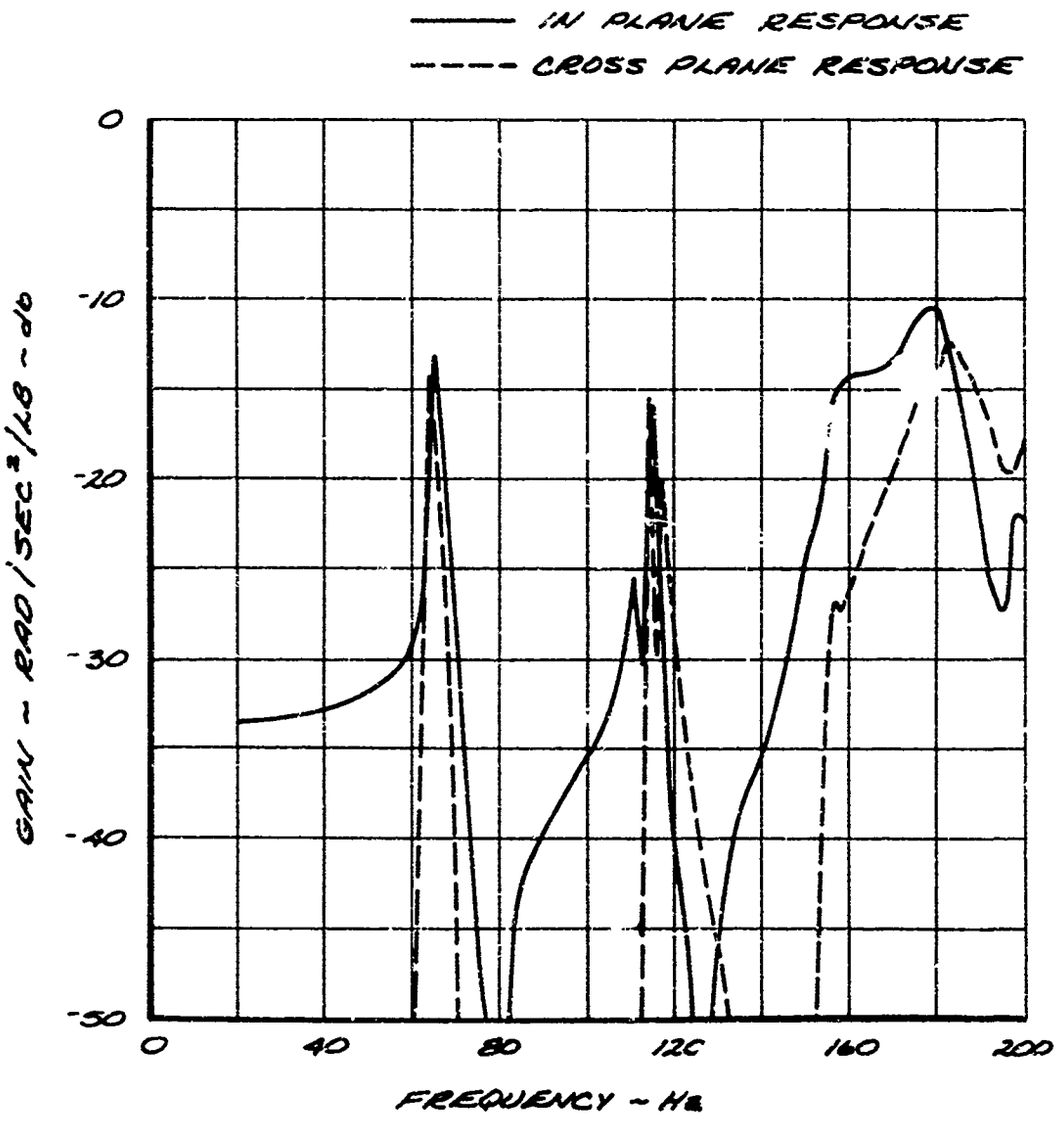

FIGURE 3-5a

EXAMPLE OF HARMONIC DISTORTION
DUE TO AIRFRAME JOINT

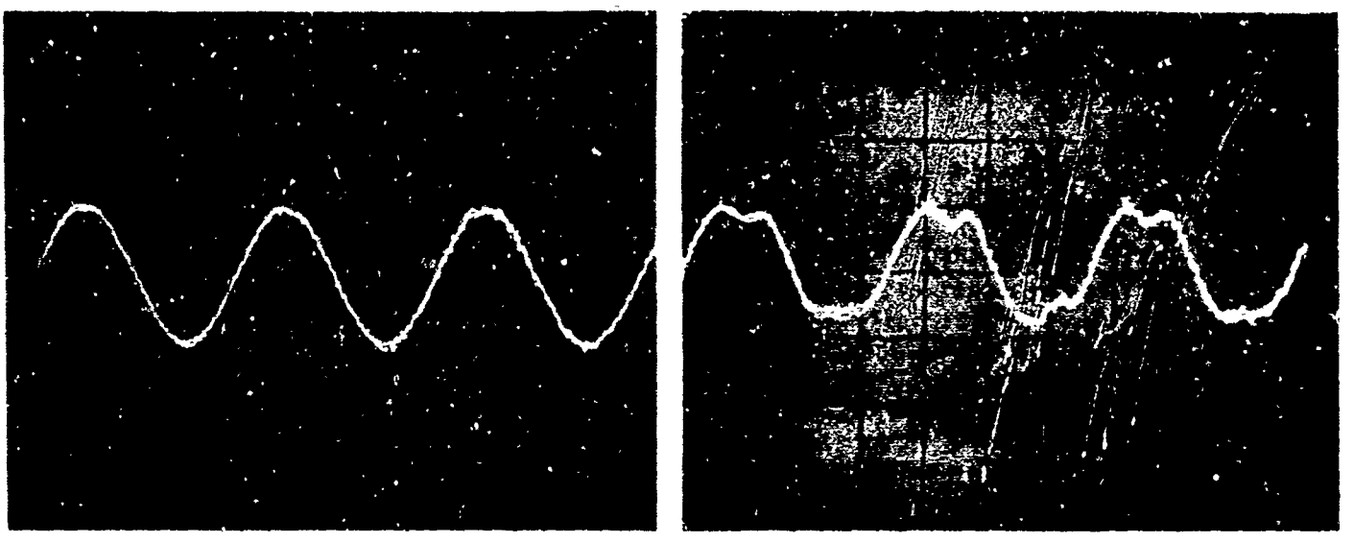

WITH SET SCREW

WITHOUT SET SCREW

FIGURE 3-5b

EXAMPLE OF NOISE GENERATION
DUE TO AIRFRAME JOINT

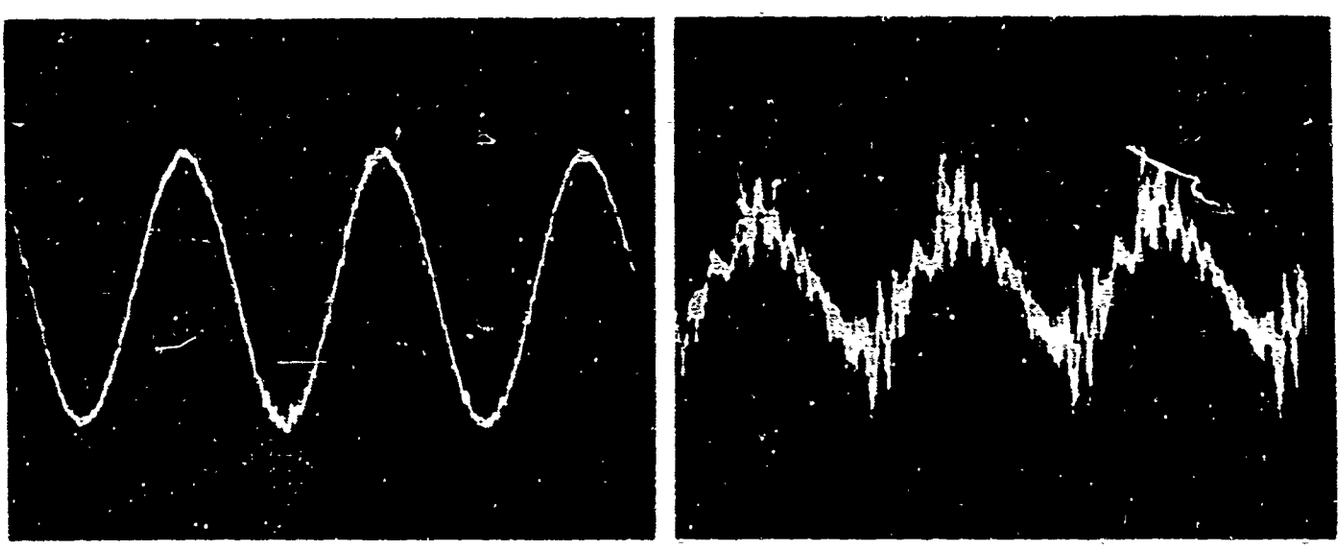

WITH SET SCREW

WITHOUT SET SCREW

Section 4.0

STRUCTURAL DYNAMIC MODELING OF AIRFRAME JOINTS

4.1 AIRFRAME REPRESENTATION

A common approach to modeling the structural dynamic characteristics of tactical missiles consists of developing a non-uniform beam model using a lumped parameter representation for the distributed stiffness and weight. Mode shapes and frequencies are computed for this representation by a variety of standard modal analysis procedures in order to provide generalized coordinates for use in all types of structural dynamic and aeroelastic response studies. The adequacy of the non-uniform beam model is of course dependent upon structural details peculiar to the individual missile design, with particular emphasis in the present study focused on the load/deflection behavior of the missile joints.

The development of the lumped parameter representation for the airframe weight and stiffness distribution (with the exception of the joint compliance characteristics) is usually a straightforward process involving the simple geometric and material properties of the structure. Mechanical joints, however, constitute a more difficult and less straightforward modeling task.

The results of the industry survey indicate that load/deflection characteristics of mechanical joints in missile airframes are most frequently represented by a flexural or rotational spring. Some beam modal analysis programs directly admit the assumed joint stiffness or its reciprocal, the joint compliance, while other programs require that the joint effects be accounted for by reducing the airframe stiffness in the local region of the joint. One advantage of this latter procedure from a conceptual standpoint is that the amount of local stiffness reduction (required to account for the joint compliance contribution) provides a direct basis for judging the significance of the joint relative to the basic airframe stiffness. A simple relationship between these two common methods for representing joint compliance can be shown by equating the net change in slope per unit moment over the reference airframe length selected for the local stiffness reduction as follows:

Reduced Stiffness

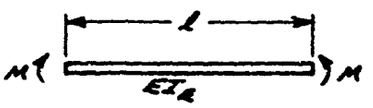

Rotational Spring Model

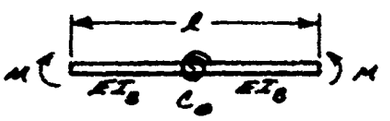

$$\frac{\ell}{EI_E} = \theta/M = C_\theta + \frac{\ell}{EI_B}$$

where:

ℓ = reference length over which airframe stiffness is assumed to be reduced.

θ/M = total bending slope change per unit moment over the reference length.

I_θ = basic (unmodified) airframe section properties in the region of the joint.

I_E = effective (reduced) airframe section properties in the region of the joint.

E = material flexural modulus of elasticity.

C_θ = rotational compliance attributable to the joint

Combining these expressions and letting K_ℓ denote the stiffness loss or reduction ratio, $K_\ell = I_E/I_\theta$

$$C_\theta = \frac{\ell}{EI_\theta}\left[\frac{1}{K_\ell} - 1\right]$$

and:

$$K_\ell = \frac{1}{1 + \frac{EI_\theta C_\theta}{\ell}}$$

In comparing the two methods for joint representation, the selection of the effective length for the joint influence on airframe stiffness is somewhat arbitrary. Both models are idealizations which oversimplify the structural deformation in the local region of the joint. Additionally, the deflection models for the two methods are equivalent only in the sense of matching slopes for applied moments. The significance of this difference is usually small if the effective length is on the order of the body diameter or less. Modal analyses were conducted for the tactical missile example given in Section 3.1 using both methods of joint representation for comparison. An effective length of half a body diameter for joint induced stiffness loss was used in this comparison, and virtually no differences in either frequencies or mode shapes were noted for the first three modes. The choice of half a body diameter for a reference length in judging joint effects appears

reasonable and basing the reference length on body diameter will be shown to be useful from a dimensional analysis and scaling standpoint in parametric studies.

4.2 DETERMINATION OF JOINT COMPLIANCE

The more difficult question in modeling tactical missile airframe joints is not how but what to model. Compliance estimates based on local section properties and fastener elastic characteristics are invariably unconservative (low). If representative missile hardware exists, one approach is to perform either static or dynamic load/deflection tests in which joint compliances are directly measured. Another common experimentally based technique is to match by trial and error a measured set of mode shapes and frequencies, assuming joint compliances to be the only unknowns in the modal analysis representation. An attempt to automate this approach is described in Section 6.0.

In some instances a very similar joint has been used in an earlier application and an extrapolation of its compliance characteristics can be made with acceptable confidence. This is not always the case, however, and there are many examples where a given joint design behaves quite differently on different airframes or in different locations.

Lacking experimental data or the opportunity to test representative hardware, which is usually the case in pre-design or early design studies, the analyst is confronted with the task of making a best judgement estimate of joint compliance characteristics. One approach to joint compliance estimation being used by several of the respondents to the industry survey is that outlined by Alley and Leadbetter of NASA Langley in Reference 1. In this reference Alley and Leadbetter present order of magnitude relationships between joint flexural compliance and joint type which they derived from launch vehicle test data. The compliance characteristics are classified from excellent (small compliance) to loose (large compliance) according to the table shown in Figure 4-1 which covers the various types of joints examined in their study.

The relationship of the magnitude of joint compliance to the joint classification is shown in the curves in Figure 4-1. Alley and Leadbetter established these curves based on 10 measured values of compliance and the assumption that the compliance is inversely proportional to the third power of the airframe diameter. The curves given in their figure may be approximated by the following relationship.

$$C = A\left(\frac{20}{D}\right)^3$$

where

C = flexural compliance, radians/inch-pound

D = diameter of the airframe at the joint location, inches

A = compliance coefficient, radians/inch-pound

The magnitude of the compliance coefficient A is a function of compliance classification and is found in the following table.

COMPLIANCE CLASSIFICATION	COMPLIANCE COEFFICIENT - A (Radians/Inch-Pound)	
	NOMINAL	RANGE
Excellent	$1(10)^{-10}$	$< 3(10)^{-10}$
Good	$1(10)^{-9}$	$3(10)^{-10}$ to $3(10)^{-9}$
Moderate	$1(10)^{-8}$	$3(10)^{-9}$ to $3(10)^{-8}$
Loose	$1(10)^{-7}$	$> 3(10)^{-8}$

4.3 JOINT COMPLIANCE COMPARISONS

The results of the industry survey provide a basis for comparing some of the compliance values which have been assigned to various tactical missile joints. Using the Alley/Leadbetter proposed classification criteria as a framework for comparison, Figure 4-2 presents joint compliance estimates for four tactical missiles ranging from 2.75" to 18" in diameter. Although only data for single joints are shown for Sidewinder and Thor, the range of Standard ARM joint compliances is seen to vary nearly two orders of magnitude. An additional comparison with the "NASA" rating criteria using the Standard ARM as an example is given in Figure 4-3. In this comparison, an additional parameter, stiffness reduction ratio (K_R) equivalent to the joint compliance has been computed using the expression for K_R developed in Section 4.1. It is particularly revealing to note that for this airframe, even the joints considered "good" represent a local (half body diameter) stiffness loss of nearly 70 per cent, while the "moderate" joints approach 95 percent stiffness loss.

The applicability of this conclusion to other missiles is shown in Figure 4-4 which is based solely on the joint classification criteria proposed in Reference 1, in combination with the missile diameters and average airframe stiffness properties listed in the Industry Survey (Appendix I). The figure is not intended to show actual joint characteristics of these missiles but only the influence that "Excellent", "Good", or "Moderate" joints would have on local stiffness. The "Test Specimen" listed in the bottom row refers to the simple models used in the test program described in Section 7.0.

FIGURE 4-1

JOINT RATING SYSTEM FROM ALLEY AND LEADBETTER (REFERENCE 1)

EXCELLENT JOINT BUTT WELDED SKIN HEAVY BOLTED, PRELOADED	
GOOD JOINT HEAVY FLANGE BOLTED THREADED DIAPHRAGM MARMAN BANDS	
MODERATE JOINT RIVETED, LAPPED RIVETED TO INNER RING SCREW SECTION WITHOUT BUTT	
LOOSE JOINT LIGHT FLANGES, BOLTED OR RIVETED LAPPED WITH SCREW FASTENERS EQUALLY SPACED BRACKETS	BRACKET

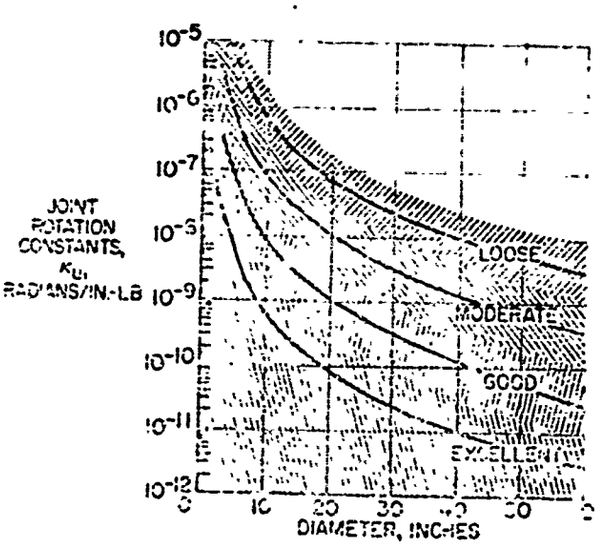

FIGURE 4-2

TACTICAL MISSILE JOINT COMPLIANCE VS. DIAMETER COMPARISON WITH "NASA" CRITERIA

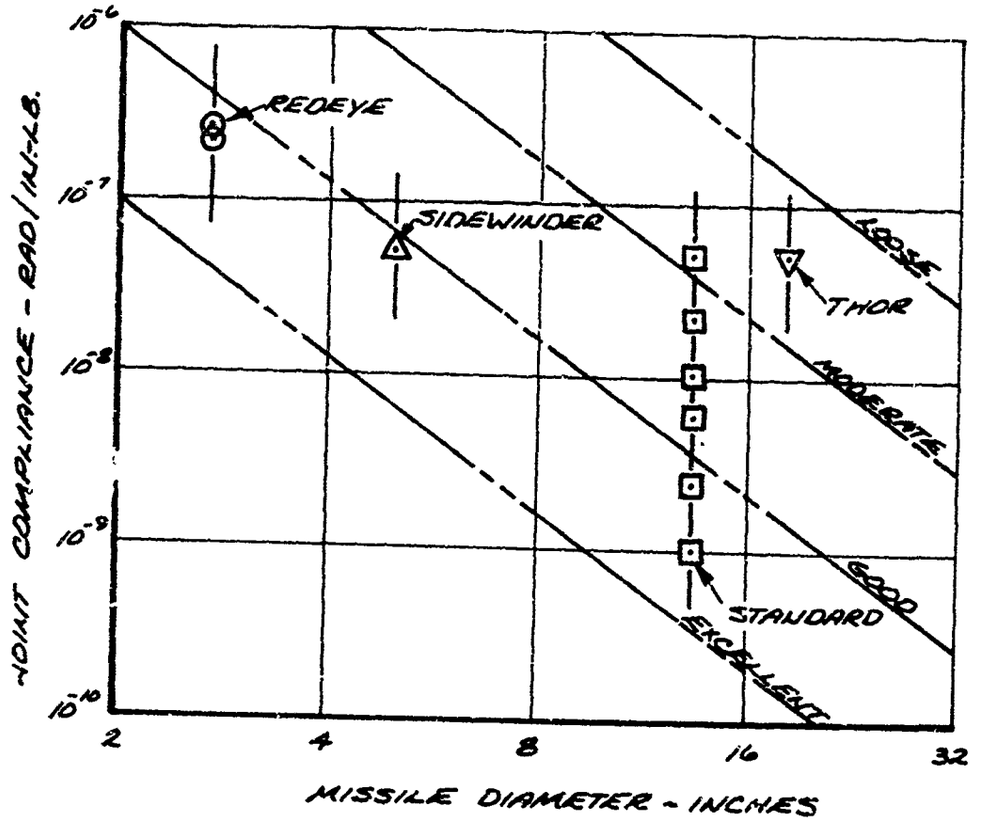

FIGURE 4-3

COMPARISON OF STO ARM JOINTS WITH "NASA" CRITERIA

NO.	JOINT DESCRIPTION		LOCATION	"NASA" RATING RANGE (REF. 4)	COMPLIANCE $C_\theta (10)^8$	STIFFNESS RATIO K_R
	TYPE	FIG. NO.	η_o			
1	RING	I-19	18	GOOD	0.75	.269
2	TENSION	I-20	23	MODERATE	5.0	.052
3	RING	I-21	35	MODERATE	2.0	.117
4	TENSION	I-22	43	EXCELLENT	0.1	.609
5	SHEAR	I-23	88	GOOD	1.0	.330
6	TENSION	I-24	93	GOOD	1.0	.372

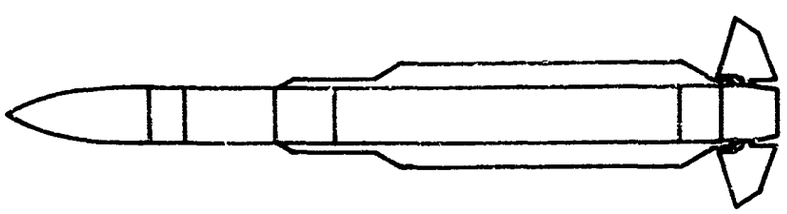

FIGURE 4-4

MISSILE JOINT CLASSIFICATION COMPARISON

$$1/I_R = 1 + \frac{EIC_\theta}{D/2} = 1 + f\left(\frac{Et}{D}\right)$$

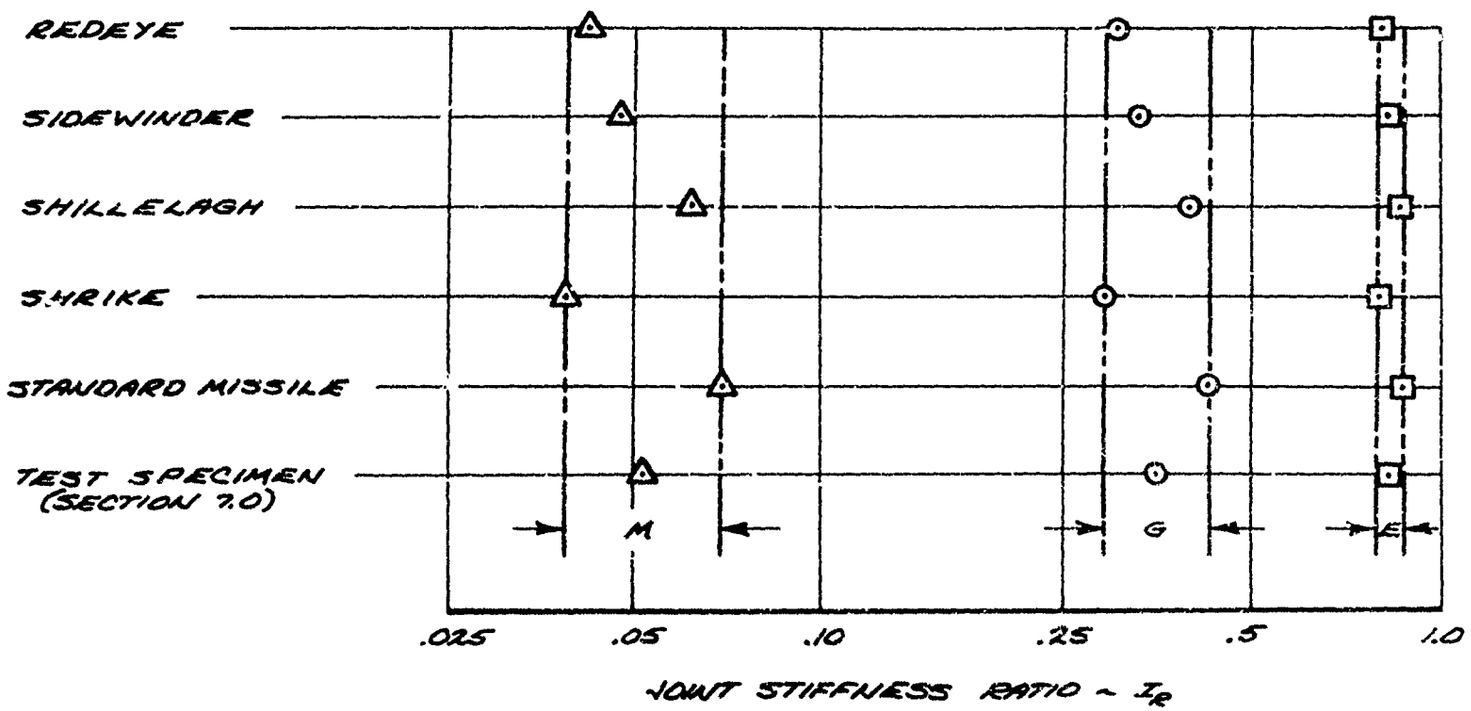

Section 5.0

PARAMETRIC STUDIES

5.1 JOINT STIFFNESS AND LOCATION

The purpose of the parametric study discussed in this section is to determine and illustrate the effects of variations in joint stiffness and location on missile response characteristics. Emphasis is placed initially on studying effects rather than the causes of the various joint parameters in order to arrive at an understanding of their relative importance.

The primary tool used in the parameter study is a standard beam modal analysis program. This program accepts a lumped parameter beam bending model for the missile structure under consideration and generates mode shape, shear, bending moment, and resonant frequency information. The approach taken in determining the influence of the joint parameters on missile response characteristics has generally been to investigate a single parameter at a time. The joint compliance values used in this report are reciprocals of the flexural spring rates attributed to the joints. For the purpose of the parametric study, only flexural or rotational compliances have been considered at joints since shear deflections are generally a second order effect.

A non-dimensional presentation of the results is shown to provide a useful basis for estimating the effects of changes in joint compliance and location on the frequencies of a uniform beam. These trends developed initially for uniform beams with single joints are shown to be extrapolatible with surprising accuracy to uniform beams with multiple joints. As might be expected, however, some discrepancies are likely in applying the results to non-uniform beams representative of actual tactical missiles. One example based on an actual missile with five joints nevertheless indicates that good qualitative estimates of joint effects on the first mode frequency are possible.

5.1.1 Method of Analysis. The modal analysis program used in the parametric study is based on a modified Holzer-Myklestad method. A missile can be described analytically as a non-uniform elastic beam (the main beam) to which various appendages are attached. Joint local deformation characteristics can be simulated by placing local springs at stations where joints occur. The main beam is represented as a series of lumped masses and inertias connected by weightless beam elements. The beam elements represent the average stiffness properties between the mass stations. The appendages are represented in the same manner as the main beam and attachment of an appendage to the main beam may be accomplished with local springs representing attachment compliances. The computer

program is capable of handling bending, torsion, and longitudinal motions; however, only bending analyses for a free-free beam have been considered in these studies. The program starts with an assigned frequency and iterates with increasing frequency until the boundary conditions are met and a natural frequency is found. At each natural frequency found by the program, the modal displacement at some selected normalization station (in these studies the first station) is set equal to unity. The deflections, slopes, bending moments, and shears are obtained at all missile stations relative to the displacement of the first station. Hence, all quantities are obtained as "normalized" values.

For the purposes of the parametric study a "nominal" uniform beam was selected which has weight, stiffness, and a first mode resonant frequency (50.188 Hz) similar to a representative tactical missile. The schematic diagram below shows the "nominal" uniform beam and its associated physical properties.

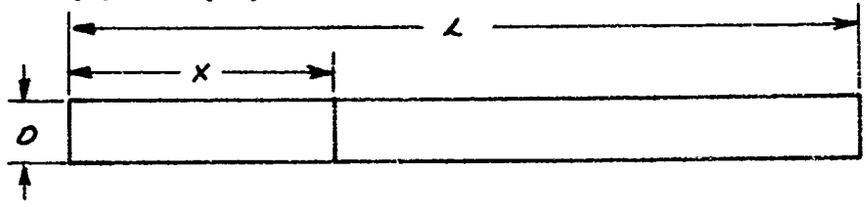

L	=	176 IN	f_{o_1}	=	50.188 Hz
D	=	13.5 IN	W/L	=	5.92 LBS/IN
EI	=	$2.9\ (10)^9$ LB-IN^2	X	=	Joint Location ~ IN

This analytical model approximates the distributed uniform beam weight as twenty one point masses. The effects of joint location and compliance on mode shape, bending moment distribution and on modal frequency have been examined using this "nominal" uniform beam.

5.1.2 Joint Location Effects. Figure 5-1 shows the bending moment distribution over the half span of the "nominal" uniform beam for the first three bending modes. Only the half span distribution is shown since the bending moment is an even function about the midspan station for the first and third modes and an odd function about the midspan station for the second mode. The bending moment has been normalized to a unity modal displacement of the beam at 0% span. Since the deflection across a rotational joint is dependent on the magnitude of the bending moment at the joint, the importance of joint location is immediately evident. As shown, the bending moment reaches a peak at 50% span in the first and third modes while the second mode bending moment goes to zero. Hence, a soft rotational spring located at the center of the beam will produce significant changes in the modal characteristics of the first and third modes while the second mode will be unaffected.

Using a "moderate" joint as determined by the NASA criteria shown in Section 4.2, the effect of joint location on the first bending mode

shape of the uniform beam was examined. Figure 5-2 shows the first bending mode shapes for the "nominal" uniform beam with a "moderate" joint at 0% (no joint), 10%, 20%, 30%, 40%, and 50% span. Joints located between 50% and 100% span would have the same effects on the first mode characteristics as joints located between 50% and 0% span.

Figure 5-3 shows the corresponding first mode bending moment distributions which result from placing a "moderate" joint at the same range of locations along the beam. As shown, the normalized bending moment decreases when a joint is located on the beam. The change in the bending moment distribution is caused by the alteration of the mode shape and reduction in modal frequency when a joint is added to the system.

Figure 5-4 shows the effect joint location has on the first mode natural frequency of the "nominal" uniform beam for a "moderate" joint. The maximum reduction in first mode frequency occurs when the joint location is at 50% span as might be expected. A joint located between 0% and 10% span causes little change in the first mode frequency while a joint location between 40% and 50% span causes a large change in the first mode bending frequency.

5.1.3 Joint Compliance Effects. Figure 5-5 shows the effect of joint compliance on the first bending mode shape of the "nominal" uniform beam with a joint located at 50% span. As expected, the mode shape becomes more deformed at the joint location as the joint stiffness decreases from no joint to a "good" joint to a "moderate" joint. Figure 5-6 shows the resulting bending moment distributions for no joint, for a "good" joint, and for a "moderate" joint. Again the distribution becomes increasingly altered as the joint spring becomes softer. Figure 5-7 shows the effect of joint stiffness on the reduction of the first mode bending frequency due to joint location.

5.1.4 Non-dimensional Presentation. Based on the uniform beam study, a useful non-dimensional relationship can be derived between joint compliance and beam stiffness. This relationship provides a means of easily assessing the significance of altering a joint parameter. The slope change across a rotational joint is equal to the product of the bending moment at the joint and the joint compliance ($\Delta\phi_j' = MC_\phi$). The change in slope per unit length on a uniform beam without joints is equal to the bending moment divided by the beam stiffness ($\Delta\phi_B'/\ell = M/EI$). A compliance ratio per unit beam length is obtained by dividing the joint rotation per unit moment by the beam rotation per unit length, $\Delta\phi_j'/\Delta\phi_B'/\ell = EIC_\phi$. This term can be conveniently non-dimensionalized by dividing by the total beam length ℓ. A nondimensional compliance ratio, EIC/ℓ, is thus obtained which relates joint compliance, beam stiffness, and beam length. This expression, not surprisingly, is directly related to the stiffness reduction ratio derived in Section 4.1.

$$1/\alpha_R = 1 + \frac{EI_B C_\phi}{\ell}$$

Using total beam length to non-dimensionalize the compliance ratio offers the advantage of general application to all uniform beams regardless of fineness ratio (length divided by diameter). The use of body diameter as a basis for non-dimensionalizing, however, is believed to offer better physical insight in judging the significance of joint compliance relative to airframe stiffness. A reference length based on diameter also permits direct comparison with the joint compliance rating system discussed in Section 4.2. The results presented on this basis, however, apply explicitly only for airframes with a fineness ratio of 13 as used in the parametric study. Both non-dimensionalizing parameters are given in Tables 5-1, 5-2 and 5-3 which summarize in tabular form the effects of non-dimensional joint compliance and location on the mode frequencies of a uniform beam. Corresponding plots of the first mode frequency ratio versus compliance ratio (EIC/L) and stiffness ratio (K_R) are presented in Figures 5-8 and 5-9 respectively. It is significant to note that a single "moderate" joint at the midspan of a uniform beam can be expected to reduce the first mode frequency by approximately 35 percent.

5.1.5 Multiple Joint Applications. The uniform beam results for a single joint as displayed in Figures 5-8 and 5-9 can be extrapolated to multiple joint configurations by a simple summing procedure in which a number of joints of various compliances at arbitrary locations are referenced and summed as an equivalent single joint compliance located at a common reference station such as the midspan. The steps in this procedure are as follows

1. At each desired joint location determine the resulting frequency ratio for a single joint of specified compliance at that location.

2. Determine the equivalent joint compliance which would be required at a common reference station such as the midspan to produce the same frequency ratio.

3. The sum of the individual equivalent joint compliances yields an equivalent single joint at the reference station.

4. The frequency ratio associated with this single equivalent joint is found to give a very close estimate of the multiple joint effect on the first mode frequency ratio for a uniform beam.

An example of the application of this procedure is presented in Table 5-4. The "calculated" frequency ratios for the multiple joint configurations listed were determined by modal analysis, with the "estimated" values determined by the procedure described. In this instance, the use of compliance ratio, EIC/L, offers an advantage over

stiffness ratio, K_R, in that the incremental equivalent compliances can be added directly.

5.1.6 Tactical Missile Application. For an actual tactical missile, non-uniformities exist in both the mass and stiffness distribution in addition to multiple joints. The effect of these considerations would be expected to severely limit the applicability of the uniform beam results in estimating joint effects on an actual missile. The following example, however, illustrates that a good qualitative estimate of joint compliance effects is nevertheless possible. Figure 5-10 displays a typical airframe stiffness distribution, in this case for the medium range Standard Missile. The significance of the narrow EI spikes showing discontinuous increases in airframe stiffness which are often meticulously computed and included in modal analysis computations is virtually zero, having very little effect in theory as shown by the calculated frequency changes in the figure. This conclusion, however, definitely does not apply in the case of discontinuous decreases in EI as will be demonstrated in the test results presented in Section 7. The following table lists the five principal airframe joints, their compliances and locations, and the comparison between the computed (modal analysis) and estimated frequency ratios by the procedure of Section 5.1.5.

STANDARD MISSILE (MR) JOINT CHARACTERISTICS

Joint Location	Compliance $C_\theta \times (10)^8$	Compliance Ratio $EIC/L(10)^2$	
		Actual	Equiv.
.22	1.5	24.70	5.06
.35	0.6	9.85	6.52
.41	0.5	8.25	6.90
.87	1.15	18.95	0.88
.92	1.0	16.45	0.31

$\Sigma \left(\frac{EIC}{L}\right)_{EQ} = .1967$

1st Mode Frequency Ratio		Error
Calculated	Estimated	%
.834	.810	3

The implied accuracy of the estimate is somewhat misleading since an average airframe stiffness must be assumed for the total airframe and the answer is obviously sensitive to this assumption. The answer does

suggest, however, that the procedure may be useful in providing good qualitative estimates of joint effects.

5.2 CROSS PLANE SPRING COUPLING AT AIRFRAME JOINTS

5.2.1 Introduction. Double peaked modes are often observed in the vibration testing of tactical missiles. This condition is most usually accompanied by substantial energy transfer or cross talk between in-plane and out-of-plane response. The cause of this coupling can frequently be traced to the behavior of one or more of the airframe joints. "Breaking" and retorqueing of the joints will in many instances significantly alter or in some cases eliminate this response characteristic. One of the major problems created by this type of mechanical joint behavior is the uncertainty it introduces in describing missile airframe response for control system design studies. One typical frequency response, measured on the nose of a grain-out extended range Standard Missile for constant force excitation at the tail station, is presented in Figure 5-11. Peaks occur at both 63 Hz and 66 Hz. The peak at the lower frequency is 1.5 db or about 20 percent greater than the peak at the higher frequency. It has been determined that for this airframe the severity of the double peak characteristic is primarily controlled by the forward-most joint which is a split ring continuous land design (Figure 1-15). Reseating and overtorqueing of the coupling nut will generally bring the peaks closer together in frequency and increase the magnitude of the peak response.

The objective in this section is to develop a conceptual model for the source of elastic coupling in airframe joints and to examine joint coupling effects on airframe response through parameteric analysis.

5.2.2 Conceptual Model for Joint Elastic Coupling. It is believed that joint elastic coupling is caused by irregularities in the mating surfaces of the joint. These irregularities produce a non-axially symmetric load distribution in the joint and, hence, create spring coupling characteristics. Discrete irregularities can be idealized as springs concentrated at the points of protrusions around the airframe circumference. If concentrated springs (with spring rates k_i) are assumed to be located in the plane of an airframe joint as shown below,

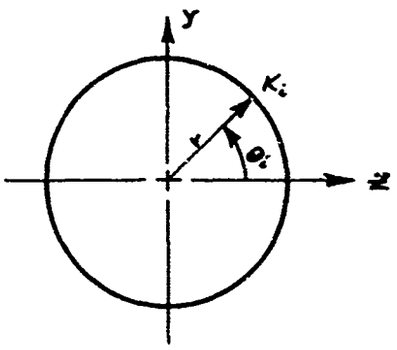

an equation can be derived expressing the bending moment across the joint in the 'Z' and 'Y' directions as a function of the spring rates k_i, angles θ_i, and joint rotations α_z and α_y. The expression for bending moment across a joint is

$$\begin{Bmatrix} M_z \\ M_y \end{Bmatrix} = -r^2 \begin{bmatrix} \sum_i K_i \sin^2\theta_i & -\sum_i K_i \sin\theta_i \cos\theta_i \\ -\sum_i K_i \sin\theta_i \cos\theta_i & \sum K_i \cos^2\theta_i \end{bmatrix} \begin{Bmatrix} \alpha_z \\ \alpha_y \end{Bmatrix}$$

or

$$\begin{Bmatrix} M_z \\ M_y \end{Bmatrix} = \begin{bmatrix} K_{zz} & -K_{zy} \\ -K_{yz} & +K_{yy} \end{bmatrix} \begin{Bmatrix} \alpha_z \\ \alpha_y \end{Bmatrix}$$

where

M = bending moment across the joint

K = rotational stiffness of the joint

α = rotation across the joint

Z, Y = two reference missile axes which are perpendicular.

A useful relationship for investigating joint coupling effects can be developed by reducing the general case to a three spring idealization. Since three points define a plane, this idealization offers a plausible model for the points of joint interface contact and becomes especially valid when the source of the preload in the joint (e.g. bolts in tension) represents a minor contribution to joint compliance.

Considering the plane of the joint for the three spring idealization, and equal spring rates:

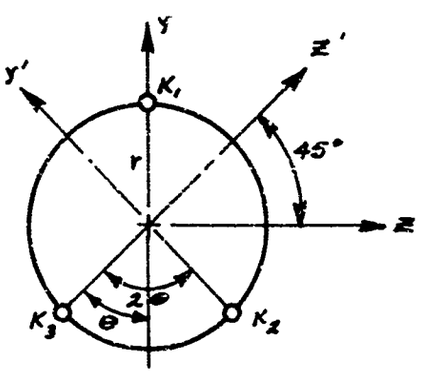

$K_1 = K_2 = K_3$

The spring matrix in the y_z coordinate system becomes:

$$\begin{Bmatrix} M_z \\ M_y \end{Bmatrix} = \begin{bmatrix} K+\Delta K & 0 \\ 0 & K-\Delta K \end{bmatrix} \begin{Bmatrix} \alpha_z \\ \alpha_y \end{Bmatrix}$$

where:

$$K = \frac{1}{2}(K_1 + K_2 + K_3) r^2$$

and

$$\Delta K = \left(1 - \frac{4}{3}\sin^2\theta\right) K$$

It is significant to note that for all values of θ a plane of symmetry exists (defined by the Y axis and the missile longitudinal axis) and that the y-z coordinates remain decoupled. The special case of axial symmetry ($\Delta K = 0$) exists when $\theta = 60°$ (120° spacing between springs).

The joint deflection characteristics viewed from a y'-z' coordinate reference rotated through 45 degrees will exhibit maximum apparent coupling through ΔK in the following transformed spring matrix:

$$\begin{Bmatrix} M_z' \\ M_y' \end{Bmatrix} = \begin{bmatrix} K & -\Delta K \\ -\Delta K & K \end{bmatrix} \begin{Bmatrix} \alpha_z' \\ \alpha_y' \end{Bmatrix}$$

Figure 5-12 presents the variation in ΔK with spacing angle θ for the three spring idealization joint model. It should be noted that the limiting case of 100 percent coupling, $\Delta K = K$ implies a zero spring about the α_y coordinate and maximum coupling in the y'-z' coordinate frame.

For actual airframes, particularly with multiple joints, coupling effects on airframe dynamic response can become sizable and quite complex. Although each joint may have a plane of symmetry with respect to its load/defelction characteristics, the probability of alignment in multiple joint planes of symmetry is quite small.

5.2.3 Joint Spring Coupling Parametric Study. A computer program which accepts generalized modal properties for a linear damped system and computes the frequency response of the desired structural transfer function has been used in the parametric study of joint spring coupling. The spring coupling term governs the response in any one plane which is solely due to an input in a plane perpendicular to the plane of response.

The equations of motion of a linear system undergoing forced vibrations may be written in matrix form and Laplace operator notation as follows:

$$\left[\left[M_{ij}\right] s^2 + \left[B_{ij}\right] s + \left[Q_{ij}\right]\right] \left\{E_i\right\} = \left\{F_i\right\}$$

where

$\left[M_{ij}\right]$ = generalized mass matrix

$\left[B_{ij}\right]$ = generalized damping matrix

$\left[Q_{ij}\right]$ = generalized spring matrix

$\left\{E_i\right\}$ = time varying generalized coordinates of the system

$\left\{F_i\right\}$ = generalized forces acting on the system

s = the Laplace operator, $sx = \frac{dx}{dt}$.

If E_f is the time varying generalized coordinate representing the forcing function,

$$\left\{F_i\right\} = \left\{A\right\} E_f$$

and substituting,

$$\left[\left[M_{ij}\right] s^2 + \left[B_{ij}\right] s + \left[Q_{ij}\right]\right] \left\{E_i\right\} = \left\{A\right\} E_f.$$

The response of the system is a linear combination of the coordinate responses, which is found by Cramer's Rule:

$$\frac{R}{F_f} = \frac{\sum_i C_i N_i}{F_f} = \frac{\sum_i C_i N_i(s)}{D(s)}$$

where

$D(s)$ = the determinant expansion of the left-hand side of the equations of motion

$N_i(s)$ = the determinant expansion of the left-hand side of the equations of motion after substituting the right-hand side into the ith column

C_i = a numerical coefficient (modal deflection at point of interest on beam)

R = the sectional response of the system to the forcing function F_f.

If the response is desired in terms of velocity or acceleration, the response equation may be multiplied by s or s^2, respectively:

$$\frac{\dot{R}}{F_f} = \frac{s\sum_i C_i N_i(s)}{D(s)}, \quad \frac{\ddot{R}}{F_f} = \frac{s^2\sum_i C_i N_i(s)}{D(s)}$$

The generalized coordinates used in the parametric study consist of in-plane and out-of-plane bending modes and in-plane and out-of-plane "hinge" modes. The bending modes have no compliance at the joint of interest, and consequently have no change of slope across the joint. The "hinge" modes treat the beam as two rigid members connected with a local spring at the joint of interest. The local spring represents the joint compliance in the two individual planes and the joint coupling characteristics between the planes.

The displacements in the "hinge" modes are such that they are mass orthogonal with respect to rigid body translation and pitch about the center of gravity. The "hinge" modes are not orthogonal to the bending modes, however, and hence in each plane we have mass coupling terms

$$M_{ij} = M_{ji} = \int_0^\ell m\, \phi_i\, \phi_j\, dx$$

where

m = running mass (mass per unit length)

ϕ_i = ith bending mode shape

ϕ_j = "hinge" mode shape

The only coupling between the two planes of motion occurs solely in the structural spring matrix. When Lagranges' equations are used to derive the equations of motion, it can be seen that the structural spring terms result from the stored energy associated with the unit deflections of all the generalized coordinates. The hinge modes store energy only by rotation at the joint, and since the bending modes have no change of slope at the joint, there is no spring coupling between the bending and hinge modes. Consequently, the spring matrix for the bending modes is a diagonal matrix. The two hinge modes have both diagonal terms and off diagonal terms, which represent energy transfer between planes. The spring terms for the hinge modes are given by the following relations:

$$\Phi_{ii} = \Phi_{jj} = (\Delta\phi'_{iz})^2 K_{zz} = (\Delta\phi'_{iy})^2 K_{yy}$$

$$\Phi_{ij} = \Phi_{ji} = \Delta\phi'_{iz}\,\Delta\phi'_{jy} K_{zy} = (\Delta\phi'_{iz})^2 K_{zy}$$

where

$\Delta\phi'$ = change of slope across the joint for the hinge modes $(\Delta\phi'_{iz} = \Delta\phi'_{jy})$

K_{zz} = joint spring in the Z plane ($K_{yy} = K_{zz}$)

K_{zy} = chosen as a parameter (a percentage of K_{zz})

i,j = mode counters of hinge mode in z and y planes, respectively.

The damping matrix used in this study, [P] , is a diagonal matrix. The [M] and [Q] matrices have the following form when considering three bending modes and one "hinge" mode in both the y and z planes:

$$[M_{ij}] = \left[\begin{array}{cccc|cccc} X & & & X & & & & \\ & X & & X & & & & \\ & & X & X & & & & \\ X & X & X & X & & & & \\ \hline & & & & X & & & X \\ & & & & & X & & X \\ & & & & & & X & X \\ & & & & X & X & X & X \end{array}\right]$$

$$[\varphi_{ij}] = \begin{bmatrix} \times & & & & & & \\ & \times & & & & & \\ & & \times & & & & \\ & & & \times & & & \times \\ & & & & \times & & \\ & & & & & \times & \\ & & & & & & \times \\ & & & \times & & & \end{bmatrix}$$

where

$$\{\xi_i\} = \left\{ \begin{array}{ll} \xi_1 = & \text{First bending mode in Z-plane} \\ \xi_2 = & \text{Second bending mode in Z-plane} \\ \xi_3 = & \text{Third bending mode in Z-plane} \\ \xi_4 = & \text{"Hinge" mode in Z-plane} \\ \xi_5 = & \text{First bending mode in Y-plane} \\ \xi_6 = & \text{Second bending mode in Y-plane} \\ \xi_7 = & \text{Third bending mode in Y-plane} \\ \xi_8 = & \text{"Hinge" mode in Y-plane} \end{array} \right\}$$

As can be readily seen, the above set of generalized coordinates is very convenient for a parametric study of joint coupling characteristics. Any change of joint coupling only involves the terms of the [Q] matrix that couple the hinge modes. If it is desired to change the joint compliance in the planes or to have different compliances in the planes, this again only involves the spring terms pertaining to the hinge modes. Consequently, the effect of variations of the joint properties can be investigated with a minimum of change to the overall set of equations of motion.

The effects of joint spring coupling on the dynamic response characteristics of a uniform beam have been studied analytically using the "nominal" beam of Section 5.1.3 with a single local flexural compliance.

The bending frequencies and mode shapes for these studies were computed using the modified Holzer-Myklestad computer program discussed in Section 5.1.1. A damping ratio of one percent of critical was assumed for all modes and the frequency response curves were computed and plotted using the transfer function program described earlier in this section. The amount of cross plane spring coupling is denoted as a percentage of the in-plane joint spring term.

Figure 5-13 shows the effect of spring coupling on the frequency response characteristics of a uniform beam with a "good" joint at 50% span. The acceleration response was computed for a point at zero span for force excitation at 100% span. The various curves are for zero, 50% and 75% cross plane spring coupling. As can be seen, the peak response decreases with increasing spring coupling and doubled peaked modes occur. Increasing attenuation exists at the center frequency as the spring coupling increases (the valley between the two peaks becomes deeper). Figure 5-14 shows the effect of joint spring coupling on the response characteristics of a uniform beam with a "moderate" joint at 50% span. The effects of spring coupling are much more pronounced for a "moderate" joint than for a "good" joint. Since the bending moment in the second mode is zero at the joint location for both of these cases no effects of joint stiffness or coupling are seen in the second bending mode.

The trend in the magnitude of joint coupling effect on the first bending mode frequency as the joint compliance is varied is illustrated in Figure 5-15. In this figure, the total frequency shift ($\Delta f/f_o$) as a function of joint elastic coupling is shown for both the "moderate" and "good" joint located at the midspan of the nominal uniform beam.

The point to be made is that relatively small amounts of elastic coupling in mechanical joints can produce substantial changes in both gain and resonant frequency characteristics. Control system body mode coupling filters typically designed for a body mode frequency tolerance of ±5 percent may be forced to cope with a much larger range of response uncertainties.

5.2.4 Spring Coupling Studies for an Actual Tactical Missile. As was pointed out earlier, Figure 5-11 shows a measured Standard Missile ER frequency response for a force excitation at the tail station. A study has been conducted which attempts the modeling of the missile in such a manner as to predict a response similar to that of Figure 5-11. The stiffness coupling terms were calculated using two sets of assumed modes which represent the missile dynamic characteristics in two orthogonal planes. The two sets consisted of four modes each. The frequency response of the resulting equations of motion was computed using the computer program previously mentioned. The Z-plane frequency responses to Z-plane force input, calculated with and without spring coupling

between the "Z" and "Y" planes, are shown in Figure 5-16. The case in which no coupling exists between the two planes shows a single sharp peak in the first mode. The case in which elastic coupling is introduced between the Z-plane and the Y-plane equal to 50 percent of the total generalized spring is shown to provide a double peaked response in close agreement with the measured data of Figure 5-11. It is felt that this joint stiffness coupling is a first order model of an important deviation from the single plane response model used in classical structural dynamic analysis of tactical missiles.

FIGURE 5-1

"NOMINAL" UNIFORM BEAM WITHOUT JOINTS
BENDING MOMENT DISTRIBUTION

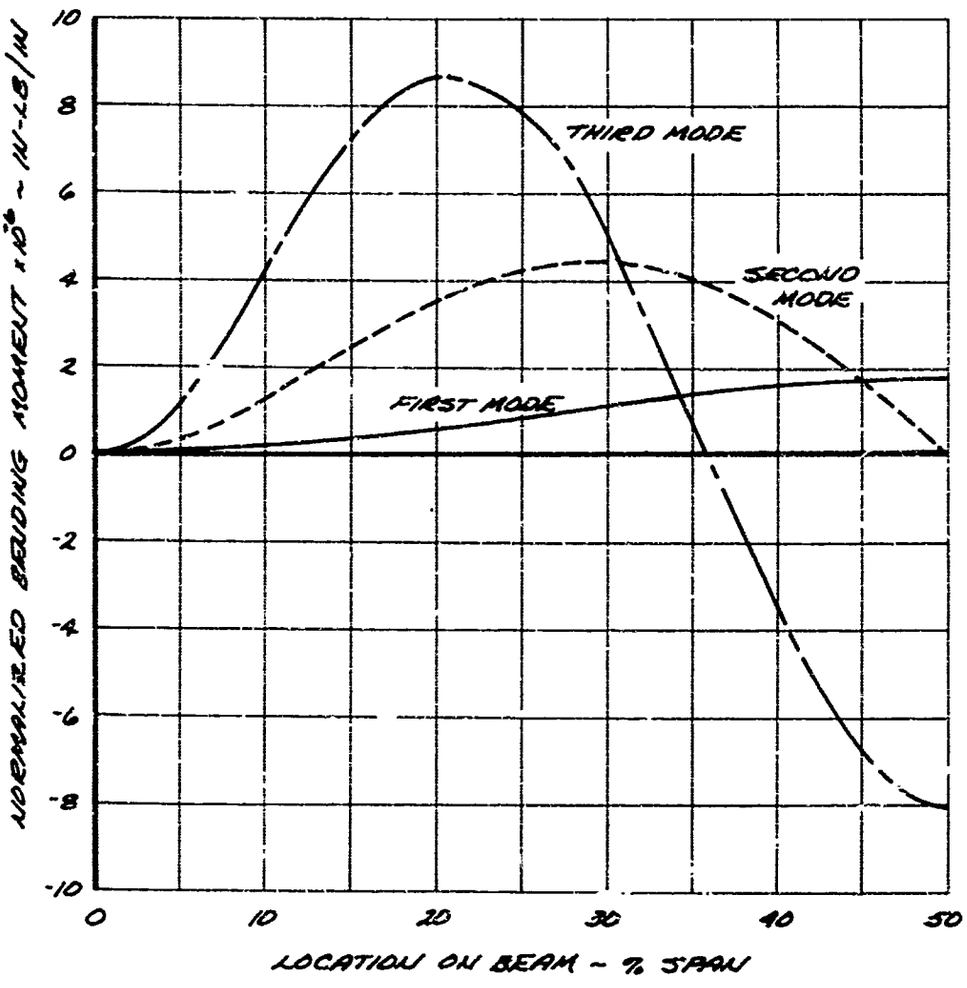

FIGURE 5-2

"NOMINAL" UNIFORM BEAM
FIRST BENDING MODE SHAPE
FOR VARIOUS LOCATIONS OF A
JOINT OF "MODERATE" COMPLIANCE

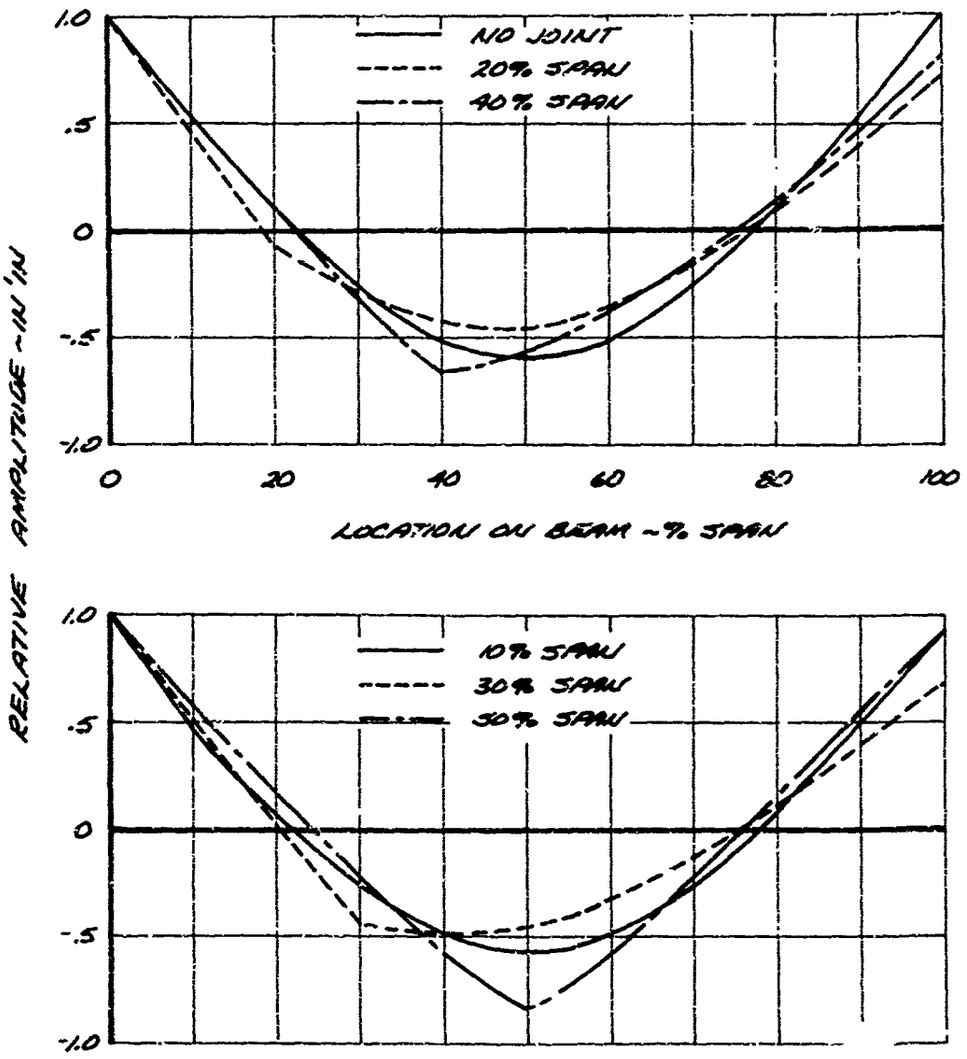

FIGURE 5-3

"NOMINAL" UNIFORM BEAM
FIRST MODE NORMALIZED BENDING MOMENT DISTRIBUTIONS
FOR VARIOUS LOCATIONS OF A
JOINT OF "MODERATE COMPLIANCE

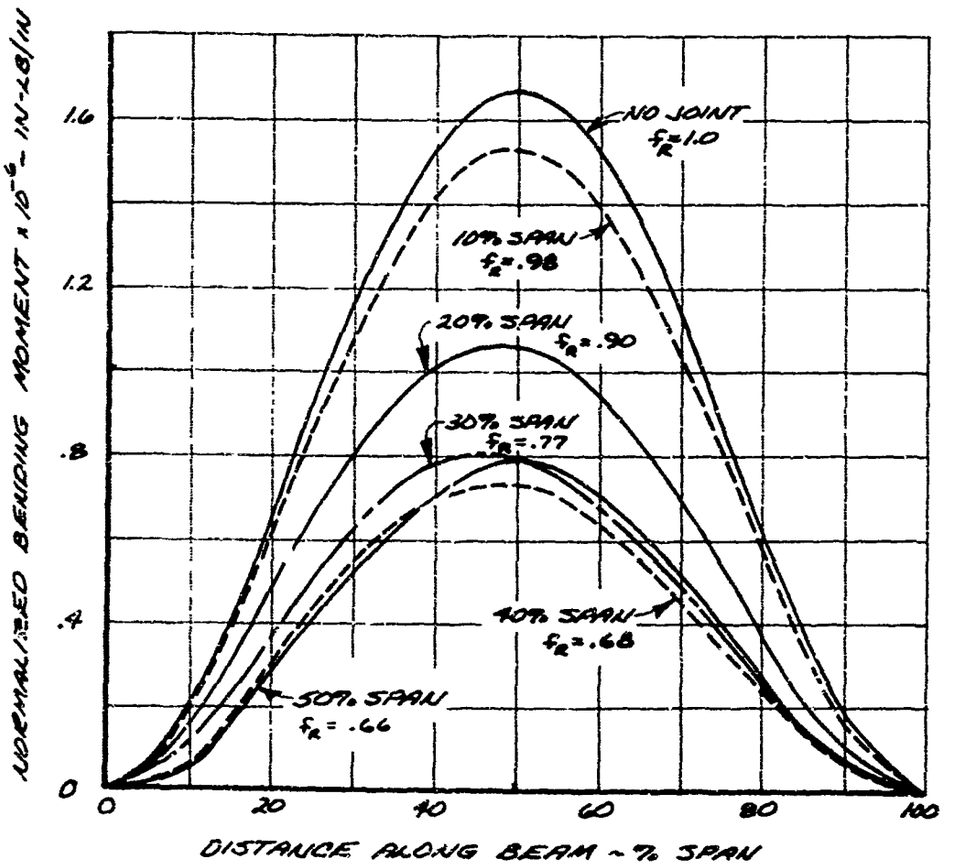

FIGURE 5-4

"NOMINAL" UNIFORM BEAM
EFFECT OF JOINT LOCATION
ON FIRST BENDING MODE FREQUENCY

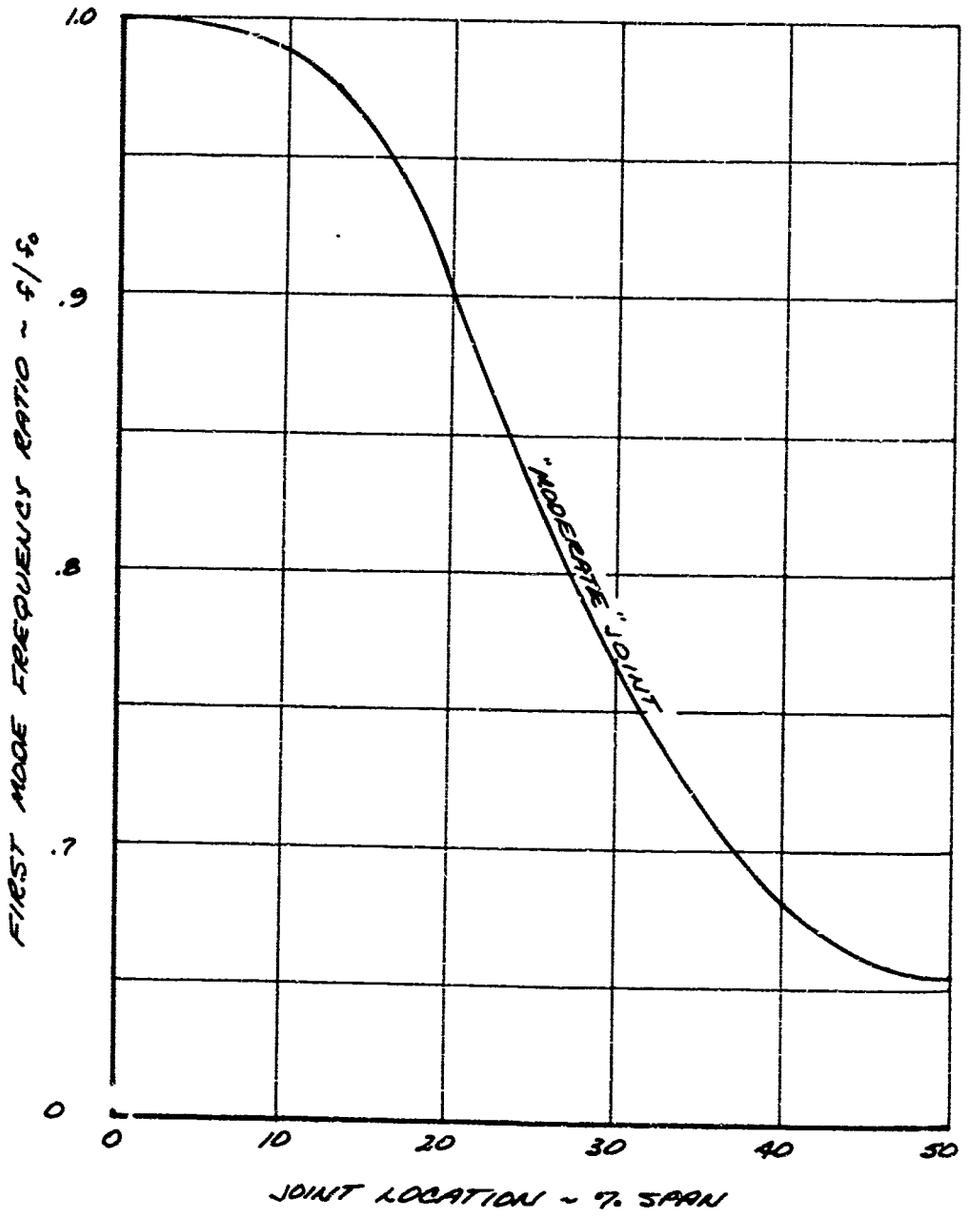

FIGURE 5-5

"NOMINAL" UNIFORM BEAM
FIRST BENDING MODE SHAPE
FOR VARIOUS JOINTS AT MIDSPAN

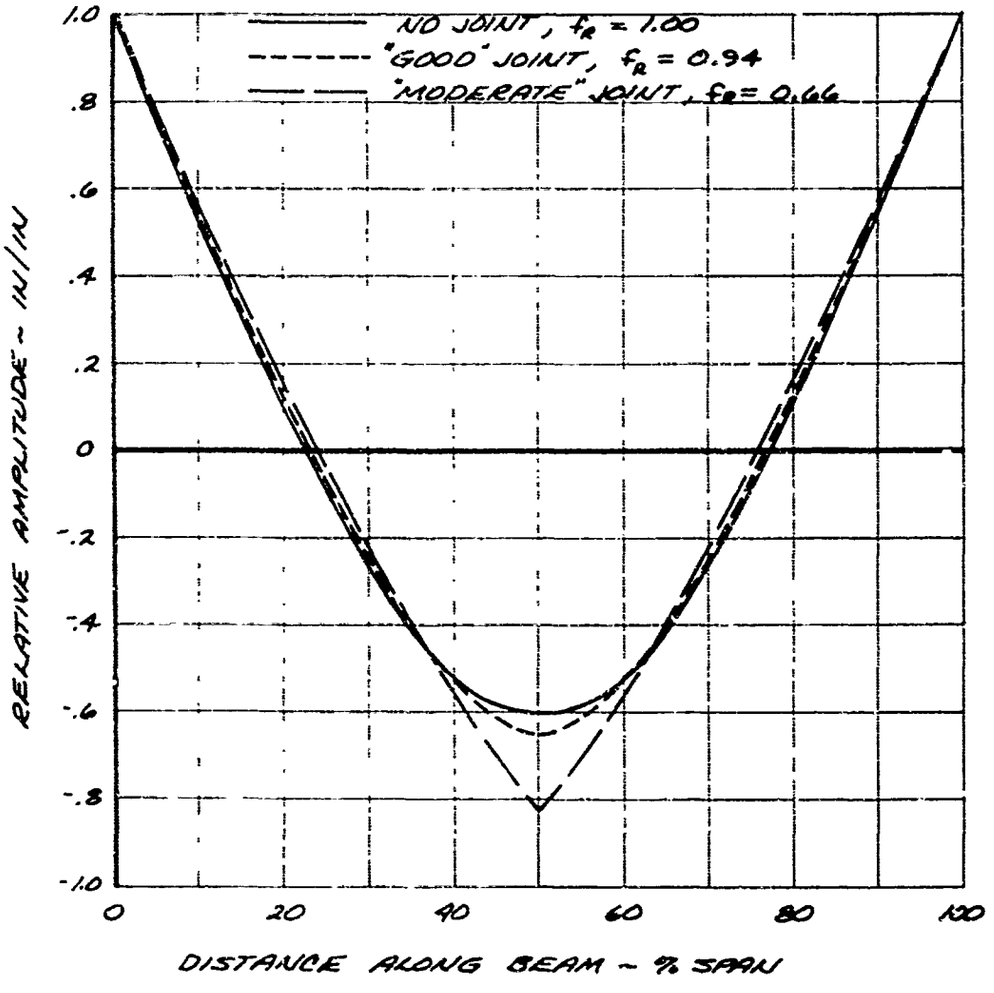

FIGURE 5-6

"NOMINAL" UNIFORM BEAM
FIRST MODE BENDING MOMENT DISTRIBUTION
FOR JOINTS AT 50% SPAN
OF VARIOUS COMPLIANCES

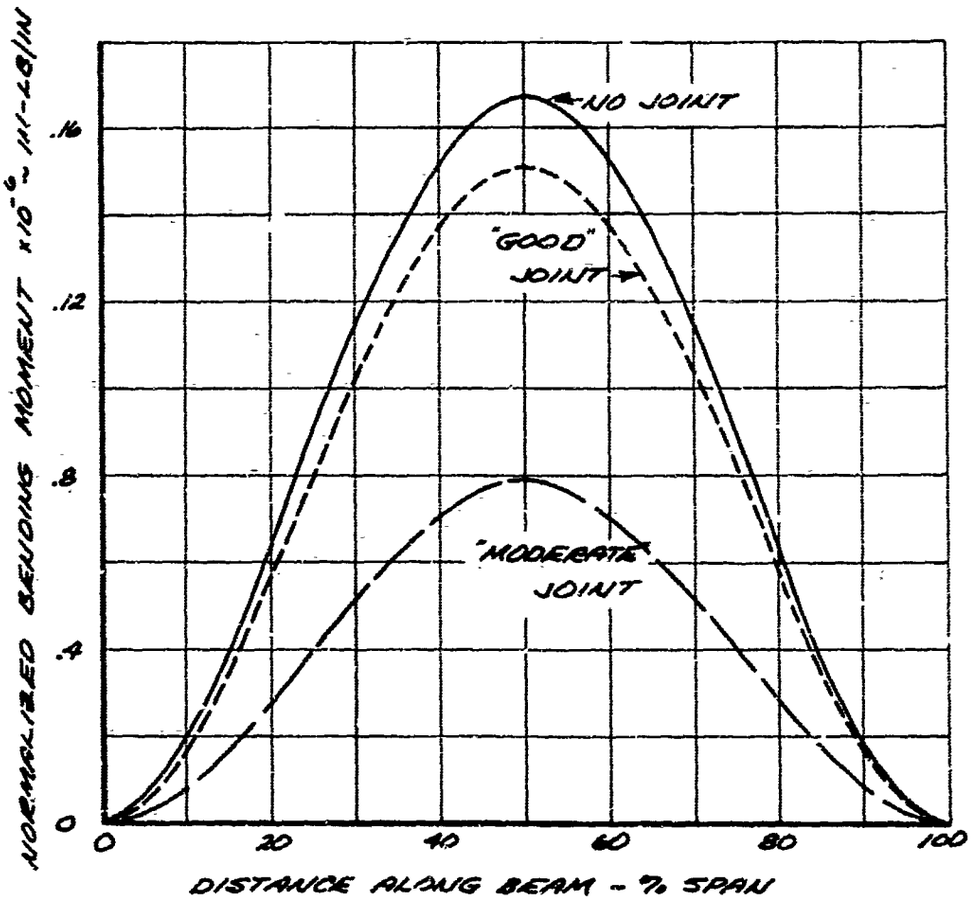

FIGURE 5-7

"NOMINAL" UNIFORM BEAM
EFFECT OF JOINT STIFFNESS AND LOCATION
ON FIRST BENDING MODE FREQUENCY

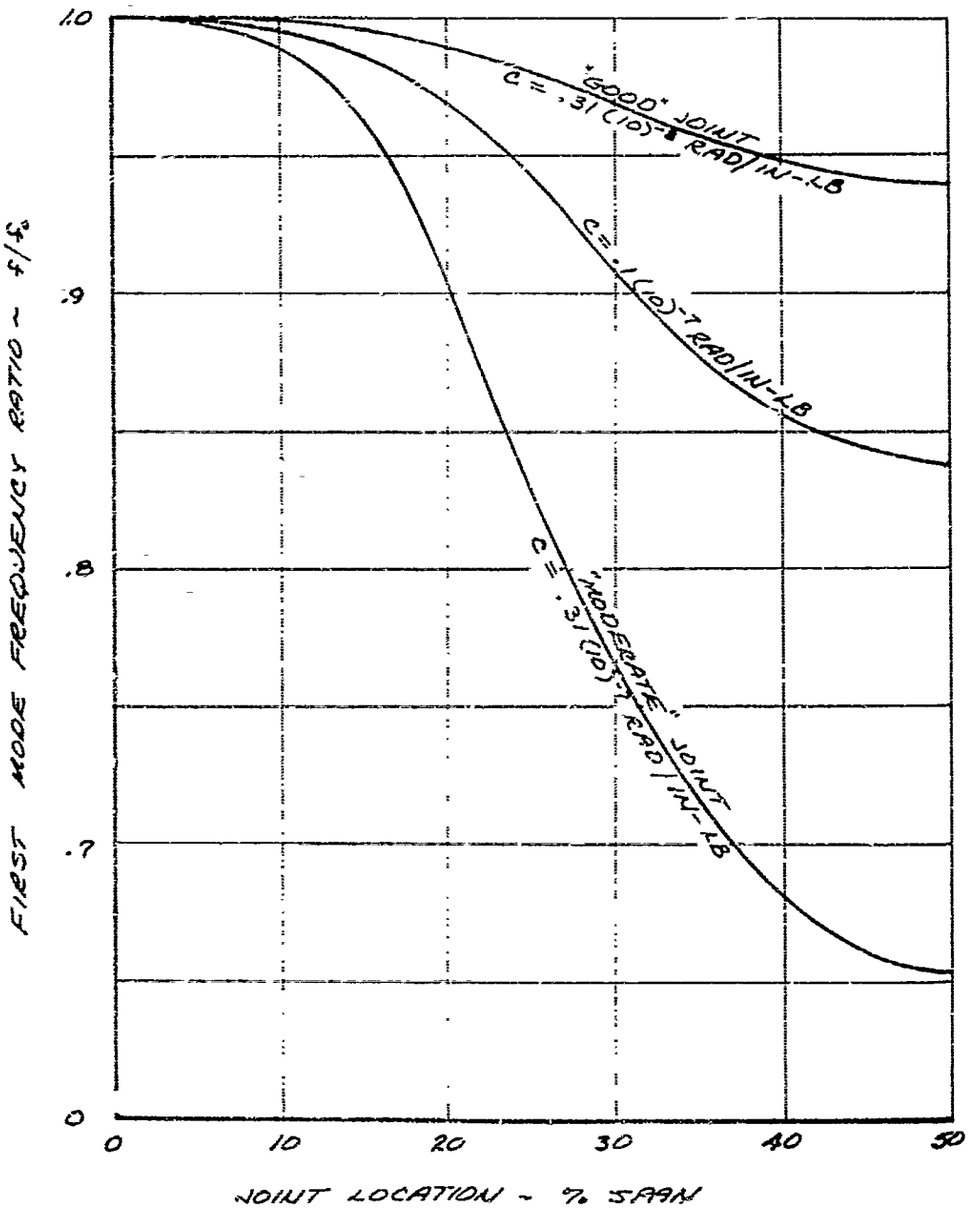

FIGURE 5-8

UNIFORM BEAM FREQUENCY RATIO
VS. JOINT COMPLIANCE RATIO
FOR VARIOUS LOCATIONS OF THE JOINT

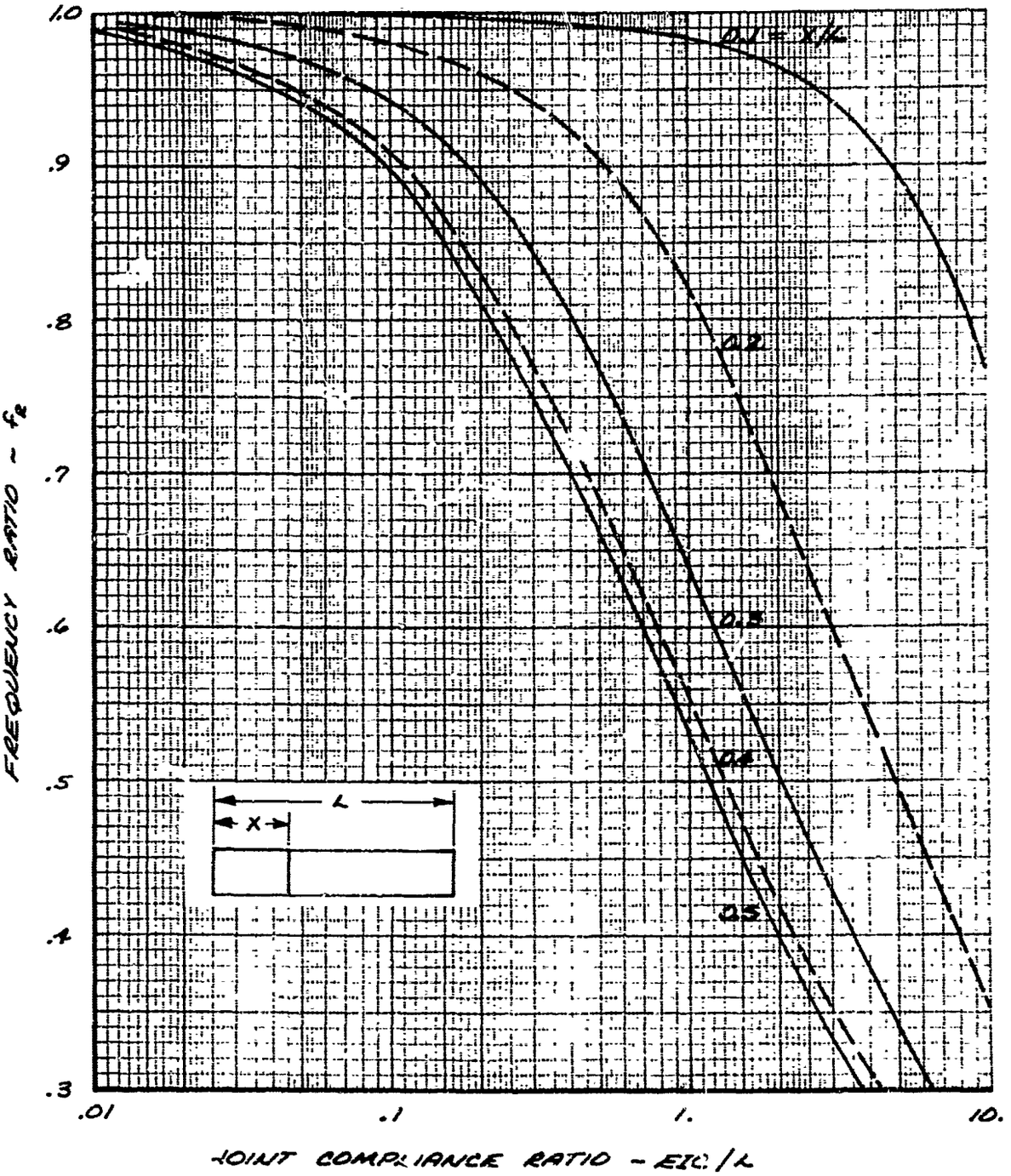

FIGURE 5-9

UNIFORM BEAM WITH A FINENESS RATIO OF 13—
FREQUENCY RATIO VS. JOINT STIFFNESS RATIO
FOR VARIOUS LOCATIONS OF THE JOINT

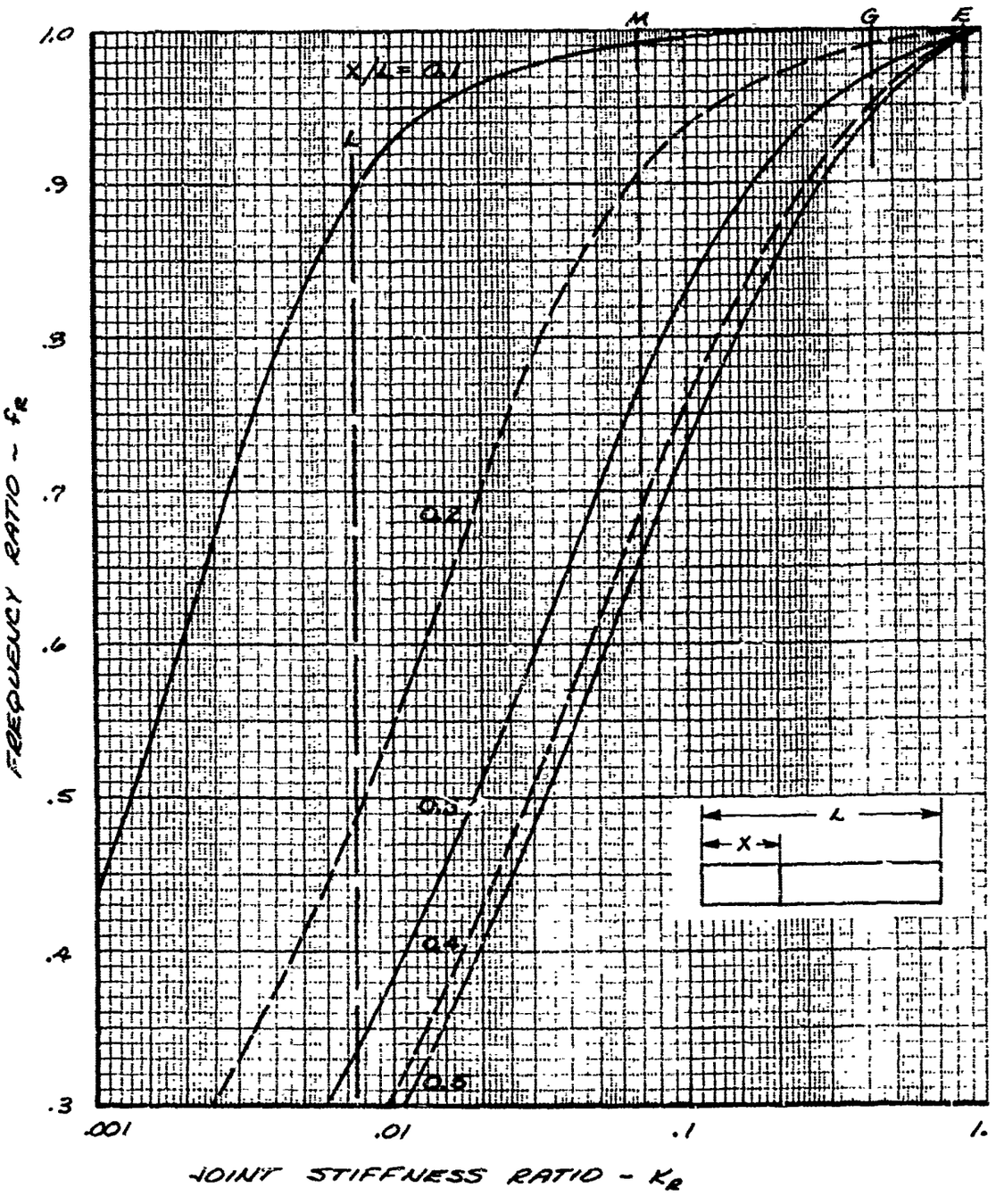

FIGURE 5-10

ACTUAL TACTICAL MISSILE
STIFFNESS DISTRIBUTION

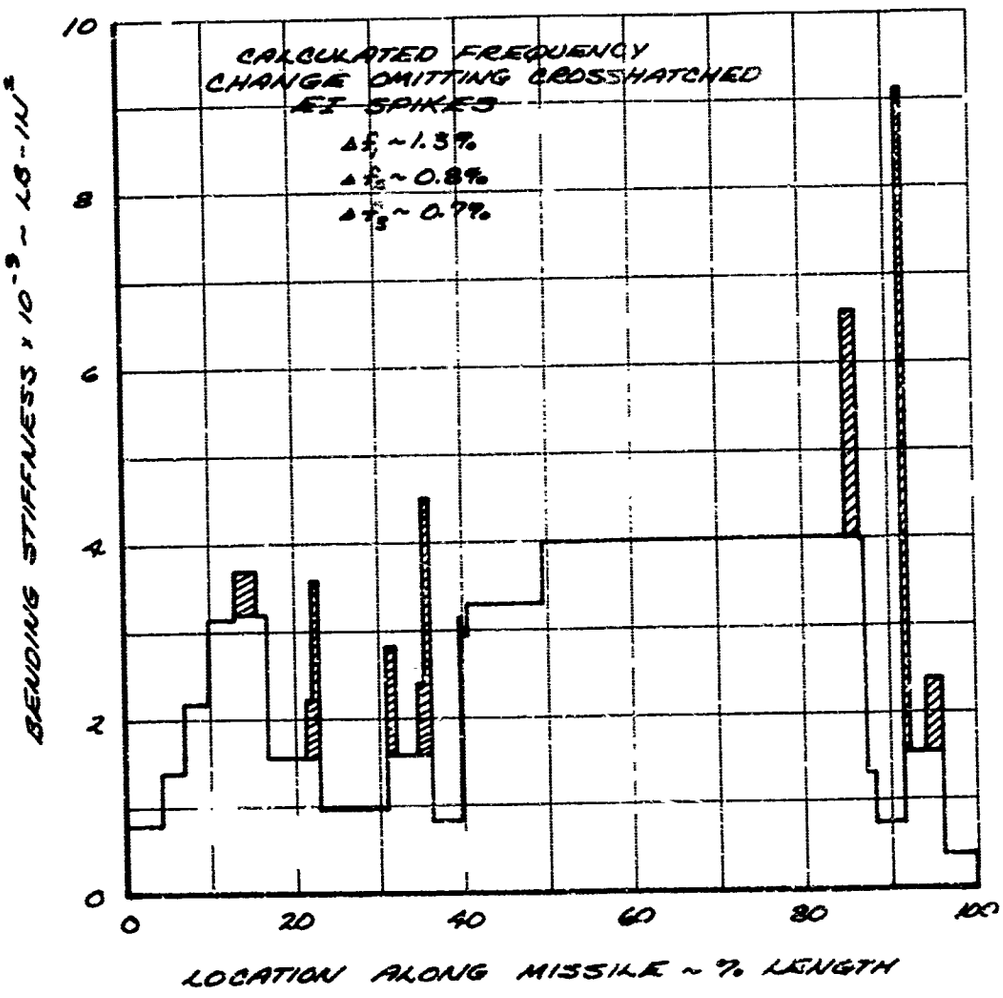

FIGURE 5-11

MEASURED FREQUENCY RESPONSE
AT THE MISSILE NOSE
DUE TO FORCE EXCITATION
AT THE TAIL STATION

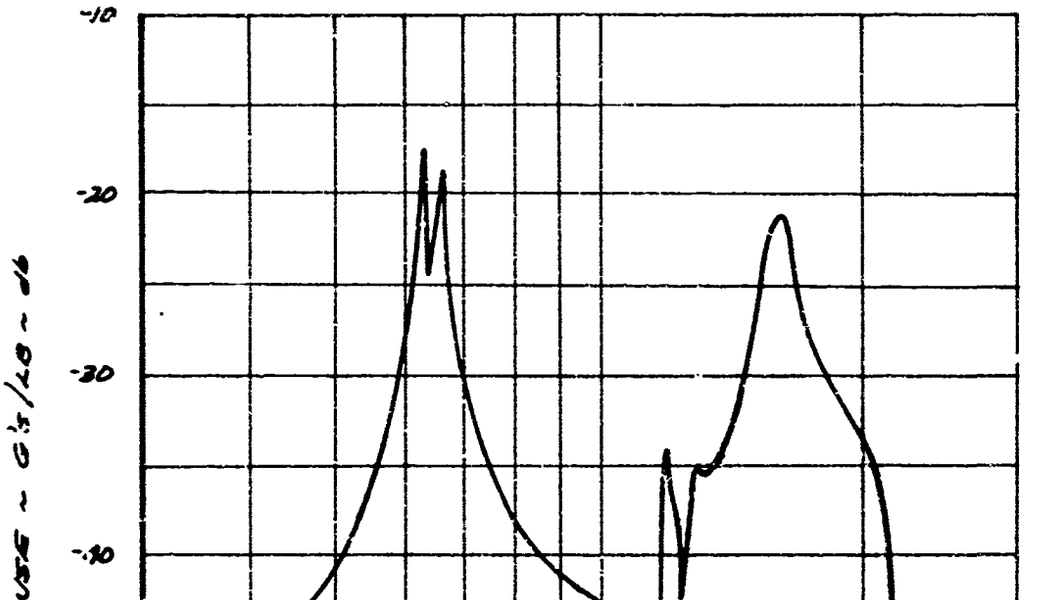

FIGURE 5-12

MECHANICAL JOINT ELASTIC COUPLING INTRODUCED BY LOAD PATH DISSYMMETRY – 3 SPRING IDEALIZATION

$$\frac{\Delta K}{K} = 1 - \frac{4}{3}\sin^2\theta$$

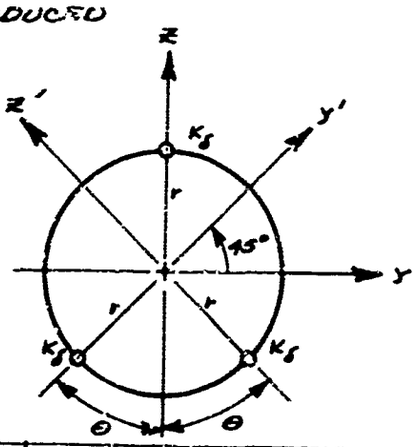

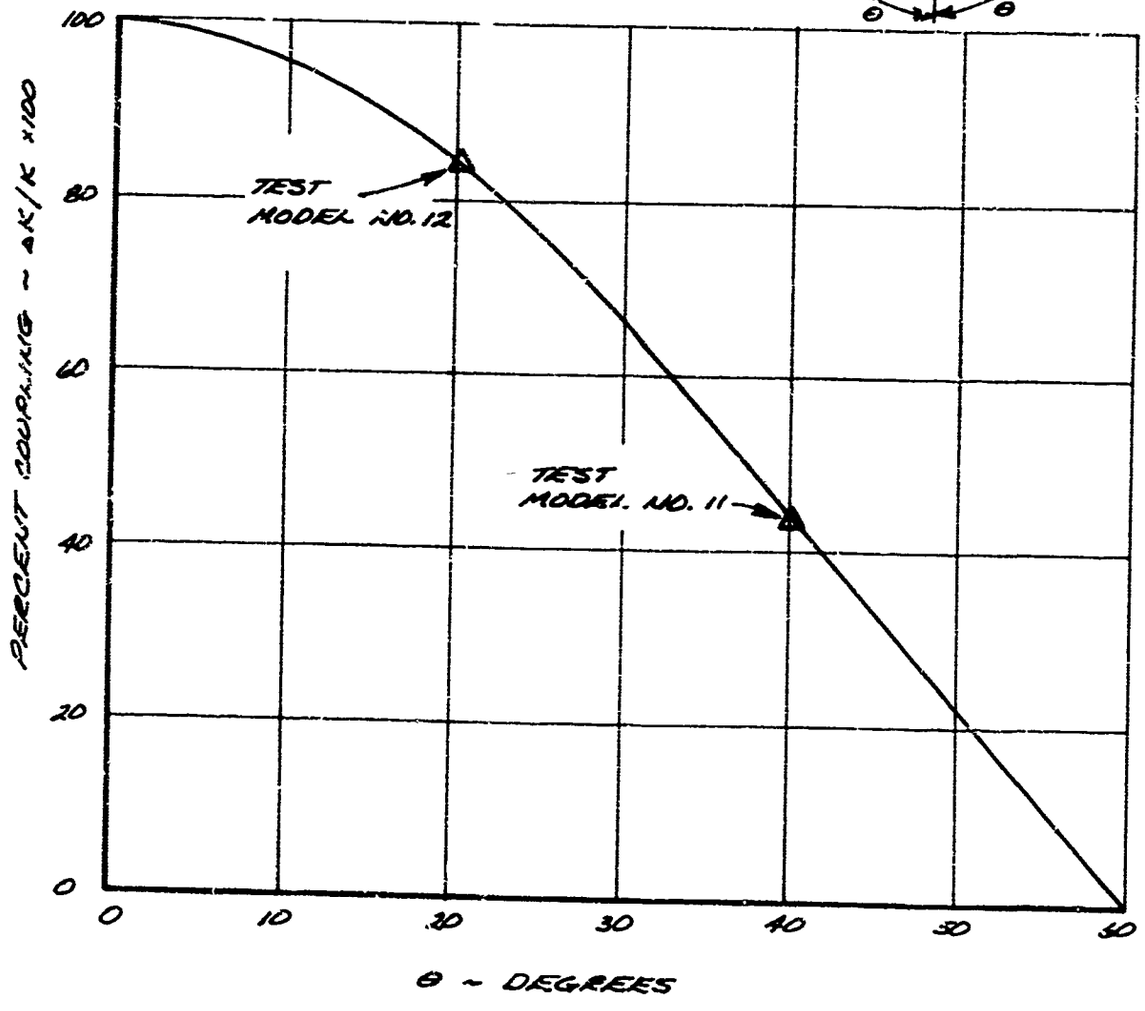

FIGURE 5-13

"NOMINAL" UNIFORM BEAM
"GOOD" JOINT AT 60% SAAN
EFFECT OF JOINT SPRING COUPLING
MAGNITUDE ON RESPONSE
AT 0% SAAN FOR EXCITATION AT 100% SAAN

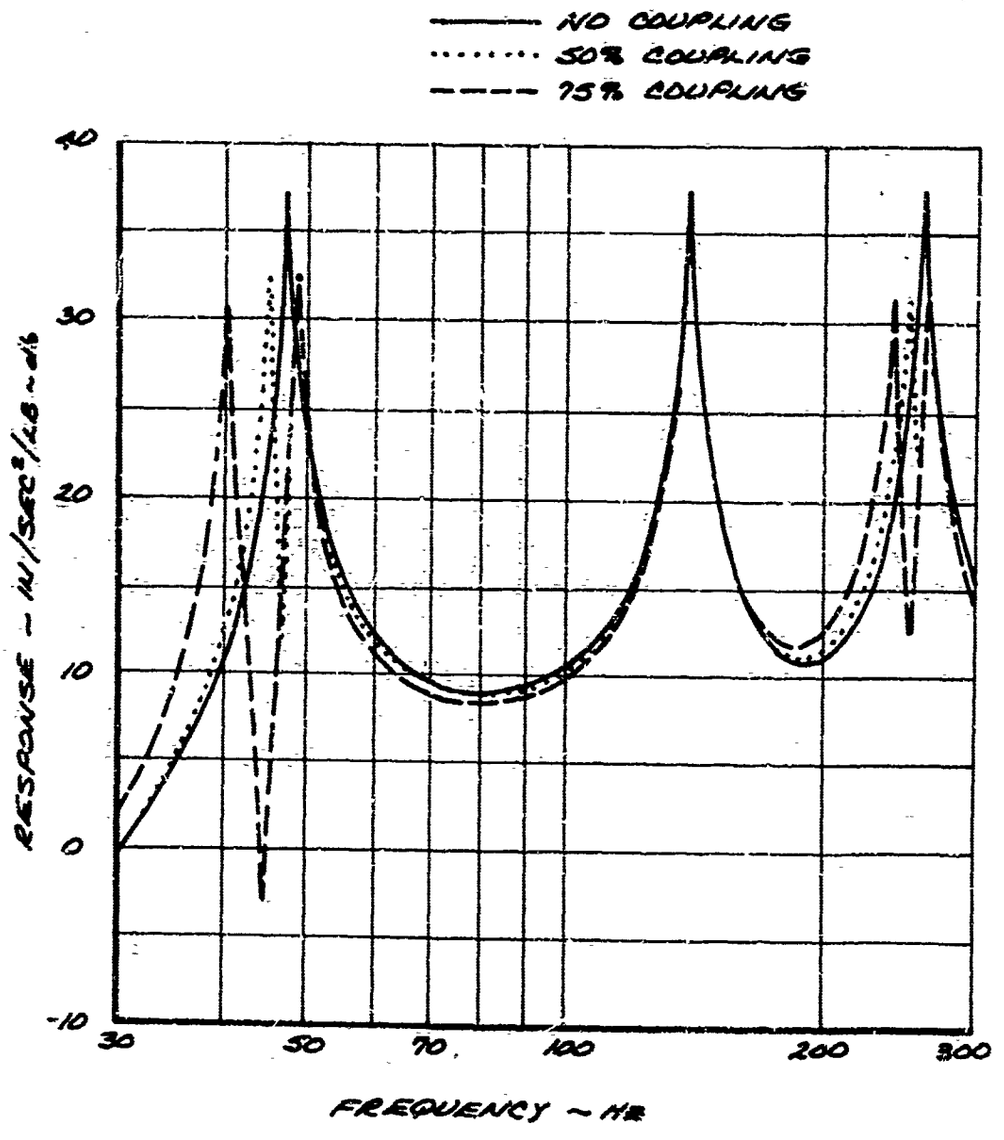

FIGURE 5-14

"NOMINAL" UNIFORM BEAM
"MODERATE" JOINT AT 50% SPAN
EFFECT OF JOINT SPRING COUPLING
MAGNITUDE ON RESPONSE
AT 0% SPAN FOR EXCITATION AT 100% SPAN

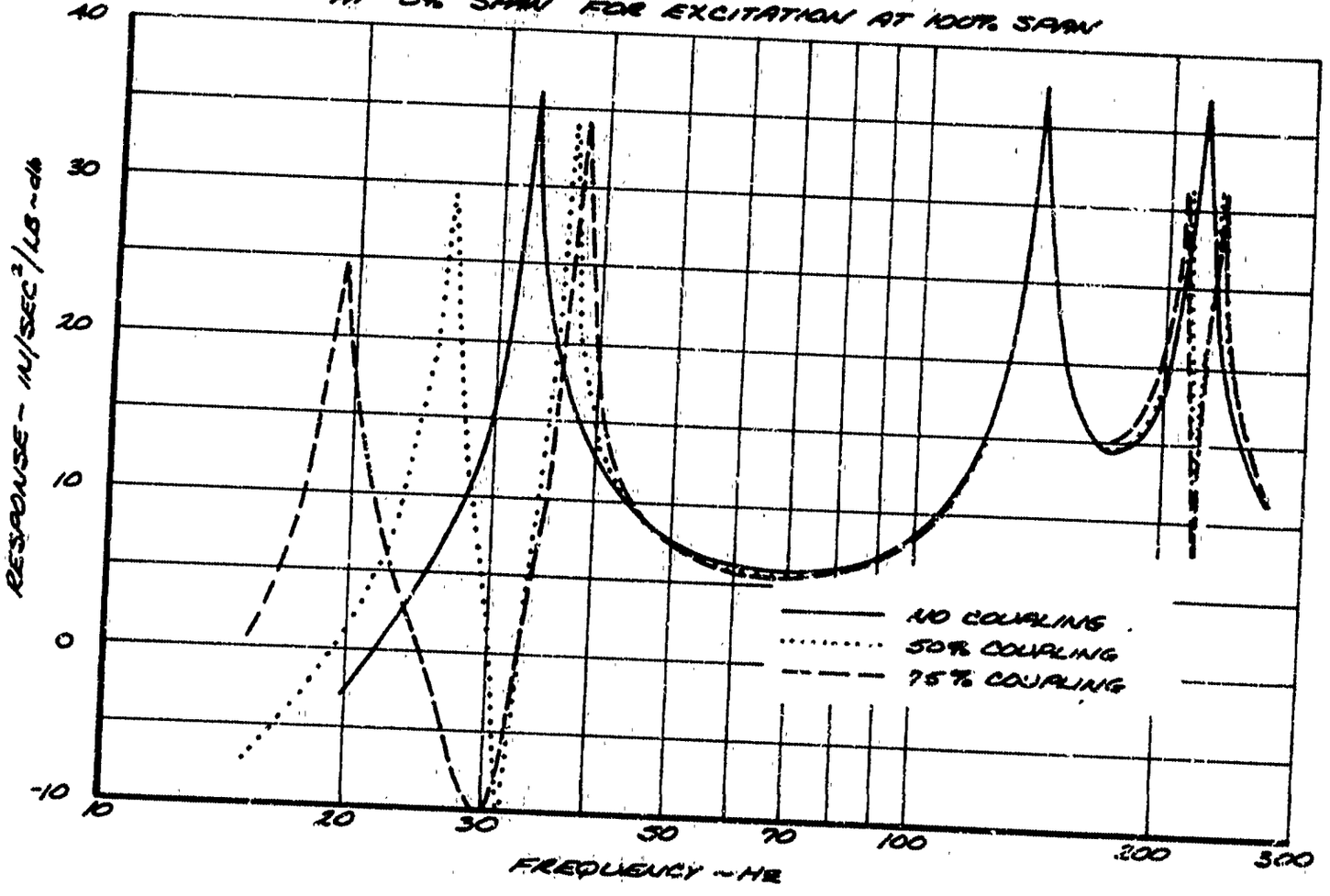

FIGURE 5-15
"NOMINAL" UNIFORM BEAM
TOTAL FIRST MODE FREQUENCY SHIFT
VS. JOINT SPRING COUPLING
(MIDSPAN JOINT ~ 0.5L)

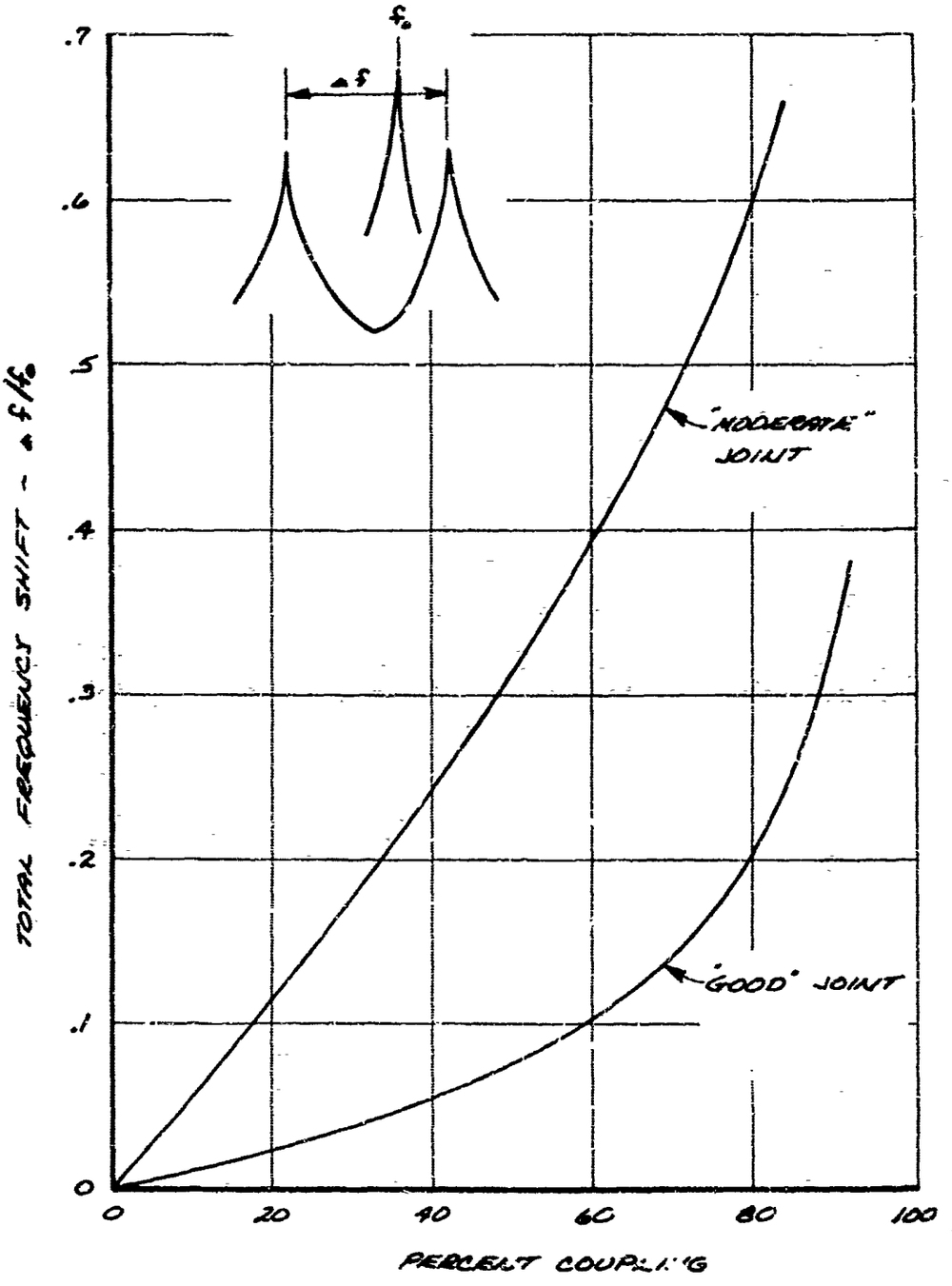

FIGURE 3-16

COMPUTED FREQUENCY RESPONSE
AT THE MISSILE NOSE
DUE TO FORCE EXCITATION
AT THE TAIL STATION

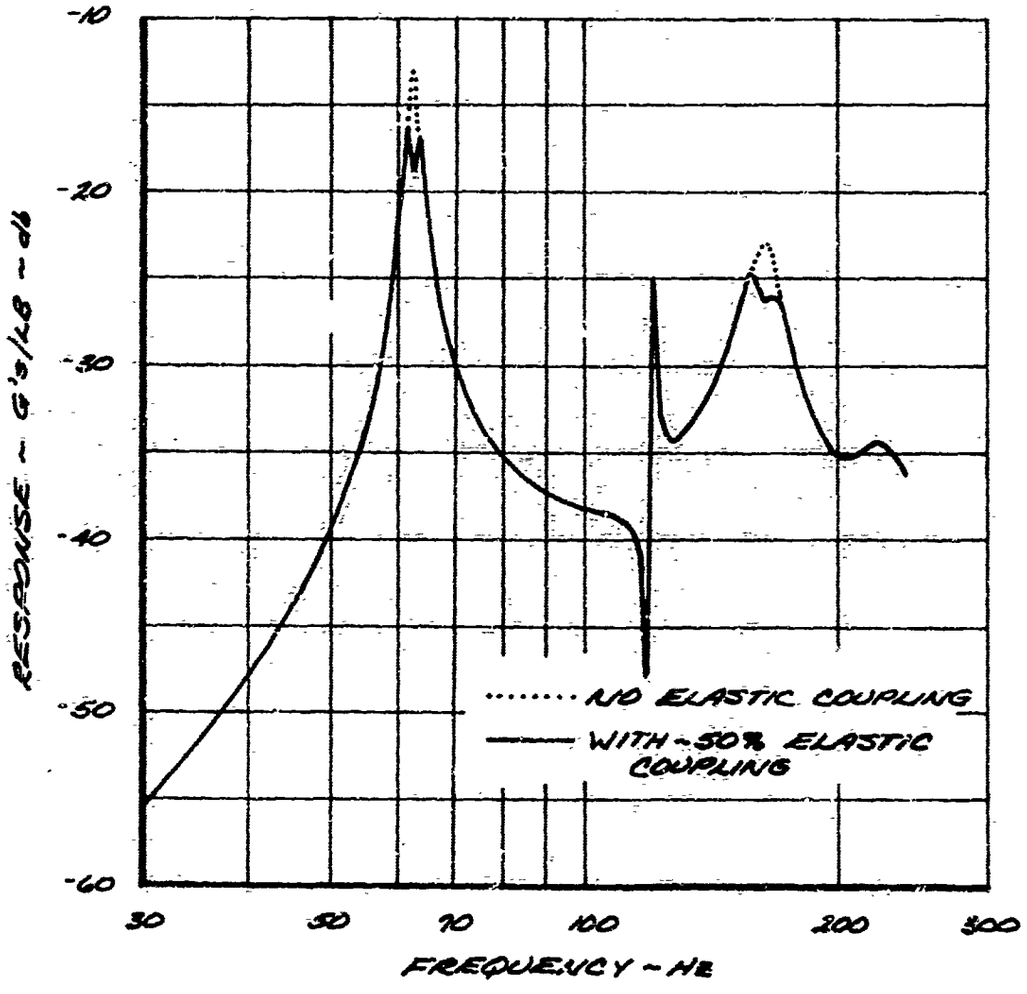

Table 5-1
FIRST MODE FREQUENCY RATIO VARIATION
WITH JOINT LOCATION AND RATING

NASA RATING	K_R	Joint Location				
		0.1	0.2	0.3	0.4	0.5
	1.0	1.0	1.0	1.0	1.0	1.0
E	.883	1.0	.999	.997	.994	.993
	.699	1.0	.997	.990	.983	.979
G	.429	.999	.990	.970	.949	.940
	.189	.997	.969	.909	.857	.838
M	.0698	.991	.904	.768	.682	.655
	.0227	.970	.730	.541	.457	.433
L	.00745	.891	.490	.337	.279	.263
	.00232	.648	.289	.194	.159	.150

Table 5-2
MODAL FREQUENCY RATIO VARIATION
WITH MIDSPAN JOINT RATING

NASA RATING	Elc. L	Freq. Ratio		
		1st Mode	2nd Mode	3rd Mode
	0	1.0	1.0	1.0
E	0.005108	.993		.995
	0.01648	.979		.985
G	0.05108	.940		.955
	0.1648	.838		.892
M	0.5108	.655		.816
	1.648	.433		.763
L	5.108	.263		.741
	16.48	.150	1.0	.732

Table 5-3
MODAL FREQUENCY RATIO VARIATION
WITH "MODERATE" JOINT LOCATION

Joint Location	Freq. Ratio		
	1st Mode	2nd Mode	3rd Mode
.1	.991	.942	.833
.2	.904	.750	.794
.3	.768	.764	.937
.4	.682	.888	.955
.5	.655	1.0	.816

Table 5-4
UNIFORM BEAM WITH MULTIPLE JOINTS
CALCULATED AND ESTIMATED FREQUENCY RATIOS

Joint Rating	Joint Locations % Span	Frequency Ratio - 1st Mode		
		Calculated	Estimated	% Error
Good	10,20,30,40,50	.869	.865	0.5
Good	20,40	.940	.940	~
Moderate	10,20,30,40,50	.478	.480	0.4
Loose	10,20,30,40,50	.169	.167	1.2
Loose	10, 30, 50	.219	.215	1.8
Loose	20,40	.255	.251	1.6

Section 6.0

EXTRACTION OF JOINT COMPLIANCES FROM MEASURED MODAL DATA

Computed modes and frequencies of a tactical missile containing joints often will vary considerably from experimental mode shapes and frequencies. Since the mass and basic stiffness properties of the missile are known with a good degree of certainty, the values used for the joint compliances must account for the discrepancies in most cases. If there are multiple joints and several modes involved, the task of iteratively adjusting compliance values by hand to produce matching results becomes laborious, time consuming, and often very frustrating. Consequently, it is desirable to automate a method that will extract the joint compliances in a manner such that theoretical results match experimental results as closely as possible. The following section of this report presents the equations, evaluation, and some limitations of an initial effort to develop such a capability.

6.1 METHOD OF ANALYSIS

A method currently being used to compute optimum trajectories is applicable to the problem (References 2 and 3). It is called the method of steepest ascent, and it uses the steepest linear slope in a function space to proceed towards the minimum (or maximum) of some computed quantity. As applied to the problem of adjusting joint compliances, it searches for a distribution of control variables (joint compliances) and unspecified initial conditions (modal slopes) that will give an optimum for a quantity (quadratic function of mode shape errors) that is a function of the integrated state variables (modal deflections) subject to constraints (boundary conditions).

In general form, the matrix differential equations to be solved for beam modal deflections, internal forces, constraint quantities, and optimizing quantity, can be expressed as

$$\{w_i'\} = \{G(w_i, \alpha_i, x)\} = [A_{ij}(w_i, \alpha_i, x)]\{w_i\} + \{F_i(\alpha_i, x)\}$$

where

$\{w_i\}$ = computed (state) quantities

$(\ )'$ = differentiation with respect to X

$\{\alpha_i\}$ = control variables (quantities to be adjusted)

$[A_{ij}], \{F_i\}$ = coefficient matrices

x = coordinate along the beam

If estimates are made for the initial values of the state variables (W) and for values of the distributed control variables (α), the equations can be integrated numerically along the length of the missile. In general the boundary conditions will not be met and the error (optimization) function will not be a minimum. It is required to alter the control variables (α), in a method that tends to satisfy the desired end results.

For small changes in α, the linear changes from the previous solution can be described by the linear perturbation equations

$$\{\delta W_i'\} = [G_{ij}(W_i, \alpha_i, x)]\{\delta W_i\} + [f_{ij}(W_i, \alpha_i, x)]\{\delta \alpha_i\}$$

where

$$[B_{ij}] = \frac{\partial [G_{ij}]}{\partial \{W_i\}}$$

$$[f_{ij}] = \frac{\partial [G_{ij}]}{\partial \{\alpha_i\}}$$

The set of equations adjoint to the perturbation equations are defined as

$$\{\lambda_i'\} = -[B_{ij}]^* \{\lambda_i\}$$

$\{\lambda_i\}$ = adjoint solutions

$[\ ]^*$ = matrix transpose

These adjoint solutions are related to the perturbation solutions by the relationship

$$(L\lambda_i]\{\delta W_i\})_{x=\ell} = \int_0^{\ell} (L\lambda_i][f_{ij}]\{\delta \alpha_i\})\,dx + (L\lambda_i]\{\delta W_i\})_{x=0}$$

where

$x = 0, \ell$ = beginning and end of the missile.

This relationship proves very useful for properly selected solutions of the adjoint equations. Let the quantity of interest at ℓ be designated $\Phi(W(\ell))$. If we define the value of $\lambda_i(\ell)$ as $\frac{\partial \Phi}{\partial (W_i(\ell))}$, the

adjoint equations can be integrated backward from $x = \ell$ to $x = 0$ to give solutions for $\{\lambda_i\}$. The left hand side of the equation relating the perturbations to the adjoint solution can be seen to equal the perturbation of Φ for this set of λ's. Looking at the right hand side of the equation, the λ's are influence coefficients that relate changes in the state variables at $x = 0$ and control variables to changes in Φ. The method of steepest ascent uses this relationship to choose the manner to vary α_i and $w_i(0)$ in order to proceed rapidly to the desired value of Φ.

The particular steepest ascent method followed is the second method outlined in Reference 3. Dropping matrix notation, a generalized weighted mean square "step size" is defined as

$$(dP)^2 = \Delta\mathbf{w}^* \mathbf{Z}^* \mathbf{Z}\, \Delta\mathbf{w} + \int_0^\ell (\delta\alpha^* U^* U \delta\alpha)\, dx$$

where

dP	=	step size
$\Delta\mathbf{w}$	=	a column of changes to $w_i(0)$ (only involves those that <u>are</u> variable)
$\delta\alpha$	=	running change in the control variables
$\mathbf{Z}, U$	=	weighting function matrices
$(\ )^*$	=	matrix transpose

The desired amount of change to the payoff quantity ($\Delta\Phi$) and the necessary changes to meet the constraints ($\Delta\Omega$) are specified and the $(dP)^2$ necessary to accomplish this is minimized. This results in the following

$$\Delta\mathbf{w} = \mathbf{Z}^{-1} \mathbf{Z}^{-1} A_{\phi/\alpha}\, \Gamma_{\phi/\alpha}^{-1}\, \widetilde{\Delta\Omega}$$

$$\delta\alpha = U^{-1} U^{-1} f^* \lambda_{\phi/\alpha}\, \Gamma_{\phi/\alpha}^{-1}\, \widetilde{\Delta\Omega}$$

where

$$\Gamma_{\phi/\alpha} = A_{\phi/\alpha}^*\, \mathbf{Z}^{-1} \mathbf{Z}^{-1} A_{\phi/\alpha} + \int_0^\ell (f \lambda_{\phi/\alpha}^*\, U^{-1} U^{-1} f^* \lambda_{\phi/\alpha})\, dx$$

$$\widetilde{\Delta\Omega} = \left\{ -\frac{\Delta\Phi}{\Delta\Omega} \right\}$$

$\lambda_{\phi/n} = [\lambda_\phi \mid \lambda_n]$ (influence functions corresponding to changes in ϕ and to the constraints, n_i)

$A_{\phi/n} = [\lambda_\phi \mid \lambda_n]_{x=0}$ (only those corresponding to $W_i(0)$ that are variable)

$f = \frac{\partial G}{\partial \alpha}$ (previously defined)

The Δ's are used to alter the initial conditions on the state variables, (W_i), and $\delta\alpha$ used to alter the control variables along the missile. The differential equations are then integrated again to give a new solution for $W_i(x)$ and the process repeated until a minimum is reached for ϕ, the payoff quantity. If the differential equations, ϕ, and n are all linear with respect to the state variables it only takes one pass to reach the answer. (In such a case, ϕ is actually a constraint, not an optimizing function).

This general method was applied to the problem of finding joint compliance values from beam bending mode data. The state variables have the form

$$\left\{ \begin{array}{c} W_i' \\ \hline W_i^2 \\ \hline \vdots \\ \hline W_i^n \end{array} \right\}$$

where each submatrix corresponds to an input mode. For each mode or submatrix we have

$$\{W_i\}^n = \left\{ \begin{array}{ll} W\sim & \text{Deflection} \\ W'\sim & \text{Slope} \\ BM\sim & \text{Bending Moment} \\ S\sim & \text{Shear} \\ \phi\sim & \text{nth mode payoff quantity} \\ \gamma\sim & \text{Mass coupling to translation} \\ \rho\sim & \text{Mass coupling to pitch} \end{array} \right\}$$

The only type of control variable that we have is joint compliance, consequently

$$\alpha = C_B, \text{ a scalar}$$

where C_B = Bending compliance

Two different sets of differential equations were used. The first uses input mode shapes to describe the loadings on the missile, and the second uses the computed shapes. In both cases a lumped mass model with constant stiffness between masses was used. The lumped masses and the concentrated joint compliances result in discontinuities in some of the differential equations, but this does not cause a problem with numerical integration.

For the first set of equations, we have (for each mode)

$$[\rho_{ij}]^n = \begin{bmatrix} 0 & 1.0 & 0 & 0 & 0 & 0 & 0 \\ 0 & 0 & -\frac{1}{EI} - C_{B_K} & 0 & 0 & 0 & 0 \\ 0 & 0 & 0 & -1.0 & 0 & 0 & 0 \\ 0 & 0 & 0 & 0 & 0 & 0 & 0 \\ (w_i - 2\phi_n)_K & 0 & 0 & 0 & 0 & 0 & 0 \\ m_K & 0 & 0 & 0 & 0 & 0 & 0 \\ (mx)_K & 0 & 0 & 0 & 0 & 0 & 0 \end{bmatrix}$$

$$\{F_i\}^n = \begin{Bmatrix} 0 \\ 0 \\ 0 \\ -(m\phi_n)_k \omega_n^2 \\ (\phi_n)_k^2 \\ 0 \\ 0 \end{Bmatrix}$$

where

EI = bending stiffness

ϕ_n = nth mode shape

$(\ )_k$ = quantity at a station k

m = mass

$\bar{x}$ = distance from center of gravity

ω_n = frequency of nth mode

The second set of equations varies from the first only in that

$$(A_{41})^n = -m_k \omega_n^2$$

and

$$(F_4)^n = 0.$$

The boundary values W_i for the initial pass are

$$\{W_i\}^n_{x=0} = \begin{Bmatrix} \phi_n \\ \phi_n' \\ 0 \\ 0 \\ 0 \\ 0 \\ 0 \end{Bmatrix}_{x=0}$$

The only boundary values that are allowed to vary are the ϕ_n''s which are adjusted by Δ in subsequent iterations. The total payoff quantity is taken to be

$$\Phi = \sum_n (\Phi_n)_{x=\ell}$$

and the constraints (one for each mode) are

$$\Omega_n = (T_n + P_n)_{x=\ell} = 0.$$

The adjoint equations are integrated backwards to obtain the influence function, once for those related to the payoff quantity and once for each of the constraints. The initial conditions for those integrations are defined by

$$\{\lambda_i(\ell)\}^{\Phi} = \frac{\partial \Phi}{\partial(W_i(\ell))}$$

for the payoff function and

$$\{\lambda_i(\ell)\}^{\Omega_n} = \frac{\partial \Omega_n}{\partial(W_i(\ell))}$$

for each of the constraints. The influence functions are then used to calculate changes to the initial deflection slopes and to the bending compliances in a manner that will reduce Φ and tend to match the constraints. The process is repeated until Φ is minimized to within a specified tolerance.

Both formulations of the deflection equations were used in demonstrating the feasibility of the overall method. The first formulation has the advantage that the input mode shapes are reflected in the beam loadings as well as the payoff quantity. It was used to make initial alterations to the compliances. In the second formulation the input mode shapes appear only in the payoff quantity. The deflections are computed in the same manner as would be done in a beam modal analysis and consequently represent computed modes. In both cases the measured frequencies are used and are considered not to be variable. The frequencies could be treated as control variables with a relatively simple altera - tion.

6.2 TEST CASE

A test case was developed for the purpose of exercising and checking out the joint compliance extraction technique. An analytical "test" case was developed which was free of experimental error. The figure and table below show this test case which consists of an idealized missile with four uniform and one nonuniform beam sections connected by four local flexural springs representing four joints.

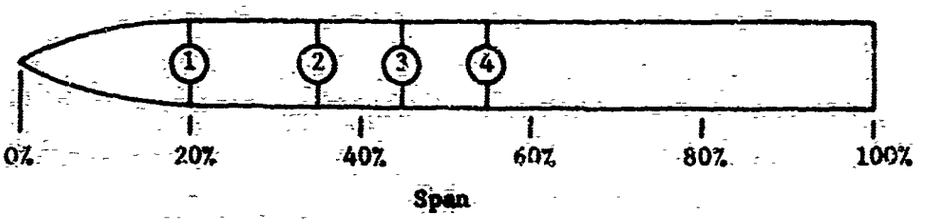

Joint Number	Span Location - %	Joint Compliance x 10^8 Rad/In-Lb	NASA Rating
1	20	1.5	G-M
2	35	0.1	E-G
3	45	0.31	G
4	55	1.0	M-G

Figure 6-1 shows the weight and stiffness distributions selected for the test case. A lumped parameter representation as discussed in Section 5.1 was used to compute the first four bending mode shapes and natural frequencies for use in the development of the compliance extraction technique. The test model natural frequencies with and without the four joints are:

Natural Frequencies With Joints (Hz)	Natural Frequencies Witout Joints (Hz)	Frequency Ratio
40.3	50.4	.800
104.5	118.3	.883
196.1	231.5	.847
313.3	389.9	.804

It can be seen, from the frequency changes shown above, that the joints selected for the test case have a significant influence on the beam bending modes and are reasonably typical of actual tactical missiles.

The first four bending mode shapes and frequencies were utilized in the joint compliance extraction computer program. The stiffness and weight distributions were assumed to be known correctly. Erroneous initial values were assumed for the four joint compliances, with the maximum error being a factor of ten from the actual compliance values. The only unknowns were the four joint compliance values. Figure 6-2 shows the error in the originally assumed compliance of the four joints, and the error which existed after each of the six computational iterations. The first three iterations used the input mode shapes in solving for the four joint compliances. The second three iterations used the mode shapes generated by the compliance extraction computer program in solving for the compliance values. The first procedure produces better results than the second procedure for this particular test case because a perfect set of input mode shapes are being used. In general this will not be the case due to the experimental error in the mode shapes. As shown, the convergence of the solution for the joint compliance values is very rapid. Only one iteration is required for the program to converge on the solution. The computed joint compliance with the largest error is that of the second joint which also has the smallest compliance of the four joints.

6.3 SENSITIVITY ANALYSIS

The joint compliance extraction program is seen to be functioning properly for the test case discussed above. However, real test data will vary from this ideal test case because of the presence of experimental error in the data. Errors will be present in both the measured mode shapes and frequencies. The sensitivities for the joint compliance of the test model to certain types of errors in the input data have been investigated.

Table 6-1 shows the effects of input modal frequency variations on the four joint compliances of the test model. The frequencies of all four modes were varied simultaneously by amounts of plus 1%, plus 2%, minus 1%, and minus 2%. The four joint compliances have a moderate

dependence on the input frequencies.

The sensitivities of the four joint compliances to the number of input modes are shown in Table 6-2. At the present time, the results are highly dependent on the number of measured modes. The zero values in Table 6-2 are the results of the program trying to assume a negative value for these particular compliances. Four joint compliances are present in the test case, and four input modes are required to produce good results. If the number of modes considered is less than the number of joints, the technique does not converge to a unique value for the joint compliances. The table below shows the compliance results obtained considering only one bending mode with two different sets of initial compliance estimates.

Joint No.	C/C Actual	
	Program Input	Program Solution
1	.1	.64
2	5.	0
3	10.	3.7
4	.1	.48
1	.67	.82
2	2.0	3.24
3	.65	.5
4	2.0	1.11

It is seen that the converged solution for the joint compliance is dependent upon the initial value used as an estimate during the first iteration when the number of modes used is less than the number of unknown joint compliances.

6.4 CURRENT RESTRICTIONS

The joint compliance extraction technique currently has several restrictions. One of the restrictions is that the number of bending modes used must equal or exceed the number of unknown joints to obtain accurate results. Also, only bending cases with free-free boundary conditions can be run using the joint compliance extraction computer program, and a method of handling appendages has not yet been devised.

The feasibility of the joint compliance extraction technique has been demonstrated. Several limitations exist at the present time, but it is felt that these restrictions can be overcome. Note has been taken of a promising technique for handling the type of problem being considered here. This technique has recently been developed by Hall,

Calkins, and Sholar of the McDonnell Douglas Astronautics Company, Huntington Beach, California (Reference 4). It is felt that this method can be modified and applied to the problem of extracting joint compliances from measured tactical missile elastic mode data.

FIGURE 6-1

JOINT COMPLIANCE EXTRACTION TECHNIQUE
TEST CASE STIFFNESS AND WEIGHT DISTRIBUTIONS

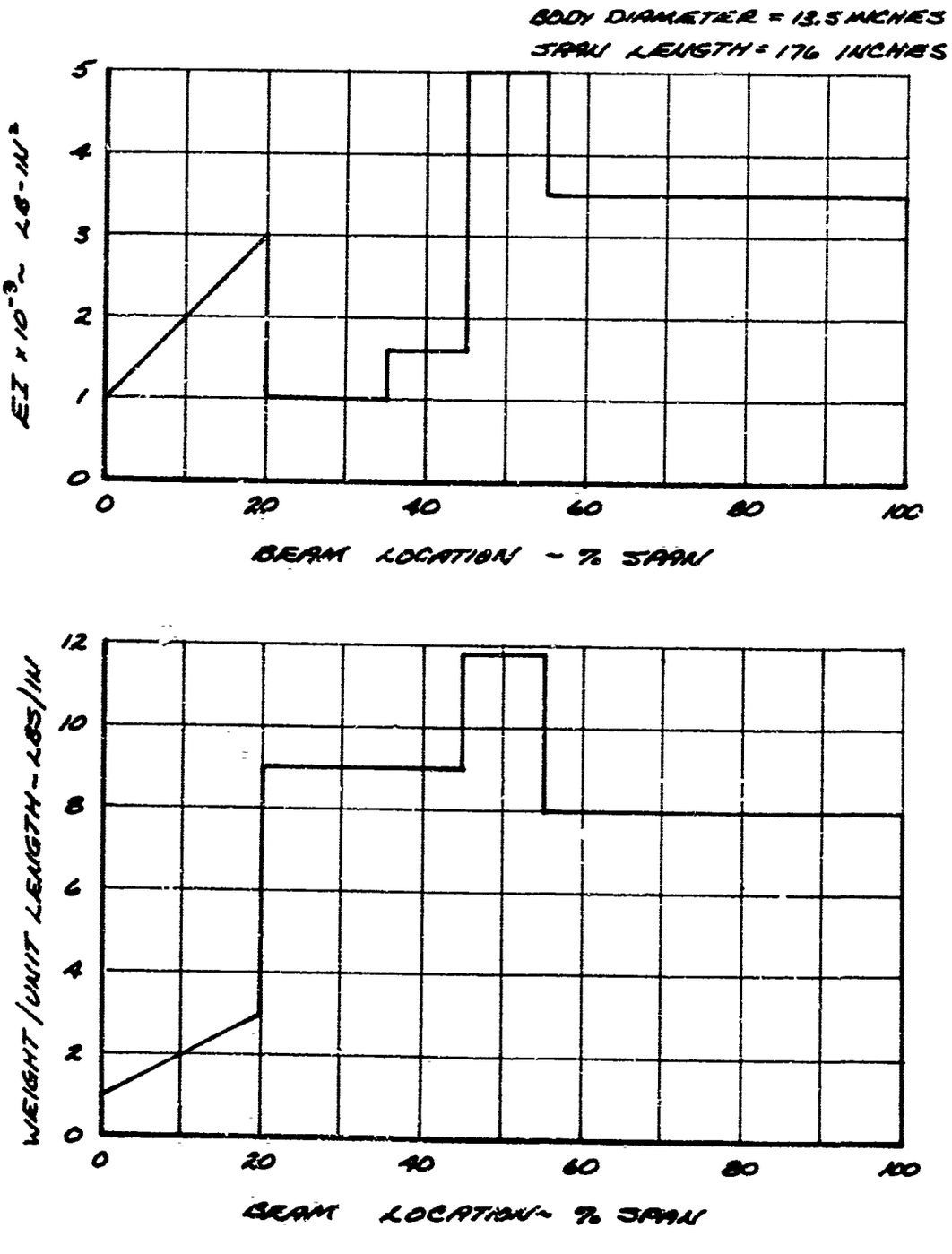

FIGURE 6-2

JOINT COMPLIANCE EXTRACTION TECHNIQUE
CONVERGENCE RESULTS

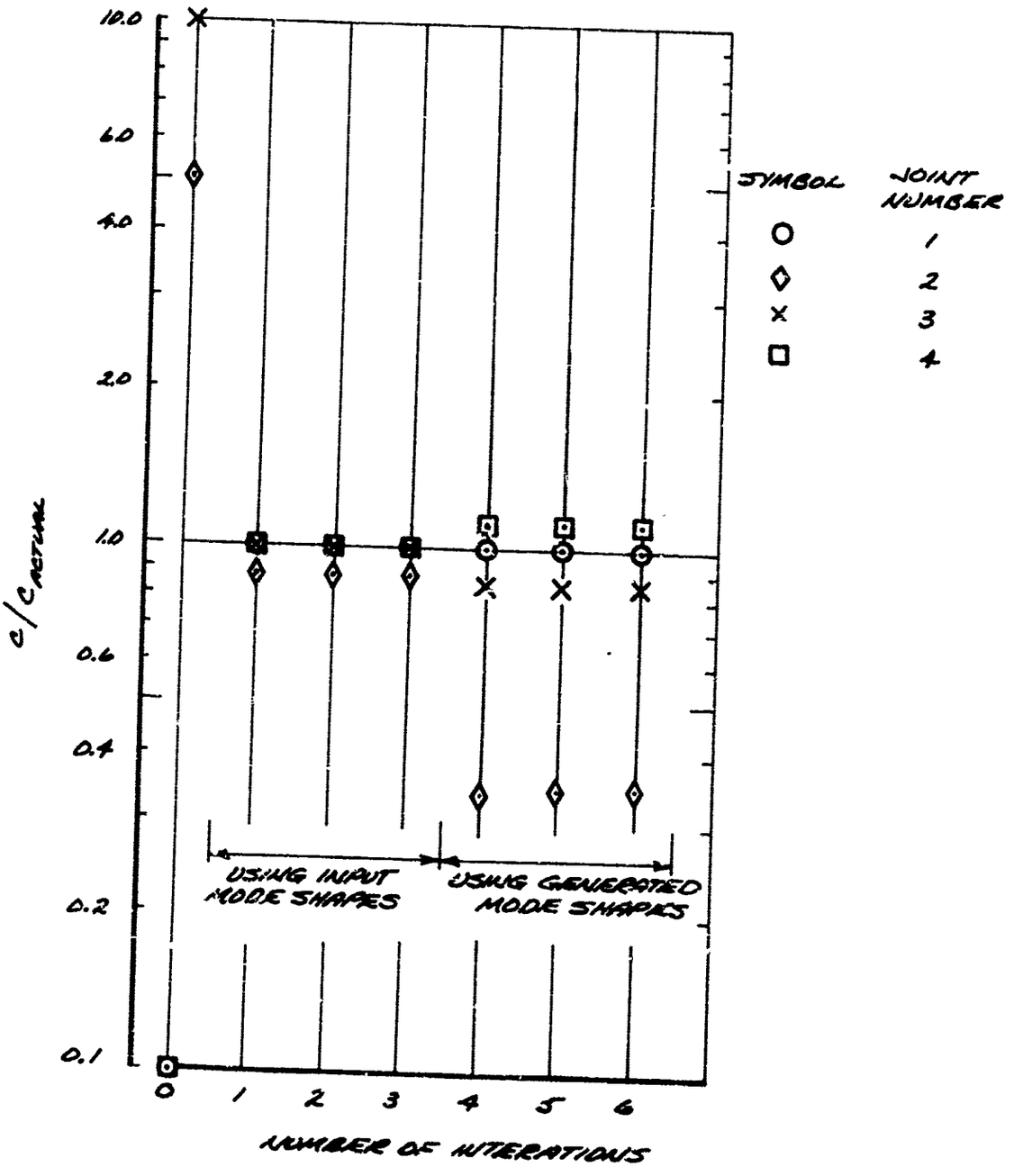

Table 6-1

SENSITIVITY OF JOINT COMPLIANCE
TO INPUT FREQUENCY ERRORS

Joint Number	Modal Frequency Variations	C/C Actual	
		Using Generated Modes	Initial Estimate
1	+2%	.888	.1
	+1%	.957	
	0	.998	
	-1%	1.06	
	-2%	1.11	
2	+2%	.348	5.
	+1%	.312	
	0	.356	
	-1%	.929	
	-2%	1.26	
3	+2%	0	10.
	+1%	1.24	
	0	.866	
	-1%	1.31	
	-2%	1.33	
4	+2%	1.63	.1
	+1%	.828	
	0	1.13	
	-1%	.946	
	-2%	1.01	

Table 6-2

SENSITIVITY OF JOINT COMPLIANCE
TO NUMBER OF MODES USED

No. of Modes Used	Joint Number	C/C Actual
1	1	.644
	2	0
	3	3.71
	4	.477
2	1	.9
	2	0
	3	5.97
	4	0
3	1	1.02
	2	0
	3	3.32
	4	.425
4	1	1.0
	2	.356
	3	.864
	4	1.13

Section 7.0

EXPERIMENTAL VERIFICATION

A limited test program using highly simplified joint test models has been conducted to illustrate and verify some of the results of the parametric analyses. A principal source of airframe joint compliance is believed to result from strain field disturbances. Almost all joints by definition represent a significant interruption and alteration of the load paths between sections. In many cases, the number of load paths is equivalent to the number of principal fasteners. The conceptual joint model discussed in Section 5.2.2 provides a useful design basis for representing both axially symmetric and non-axially symmetric joint test specimens. Physical property control is a critical requirement in developing simple inexpensive models of airframe joints. The design approach taken and described in this section has provided a total of 12 test specimens in three control groups, having physical properties easily defined and controlled, and requiring only very simple machining.

7.1 TEST MODEL

The joint simulation models consist of aluminum tubing with circumferential slots cut out at the midspan of the beams. These slots produce local strain field disturbances under loading which are intended to be analogous to those occurring in a missile airframe joint. Slot geometries were selected to provide reductions in local section properties (EI) ranging from 60 to 97.5 percent of the basic cross section. The net compliance produced by these slots is shown to be significantly larger than that predicted by considering only the area reduction over the length of the slots. The strain field disturbance is propagated a significant distance from the sectional discontinuity. In deriving an equivalent beam representation for the test models, the EI distribution in the vicinity of the joint has to be reduced in addition to the EI reduction at the joint, or a local joint compliance must be introduced at the joint in order to predict proper mode shape and frequency data.

The joint simulation models are described in Figure 7-1. Model number 1 is a uniform tube without a joint, the standard or reference for this set of models. Models 2 thru 5 have six segments of material equally spaced around the circumference. Model numbers 6 thru 10 have three equally spaced segments of material remaining from the slot cuts. Model numbers 11 and 12 are designed to be non-axially symmetric and produce elastic coupling across the joint by the mechanism discussed in Section 5.2. The segment spacing in models 11 and 12 ($\theta = 40°, 20°$) represents an estimated elastic coupling of 45 and 85 percent respectively. When excited in either of the two planes of symmetry, the response characteristics will show only one peak in the vicinity of the first mode. When

tested in any other plane, a double peaked response will result. The plane with maximum cross plane coupling will result at 45 degrees from the planes of symmetry.

7.2 TEST SETUP

The vibration testing of the joint simulation test models was conducted with the models suspended by soft springs at the nodal points of the first bending mode as shown in Figure 7-2. This figure also shows some of the equipment used during the test. A miniature accelerometer, shown mounted on the test specimen, and a Bentley distance detector were used to make response measurements on the test models. The accelerometer and probe outputs were fed through a high pass filter to an oscilloscope where the wave form was monitored and to a counter to measure the excitation frequency. An oscillator and power amplifier were used to drive an induction shaker which excited the test models in the horizontal plane.

The resonant frequencies of the joint simulation models were measured in two perpendicular planes for the symmetric models to verify that the variations in frequency due to manufacturing and measurement tolerances were small. The resonant frequencies of model number 11 and 12 were measured in the two planes of symmetry, and at angles of thirty and forty-five degrees from the planes of symmetry.

7.3 RESULTS

The results of the vibration testing of the joint simulation models are presented in Table 7-1. With the exception of test model number 10, the symmetric joint simulation models have resonant frequencies which are very close to each other for the two perpendicular (A and B) planes. With specimen number 10, a double peaked first mode was observed. Obviously, the two perpendicular planes tested were not principal stiffness planes, since a double peaked response was observed. The magnitude of the input force for these tests was so small that response amplitude measurements could not be made off resonance. At resonance, very little damping existed, and the peak response was very large.

Test specimens 11 and 12 were designed to produce the double peaked first mode response characteristics discussed in Section 5.2. Table 7-1 shows the stiffness ratios in the two principal stiffness planes and the resulting resonant frequencies. The first mode double peaks are very widely separated (similar to the type of response shown in Figure 5-16) due to the differences in stiffness between the two planes.

The effective compliance produced by the slot discontinuities in the test specimens can be represented by either of the joint models described in Section 4.1. Table 7-2A lists flexural and reduced stiff-

ness model equivalences for each test specimen based on matching the measured first mode frequencies. In the first case, the effective length of the stiffness discontinuity induced by the slot is determined, and in the second case, the rotational compliance of the equivalent joint spring is determined. Table 7-2B shows the relationship between test specimen effective compliance and the joint "rating" system previously discussed in Section 4.2.

A plot of the effective length of the stiffness discontinuity expressed in test specimen body diameters is shown in Figure 7-3. As might be expected, the effective length decreases as the number of slots (load paths) increase. It is of interest to note that for the three segment models, the effective length ranges from about 0.2 to 0.7 diameters with the average of approximately 0.5 falling in the vicinity of what would be considered a good to moderate joint.

This observation is perhaps better illustrated in Figure 7-4, which presents test specimen geometric stiffness ratio versus frequency ratio. The numbers adjacent to the data points identify the test specimens. The 6-segment models are clearly less sensitive than the 3-segment models to stiffness discontinuities. The dashed curve in this figure represents for comparison purposes the predicted relationship between frequency ratio and joint stiffness ratio for a uniform beam with a joint at the mid-span. This curve is based on the test specimen fineness ratio (L/D) of 15 and a reference length of 0.5 body diameters for the assumed span of the local stiffness reduction. Test points close to the dashed curve imply effective lengths in stiffness loss close to the 0.5 diameter assumption. The branch curve passing through point 8 connecting data for test specimens 11 and 12 reveals the dramatic influence of unsymmetric segment spacing. In this instance, the segment areas for the three specimens (8, 11, 12) are the same and it is interesting to note that the variation with segment spacing approaches the dashed curve quite closely.

7.4 CORRELATION ANALYSIS

In an effort to obtain a relatively accurate analytic determination of the equivalent beam stiffness for comparison with test results a relatively detailed finite element analysis was undertaken for one test specimen - number 10. This analysis was performed using the STARDYNE computer program, Reference 8.

The beam with a concentric circular cross section is interpreted as a cylindrical shell with a length equal to four diameters. The notching is placed at the mid-section. The ends of the shell are given a stress distribution which varies linearly in one direction and which results in a uniform moment distribution along the axis of the associated beam. The shell and loading are shown in Figure 7-5a.

Due to symmetry only one fourth of the geometric configuration need be modeled as shown in Figure 7-5b. The finite element analysis used described this portion of the geometric configuration with a set of triangular finite elements. This element accounts for both shell membrane and bending stresses. The distribution of finite elements used is shown in Figure 7-6. This figure depicts the element distribution for the unfolded shell segment so that it can be placed on a plane.

The model used has 480 triangular elements and 275 node points. Since there are 6 degrees of freedom for each node point the model has 1650 degrees of freedom. The application of boundary conditions for the quarter segment requires the constraining of 108 degrees of freedom. Thus the model has 1542 unconstrained degrees of freedom.

The analysis yielded a set of node displacements and rotations. This in turn was used to determine an equivalent compliance value for a spring placed at the notched section. The value of the computed compliance is $7.03 \times (10)^{-6}$ rad/in-lb. The measured frequency for model number 10 implies a compliance value of $7.6(10)^{-6}$ rad/in-lb. The finite element analysis compliance value agrees with the experimental value within 7.5 per cent.

FIGURE 7-1

JOINT SIMULATION MODELS

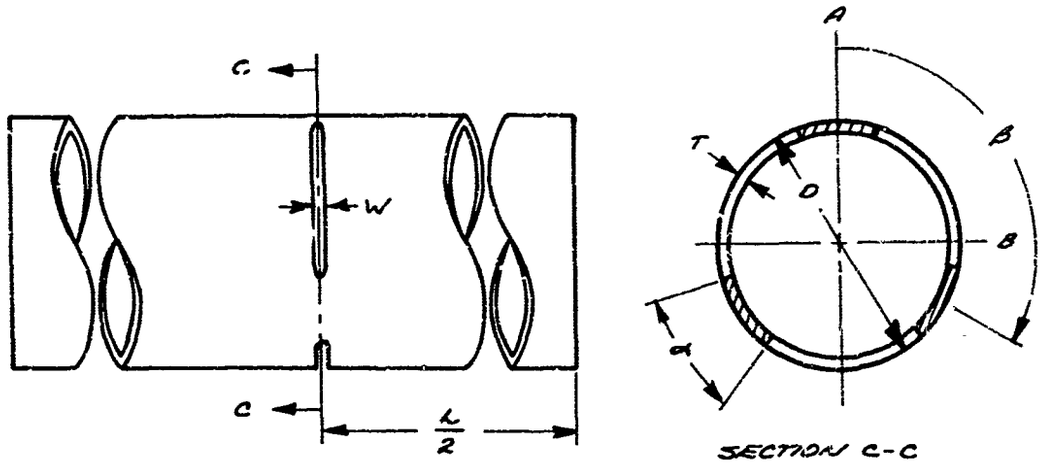

MODEL NUMBER	NUMBER OF SEGMENTS	SEGMENT SPACING (β)	SEGMENT WIDTH (α)	I_e
1	1	—	360°	1.0
2	6	0°, 60°, 120°, 180°, 240°, 300°	24°	.40
3	"	"	12°	.20
4	"	"	6°	.10
5	"	"	3°	.05
6	3	0°, 120°, 240°	48°	.40
7	"	"	24°	.20
8	"	"	12°	.10
9	"	"	6°	.05
10	"	"	3°	.025
11	3	0°, 140°, 220°	12°	.145/.055
12	"	0°, 160°, 200°	"	.184/.016

DIMENSIONS:
W = .065 INCH
L = 30.0 INCH
D = 2.00 INCH
T = .065 INCH

MATERIAL:
6061-T6 ALUMINUM

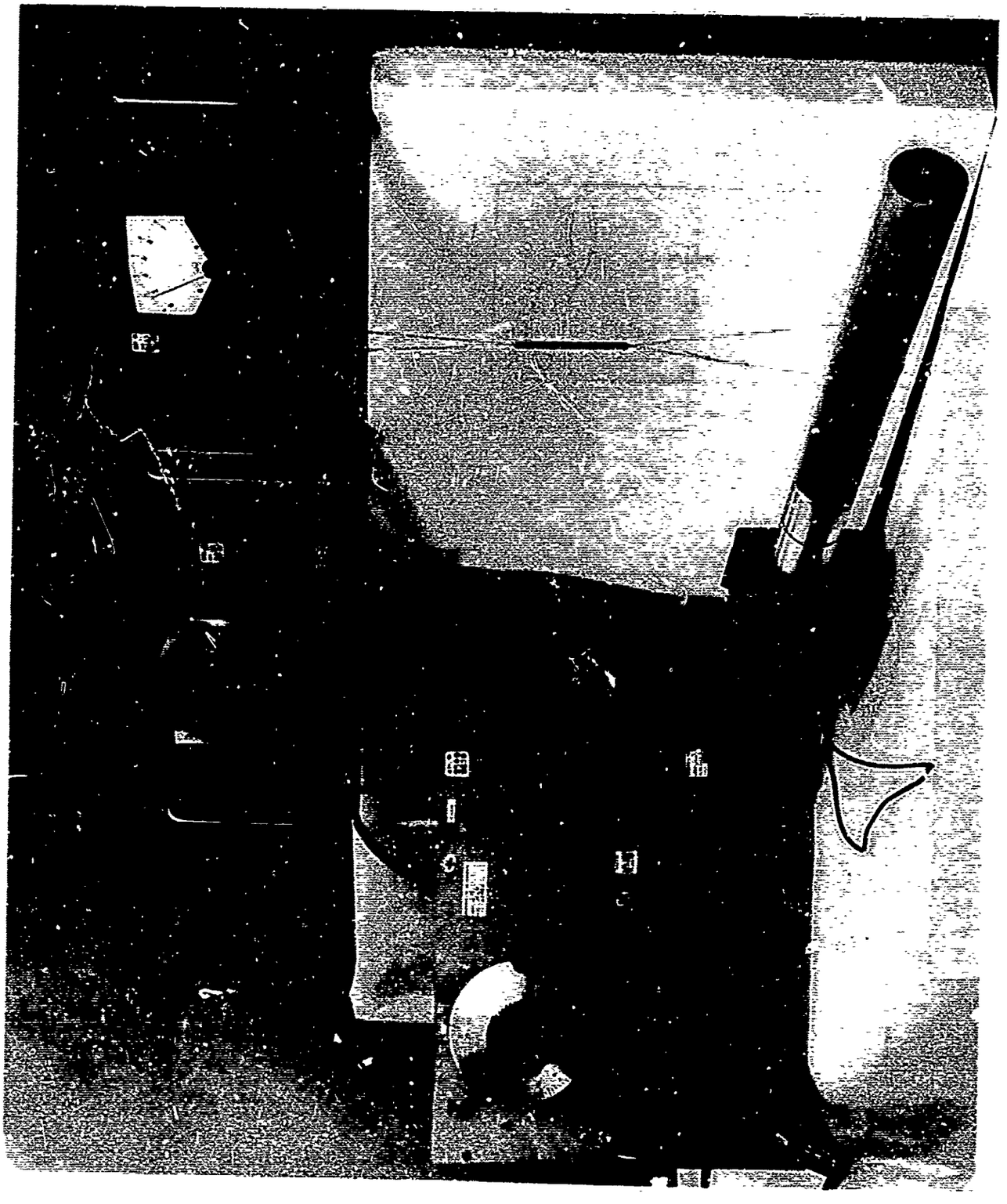

Figure 7-2 Test Setup of Joint Simulation Models

FIGURE 7-3

EFFECTIVE LENGTH OF STIFFNESS REDUCTION VS. STIFFNESS RATIO AND NUMBER OF REMAINING SEGMENTS USING TEST RESULTS

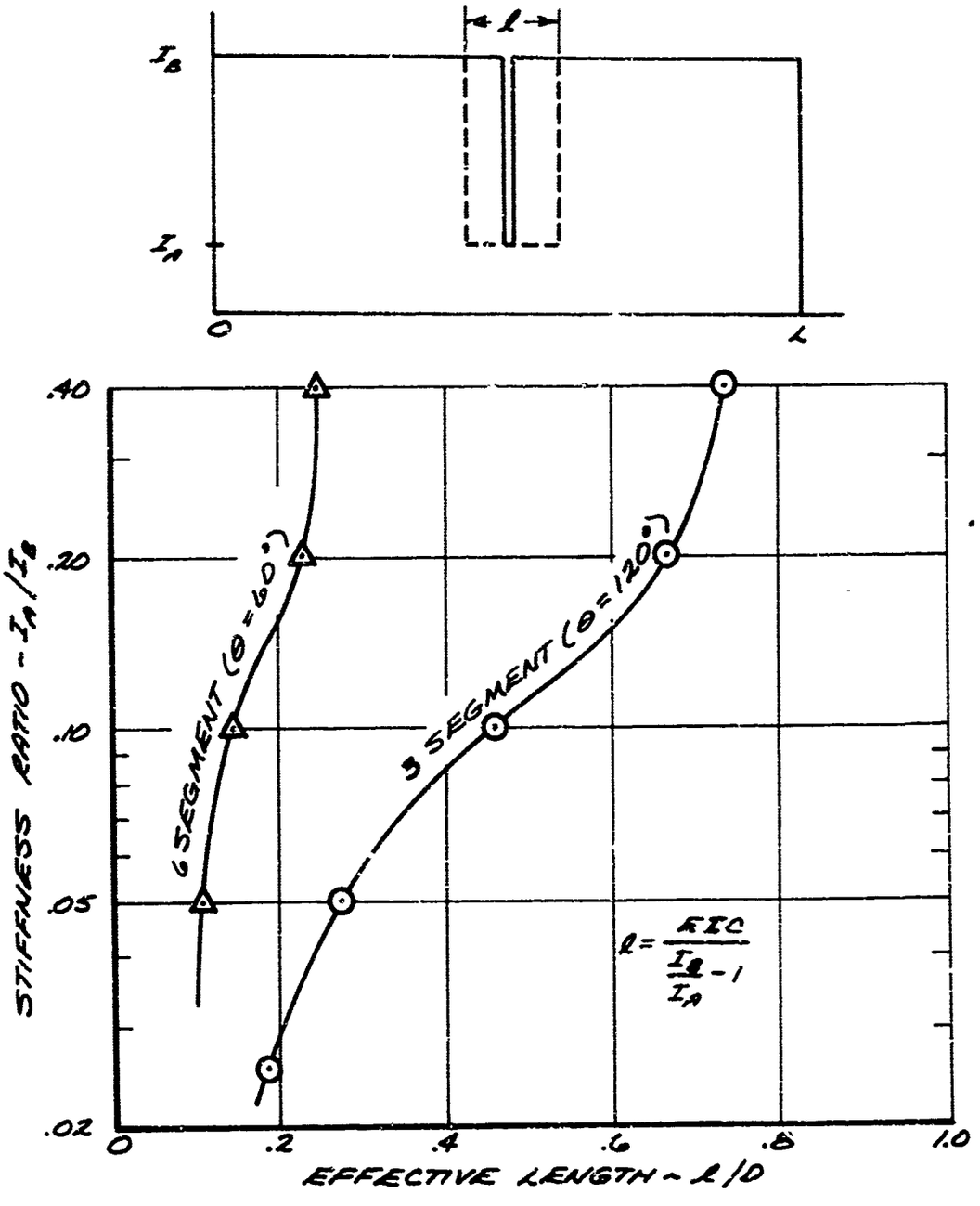

FIGURE 7-4

EI DISCONTINUITY TEST DATA - STIFFNESS RATIO VS. FREQUENCY RATIO

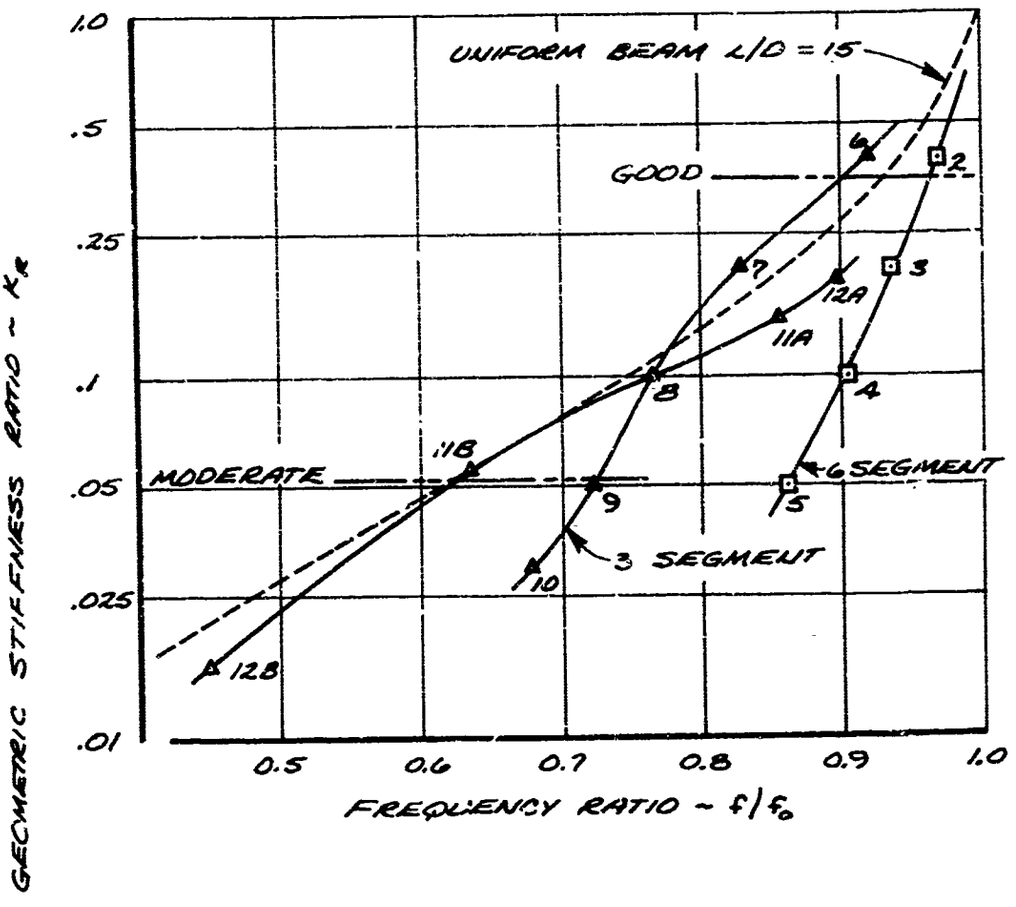

FIGURE 7-5

DESCRIPTION OF SHELL, SHELL LOADING, AND SHELL SEGMENT USED IN FINITE ELEMENT ANALYSIS

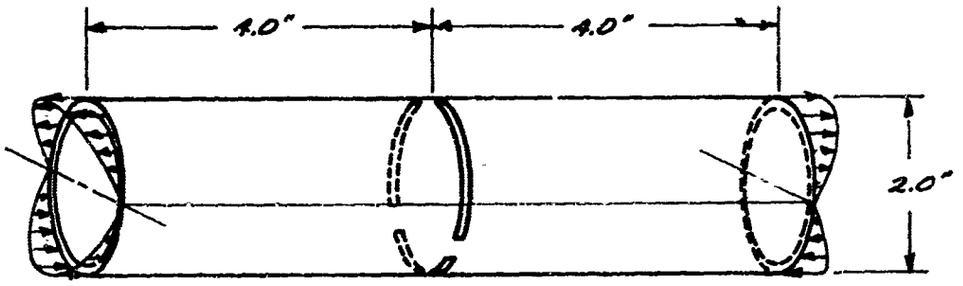

(a)

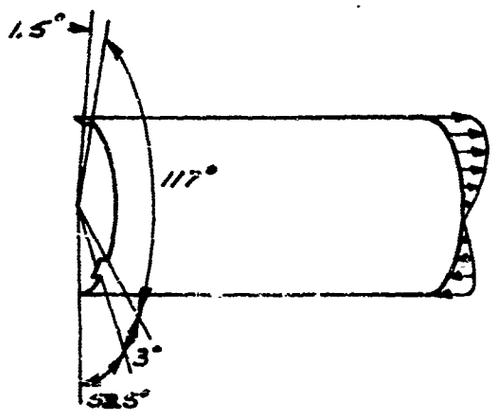

(b)

FIGURE 7-6

DISTRIBUTION OF SHELL SEGMENT
FINITE ELEMENTS

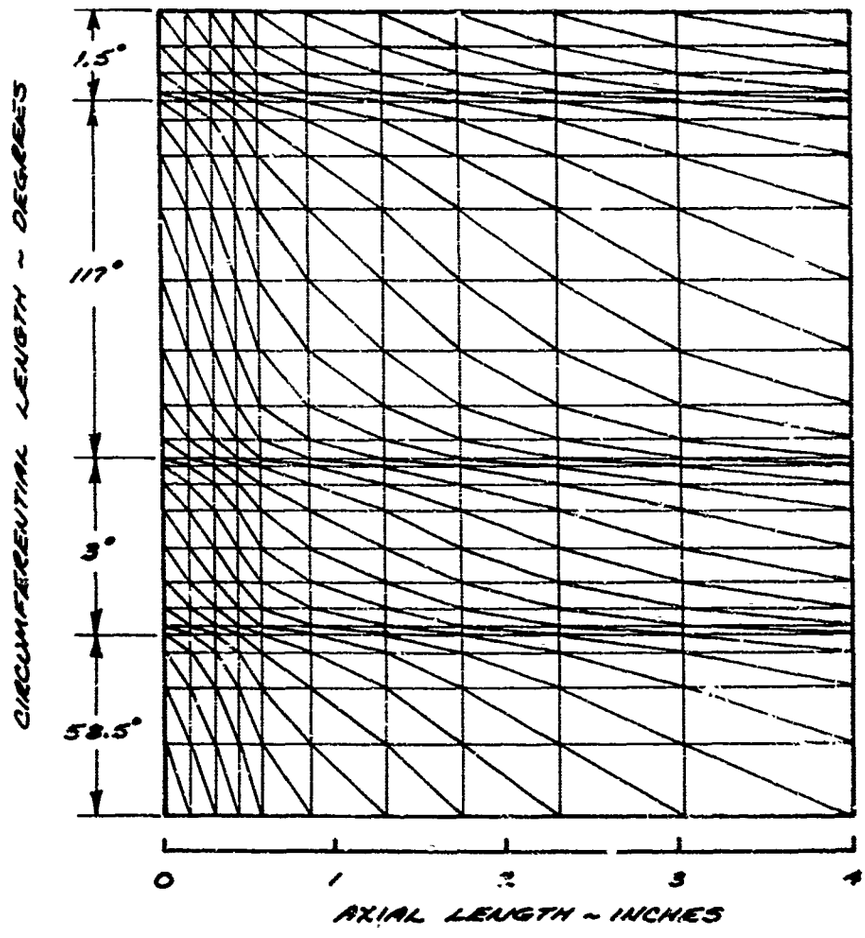

Table 7-1

Vibration Test Results
Free-Free Joint Simulation Models

Specimen Number	f_B (Hz)	f_A (Hz)	f_B/f_o	f_A/f_o	EI_c/EI_b
1	526.	526.	1.0	1.0	1.0
2	511.	510.	.971	.970	0.4
3	492.	492.	.935	.935	0.2
4	476.	475.	.905	.903	0.1
5	453.	454.	.861	.863	0.05
6	484.	484.	.920	.920	0.4
7	436.	436.	.829	.829	0.2
8	403.	402.	.766	.764	0.1
9	382.	380.	.726	.722	0.05
10	356.	356.	.677	.677	0.025
	360.	360.	.684	.684	- -
11	334.	451.	.635	.857	.0554/.1446
12	236.	472.	.449	.897	.0162/.184

f_o = First bending mode frequency of reference specimen (No. 1).

f_A = First bending mode frequency in the A plane.

f_B = First bending mode frequency in the B plane.

EI_c = Sectional stiffness of slotted region of the tube.

EI_b = Sectional stiffness of the basic tube.

Table 7-2A

COMPLIANCE AND COMPLIANCE RATIO RESULTS
FOR JOINT SIMULATION MODELS

Specimen Number	No. of Seg.	Freq. Ratio	Geometric Stiffness Ratio, I_R	Effective Length ℓ/D	Effective Compliance Rad/In-LB $(10)^6$
1	1	1.0	1.0		0
2	6	.971	0.40	.245	.4
3	6	.935	0.20	.230	1.0
4	6	.905	0.10	.150	1.4
5	6	.861	.05	.106	2.2
6	3	.920	0.40	734	1.2
7	3	.829	0.20	.666	2.9
8	3	.766	0.10	.459	4.5
9	3	.726	0.05	.274	5.7
10	3	.677	0.025	.179	7.6
11A	3	.857	.145	.359	2.3
11B	3	.635	.055	.516	9.6
12A	3	.897	.184	.332	1.6
12B	3	.449	.016	.386	25.5

Table 7-2B

TEST SPECIMEN EFFECTIVE COMPLIANCE COMPARISON
WITH JOINT RATING CLASSIFICATION

Compliance	Joint "Rating"		
	Excellent	Good	Moderate
$C_e(10)^6$ Rad/In-Lb	0.1	1.0	10.0

Section 8.0

CONCLUSIONS

In reviewing the results of this initial study of the structural dynamic properties of tactical missile joints the major points would appear to be the following.

(1) The most significant directly related work to date is that of Alley and Leadbetter (Reference 1) in which the compliance characteristics of various joints are classified from "excellent" (small compliance) to "loose".

(2) The compliance and damping characteristics of typical tactical missile joints can have a powerful influence on airframe structural dynamic response. A single joint of "moderate" compliance placed at the midspan of a typical missile; for example, could be expected to reduce the first mode frequency by approximately 35 percent.

(3) The structural efficiency of typical missile joints judged on the basis of maintaining airframe stiffness through the local region of the joint is extraordinarily low with a "good" joint rated near 40 percent, a "moderate" joint near 5 percent, and a loose joint generally below 1 percent (efficiency in this sense equals percent of local stiffness retained over a length of one-half a body diameter).

(4) Results obtained with simple test models suggest that the number of load paths and their spacing around the periphery of the joint are the determining parameters in joint compliance. The poor performance of some types of ring joints is suspected to be traceable to relatively low axial preloads (although assembly torques may be high due to friction) and a strong likelihood of only three points of contact unequally spaced.

(5) The role of unequal load path spacing in joints as a source of elastic coupling has been illustrated both by analysis and test, and a simple conceptual model presented which is believed to offer a plausible explanation and insight for this mechanism.

(6) A technique for extracting the joint compliance values from a set of measured missile elastic mode frequencies and shapes has been developed to a preliminary stage. The technique, which is based on the method of steepest ascent used originally in trajectory optimization, has been shown to be feasible for the present application. Certain limitations are present in

the method as currently implemented. These limitations are not inherent in the technique. The removal of these limitations will result in a powerful and useful analytical tool for the determination of flexural joint compliances from measured missile elastic mode test data.

(7) Finite element structural analysis approaches are believed to offer excellent potential as analytical tools in estimating joint load/deflection characteristics. Selection of the model and the interface load path assumption are critical considerations.

The next phase of this study, identified as "Phase 2, Data Acquisition and Analysis Extension Phase" is directed at accomplishing the following objectives.

(1) Developing the analytical techniques, which were formulated in Phase 1, into operational methods.

(2) Applying these operational methods to the data collected in the Phase 1 study.

(3) Developing approaches to modeling the more significant damping, cross coupling and nonlinear stiffness joint characteristics.

(4) Conducting a limited test on full scale missile joint hardware.

(5) Performing a correlation analysis to provide a basis for verification of the analytical techniques developed in Phase 2.

REFERENCES

1. Alley, Jr., V. L. and Leadbetter, S. A., "The Prediction and Measurement of Natural Vibrations on Multistage Launch Vehicles", American Rocket Society Launch Vehicles: Structures and Materials Conference Report, April 1962.

2. Bryson, A. E., and Denham, W. F., "A Steepest Ascent Method for Solving Optimum Programming Problems," pp 247-257 Journal of Applied Mechanics, June 1962.

3. Graham, R. G., "A Steepest Ascent Solution of Multiple Arc, Vehicle Optimization Problems," Space System Division, Air Force System Command SSD-TDR-63-362, Aerospace Corporation, Report No. TDR-269(4550-20)-3, December 1963.

4. Hall, B. M., Calkin, E. D. and Sholar, M. S., "Linear Estimation of Structural Parameters from Dynamic Test Data," AIAA/ASME 11th Structures, Structural Dynamics, and Materials Conference, Denver, Colorado, April 22-24, 1970.

5. Kutschka, J. D., "Standard Missile Guidance/Ordnance Joint Out-Of-Tolerance Coupling Nuts Investigation," General Dynamics Pomona Division, Report No. TM 6-420-230, 23 April 1969.

6. Maidanik, G. and Ungar, E. E., "Panel Loss Factors Due to Gas-Pumping at Structural Joints," NASA CR-954, Nov. 1967.

7. McIntyre, K. L., "Modified Holzer-Myklestad Model Analysis Final Report - CWA 245," General Dynamics Pomona Division, Report No. TM 348-15,1-3, 24 July 1961.

8. Rosen, R., "STARDYNE User's Manual," Mechanics Research Inc., Los Angeles, California, March 1970.

APPENDIX I

AEROSPACE INDUSTRY SURVEY

An aerospace industry survey on structural dynamic properties of missile airframe joints has been conducted in the form of a questionnaire. This questionnaire was distributed with the Minutes of the Aerospace Flutter and Dynamics Council Meeting held May 14 - 15, 1969 in San Antonio, Texas. The intent of the survey was to gather information from which a list of joints in common usage and the structural dynamic characteristics of importance for joints could be compiled. The primary results of the aerospace industry survey are presented in the form of a table (Table I-1).

The authors wish to express their appreciation to the following individuals and organizations who have provided the information given in this Appendix.

Mr. Thomas W. Miller	The Boeing Company Seattle, Washington
Mr. I. Baker Mr. F. A. Figge Mr. R. J. Oedy	Hughes Aircraft Co. Canoga Park, California
Mr. Bert M. Hall Mr. Gerry Kahre	McDonnell Douglas Astronautics Co. Santa Monica, California
Mr. Craig S. Porter Mr. William J. Werback	Naval Weapons Center China Lake, California
Mr. H. M. Marshall	Philco Ford Corp. Newport Beach, California

Table I-1 shows specific missile and joint properties obtained from the aerospace industry survey plus data obtained here at the Pomona Operation of General Dynamics. Only a limited number of joint compliance values have been obtained from the industry survey, and all of the compliances have been flexural compliances. No shear compliances have been reported, supporting the premise that flexural compliance is dominant to shear compliance in importance to structural dynamic analyses. Not all of those responding to the questionnaire represented joints as discrete springs, but rather some considered the bending stiffness to be some reduced value of stiffness in the area of the joint. The effect of the airframe joints on the first bending mode frequency has been obtained for six tactical missiles. The results are presented in Table I-2. A decrease in airframe stiffness as the number of joints is increased can be seen.

Table I-2

Effects of Joints on Missile First Mode Frequency

Missile	No. of Joints	First Mode Frequency Increase W/O Joints (%)
Sidewinder	4	7
SRAM	6	20
Standard ARM	6	22
Standard Missile Medium Range	7	20
Standard Missile Extended Range	7	21
Phoenix	10	40

Figures I-1 thru I-31 show diagrams of the joints listed in Table I-1. One point of interest resulting from the survey is that the damping characteristics of the joints are generally not defined, rather a percentage of the critical viscous damping is assumed for each mode in dynamic response analyses. Also, beam modal analyses are, in general, the methods employed to analyze tactical missile structures.

AEROSPACE INDUST

MISSILE	RESPONDENT	MISSILE LENGTH (IN)	NUMBER OF JOINTS IN REPLY	JOINT DIAMETER (IN)	JOINT LOCATION (% L)	TYP
REDEYE (FIM-43C)	GENERAL DYNAMICS POMONA	47	4			
				2.75	6	ORTMAN
				2.75	31	THREAD
				2.75	41	THREA
				2.75	92	ORTMAN
SIDEWINDER/CHAPARRAL (AIM-9D/MIM-72A)	NAVAL WEAPONS CENTER CHINA LAKE	115	4			
				2.7	1	THREA
				5.0	21	MARM
				5.0	26	MARM
				5.0	37	MARM
SHILLELAGH (MGM-51A)	PHILCO FORD NEWPORT BEACH	43	2			
				5.95	48	ORTMA
				5.95	83	ORTMA
SHRIKE (AGM-45A)	NAVAL WEAPONS CENTER CHINA LAKE	120	4			
				7.3	13	SHEA
				8.0	24	SHEA
				8.0	48	SHEA
				8.0	58	CONTI
FALCON (GAR-11)	HUGHES AIRCRAFT CANOGA PARK	86	7			
				9.2	30	RIVET
				10.7	37	RIVET
				11.4	57	RIVET
				11.4	60	RIVET
				9.8	77	RIVET
				9.3	85	RIVET
				9.3	86	(8) SHE
STANDARD MISSILE EXTENDED RANGE AFTER BOOSTER SEPARATION (RIM-67A)	GENERAL DYNAMICS POMONA	159	8			
				13.5	25	CONTIN
				13.5	34	RIVET
				13.5	39	(4) TEN
				13.5	41	RIVET
				13.5	49	(4) TEN
				13.5	83	(16) TEN
				13.5	90	(16) TEN
				13.5	100	MARMO

TABLE I-1
INDUSTRY SURVEY RESULTS

B

TYPE OF JOINT	AVERAGE AIRFRAME STIFFNESS ADJACENT TO JOINT ($LB-IN^2$)	JOINT COMPLIANCE (RAD/IN-LB)	METHOD BY WHICH COMPLIANCE WAS OBTAINED	FIGURE NUMBER
ORTMAN KEY - THREADED	$7.0\ (10)^6$	——	——	I-1
THREADED COUPLING RING	$8.2\ (10)^6$	$2.5\ (10)^{-7}$	[VIBRATION TESTS OF SIMULATED JOINTS]	[I-2]
THREADED COUPLING RING	$8.0\ (10)^6$	$2.0\ (10)^{-7}$		
ORTMAN KEY	$8.2\ (10)^6$	——	——	I-3
THREADED COMPRESSION	——	——	——	I-4
MARMON CLAMP	$1.0\ (10)^8$	$5.0\ (10)^{-8}$	["GOOD" JOINT SELECTED FROM REF. 1]	[I-5]
MARMON CLAMP	$1.0\ (10)^8$	$5.0\ (10)^{-8}$		
MARMON CLAMP	$1.0\ (10)^8$	$5.0\ (10)^{-8}$		
ORTMAN KEY	——	——	——	I-6
ORTMAN KEY	——	——	——	I-7
SHEAR SCREWS	$1.0\ (10)^8$	——	——	——
SHEAR SCREWS	$6.5\ (10)^8$	——	——	——
SHEAR SCREWS	$7.9\ (10)^8$	——	——	——
CONTINUOUS THREADS	$6.3\ (10)^8$	——	——	——
RIVETS	$1.5\ (10)^8$	——	——	I-8
RIVETS	$1.9\ (10)^8$	——	——	I-9
RIVETS	$2.5\ (10)^8$	——	——	I-10
RIVETS	$2.5\ (10)^8$	——	——	I-11
RIVETS	$2.3\ (10)^8$	——	——	I-12
RIVETS	$1.7\ (10)^8$	——	——	I-13
(8) SHEAR SCREWS	$1.5\ (10)^8$	——	——	I-14
CONTINUOUS LAND RING	$1.2\ (10)^9$	$1.5\ (10)^{-8}$	[MATCH OF MISSILE VIBRATION MODE SURVEY RESULTS]	I-15 (SIMILAR TO I-16)
RIVET (FIBERGLASS WRAP)	$1.1\ (10)^9$	$0.1\ (10)^{-8}$		
(4) TENSION BOLTS	$2.1\ (10)^9$	$0.6\ (10)^{-8}$		[I-16]
RIVET (FIBERGLASS WRAP)	$1.7\ (10)^9$	$0.1\ (10)^{-8}$		
(4) TENSION BOLTS	$2.8\ (10)^9$	$0.6\ (10)^{-8}$		I-17
(16) TENSION BOLTS	$2.5\ (10)^9$	$0.24\ (10)^{-8}$		(SIMILAR TO I-23)
(16) TENSION BOLTS	$1.2\ (10)^9$	$0.24\ (10)^{-8}$		
MARMON CLAMP (EXPLOSIVE)	$2.4\ (10)^9$	——	——	I-18

(CONT.)

TABLE I-1 AEROSPACE INDUSTRY SURVEY RESULTS (CONT.)

MISSILE	RESPONDENT	MISSILE LENGTH (IN)	NUMBER OF JOINTS IN REPLY	JOINT DIAMETER (IN.)	JOINT LOCATION (% L.)	TY
STANDARD ARM (AGM - 78B)	GENERAL DYNAMICS POMONA	179	6			
				13.5	18	DISCON
				13.5	23	TENS
				13.5	35	DISCO
				13.5	43	(8) TEN
				13.5	88	(18) SHL
				13.5	93	(8) TE
PHOENIX (AIM - 54A)	HUGES AIRCRAFT CANOGA PARK	≈156	10			
				≈15	22	COUPL
				≈15	23	SHEA
				≈15	34	
				≈15	37	
				≈15	55	
				≈15	56	
				≈15	79	
				≈15	81	
				≈15	91	
				≈15	94	
SRAM (AGM - 69A)	THE BOEING CO. SEATTLE	≈168	6			
				——	4	
				10.3	14	(12) SHA
				15.4	31	BAYON
				——	38	
				17.1	41	(43) SA
				——	88	
THOR/DELTA	McDONNELL DOUGLAS SANTA MONICA	——	1			
				18.	5	MARM
WALLEYE (YAGM - 62A)	NAVAL WEAPONS CENTER CHINA LAKE	136	2			
				15.	20	MODIF
				15.	76	MODIF

B

ON)	TYPE OF JOINT	AVERAGE AIRFRAME STIFFNESS ADJACENT TO JOINT (LB-IN²)	JOINT COMPLIANCE (RAD/IN-LB)	METHOD BY WHICH COMPLIANCE WAS OBTAINED	FIGURE NUMBERS
	DISCONTINUOUS LAND RING	$2.4\ (10)^9$	$0.75\ (10)^{-8}$	[MATCH OF MISSILE VIBRATION MODE SURVEY RESULTS]	I-19
	TENSION CLAMP	$2.5\ (10)^9$	$3.0\ (10)^{-8}$		I-20
	DISCONTINUOUS LAND RING	$2.5\ (10)^9$	$2.0\ (10)^{-8}$		I-21
	(8) TENSION BOLT	$4.3\ (10)^9$	$0.1\ (10)^{-8}$		I-22
	(18) SHEAR SCREWS	$1.4\ (10)^9$	$1.0\ (10)^{-8}$		I-23
	(2) TENSION BOLT	$1.1\ (10)^9$	$1.0\ (10)^{-8}$		I-24
	COUPLING RING	—	—	—	I-25, I-26
	SHEAR BOLTS	—	—	—	I-25
	———	—	—	—	[I-27, I-28, I-29]
	———	—	—	—	
	———	—	—	—	
	———	—	—	—	
	———	—	—	—	
	———	—	—	—	
	———	—	—	—	
	———	—	—	—	
	———	—	—	—	—
	(12) SHEAR BOLTS	—	—	—	I-30
	BAYONET SPLINES	—	—	—	I-31
	———	—	—	—	—
	(43) SHEAR BOLTS	—	—	—	(SIMILAR TO I-30)
	———	—	—	—	—
	MARMON CLAMP	—	$4.9\ (10)^{-8}$	FROM MODAL SURVEY	—
	MODIFIED MARMON CLAMP	—	—	—	—
	MODIFIED MARMON CLAMP	—	—	—	—

FIGURE I-1

MISSILE: REDEYE (FIM-43C)

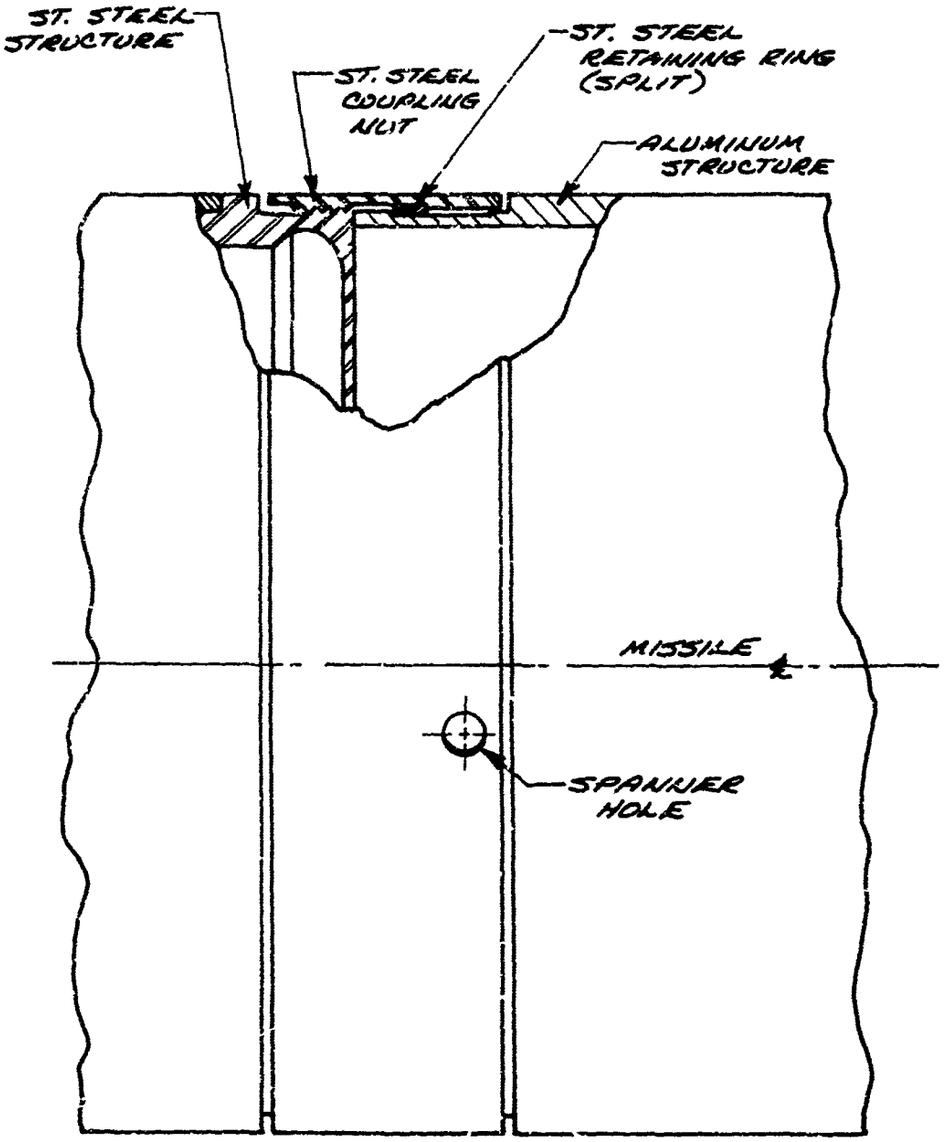

JOINT LOCATION: 69% AIRFRAME LENGTH
JOINT DIAMETER: 2.75 INCHES
SCALE: 2X

FIGURE I-2

MISSILE: REDEYE (FIM-43C)

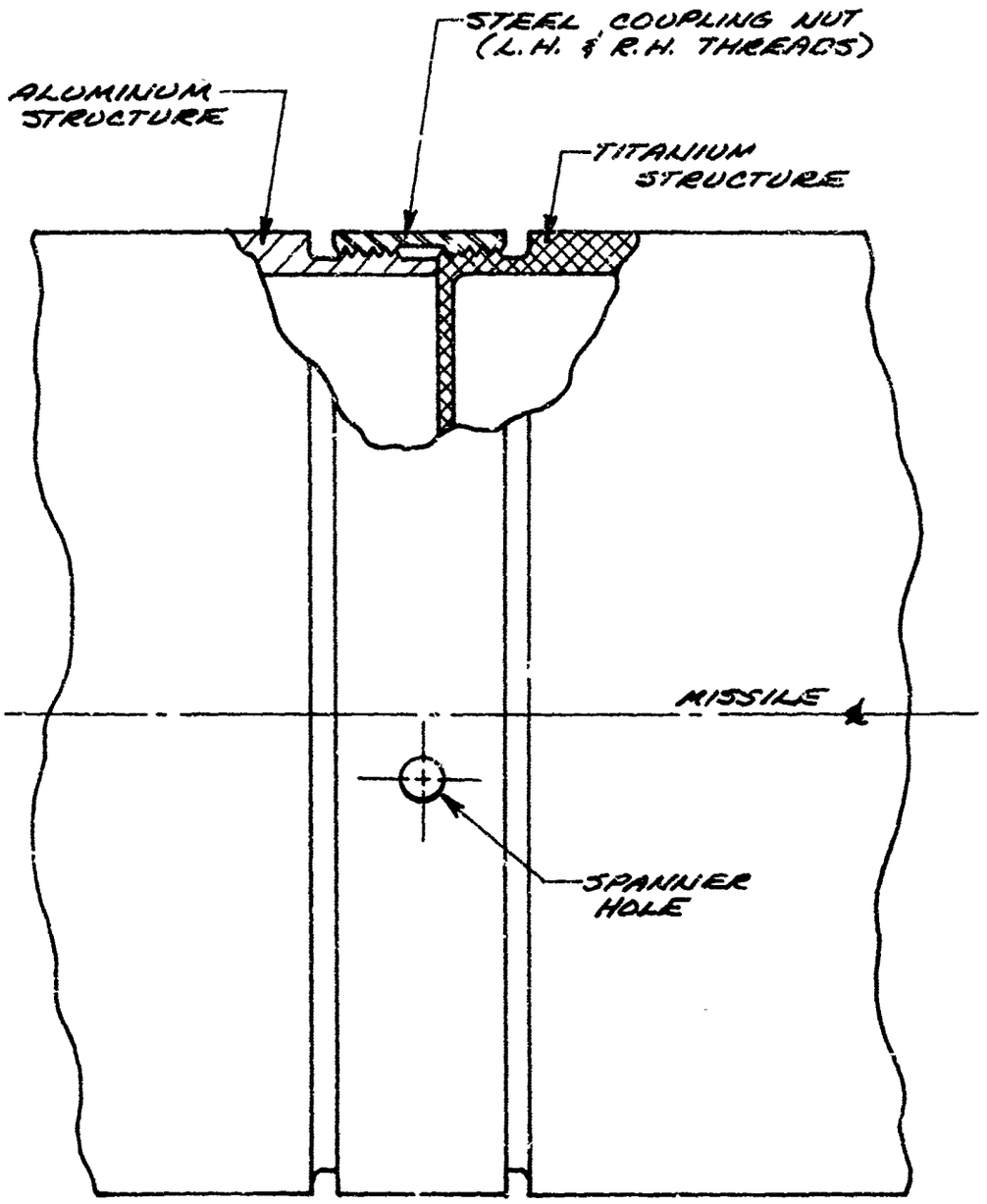

JOINT LOCATION: 31 % AIRFRAME LENGTH

JOINT DIAMETER: 2.75 INCHES

SCALE: 2X

FIGURE I-3

MISSILE: REDEYE (FIM-43C)

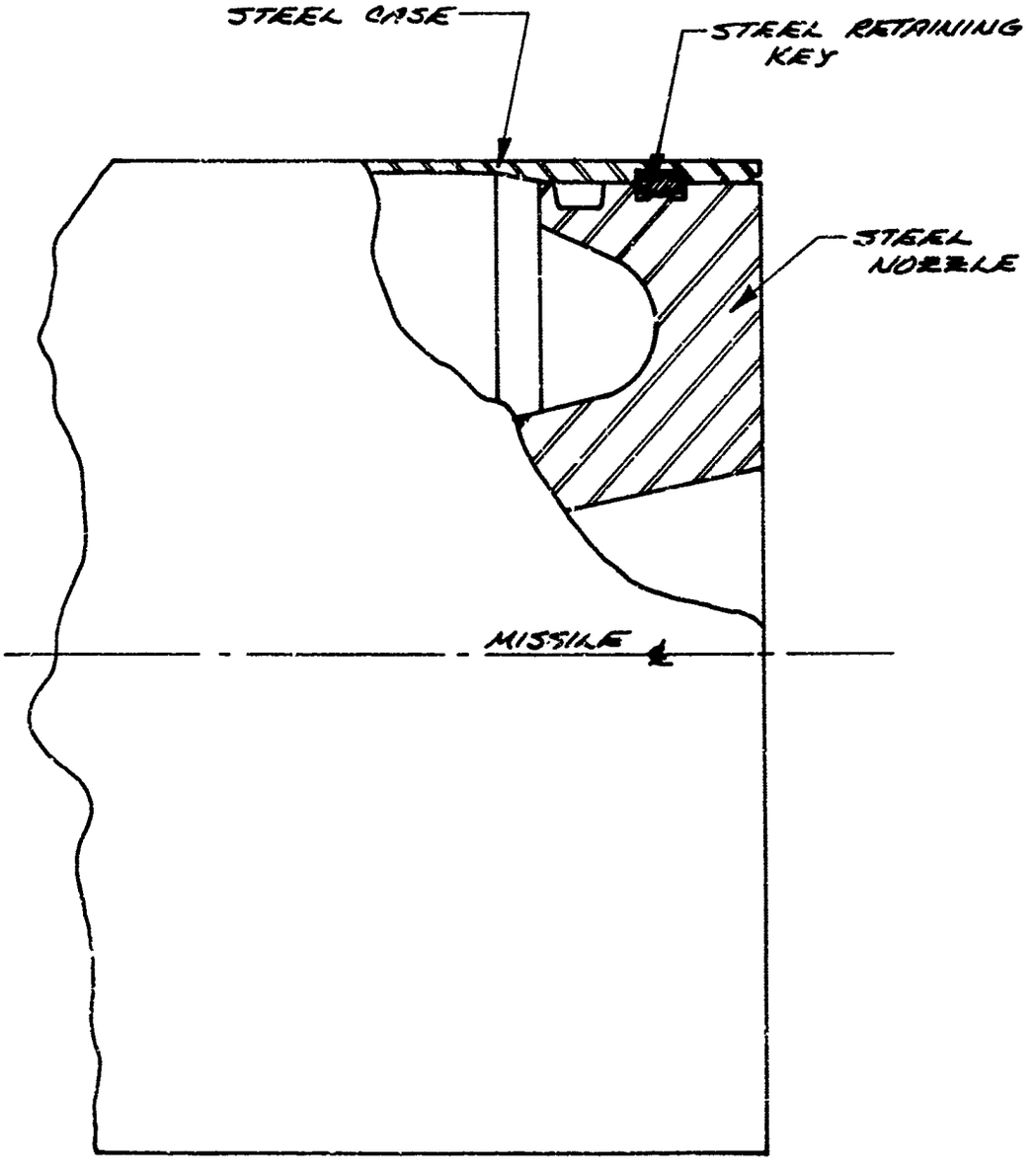

JOINT LOCATION: 92 % AIRFRAME LENGTH
JOINT DIAMETER: 2.75 INCHES
SCALE: 2X

FIGURE I-4

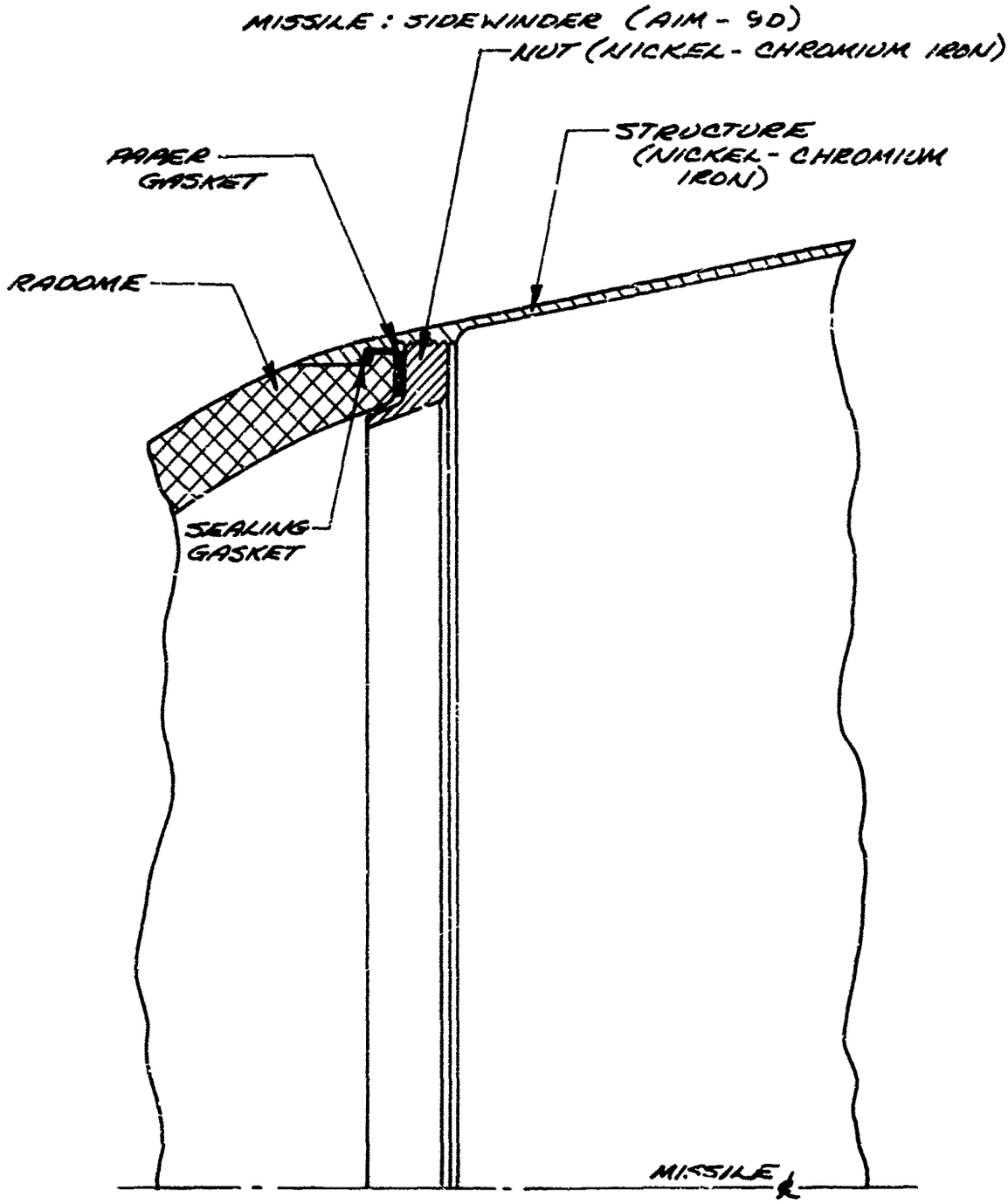

JOINT LOCATION : 19% AIRFRAME LENGTH
JOINT DIAMETER : 2.7 INCHES
SCALE : 2X

FIGURE I-5

MISSILE : SIDEWINDER (AIM-9D)
JOINT LOCATION : 21% AIRFRAME LENGTH
JOINT DIAMETER : 5.0 INCHES
SCALE : 2X

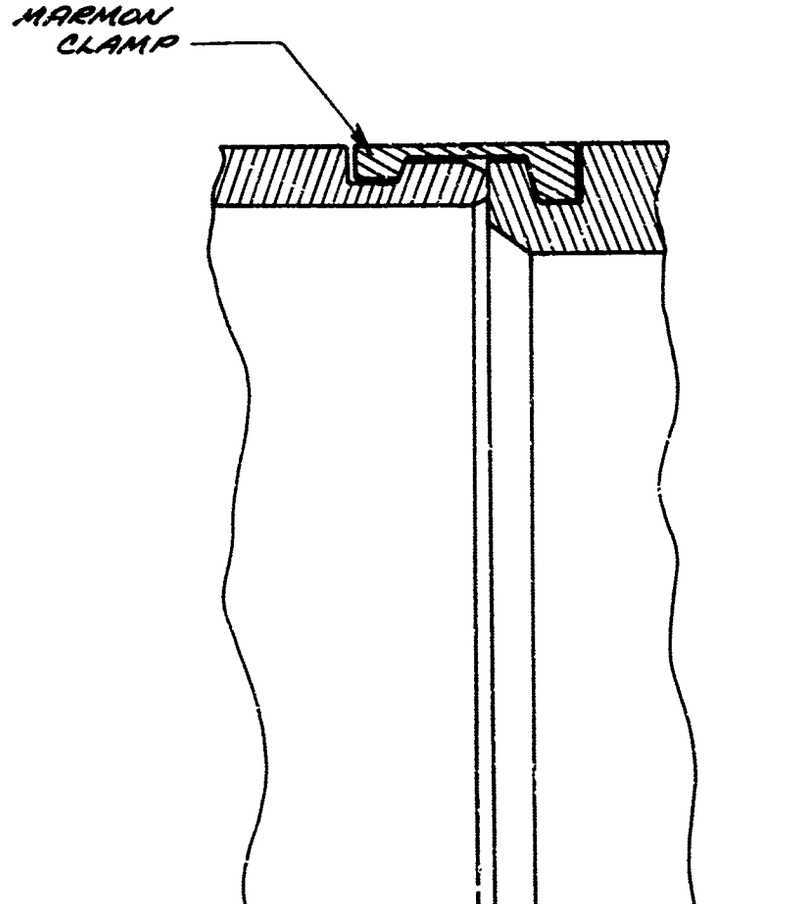

FIGURE I-6

MISSILE : SHILLELAGH (MGM-51A)
JOINT LOCATION : 48% AIRFRAME LENGTH
SCALE : FULL

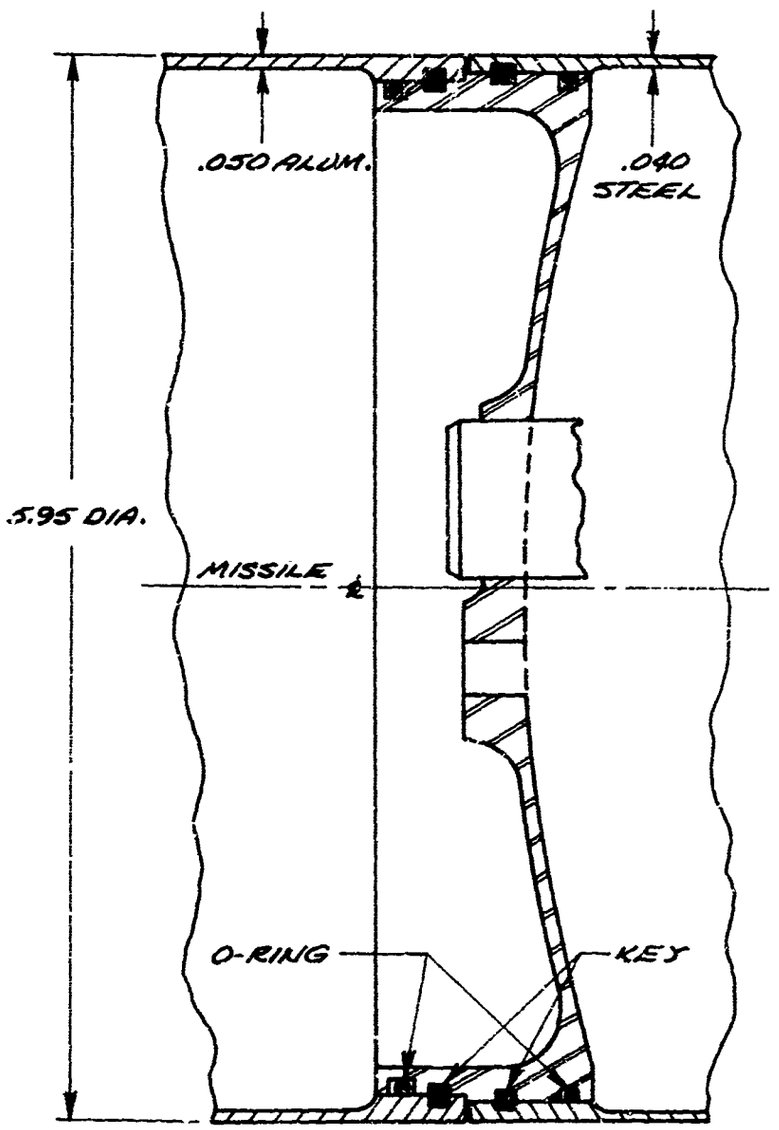

FIGURE I-7

MISSILE: SHILLELAGH (MGM-51A)
JOINT LOCATION: 83% AIRFRAME LENGTH
JOINT DIAMETER: 5.95 INCHES
SCALE: FULL

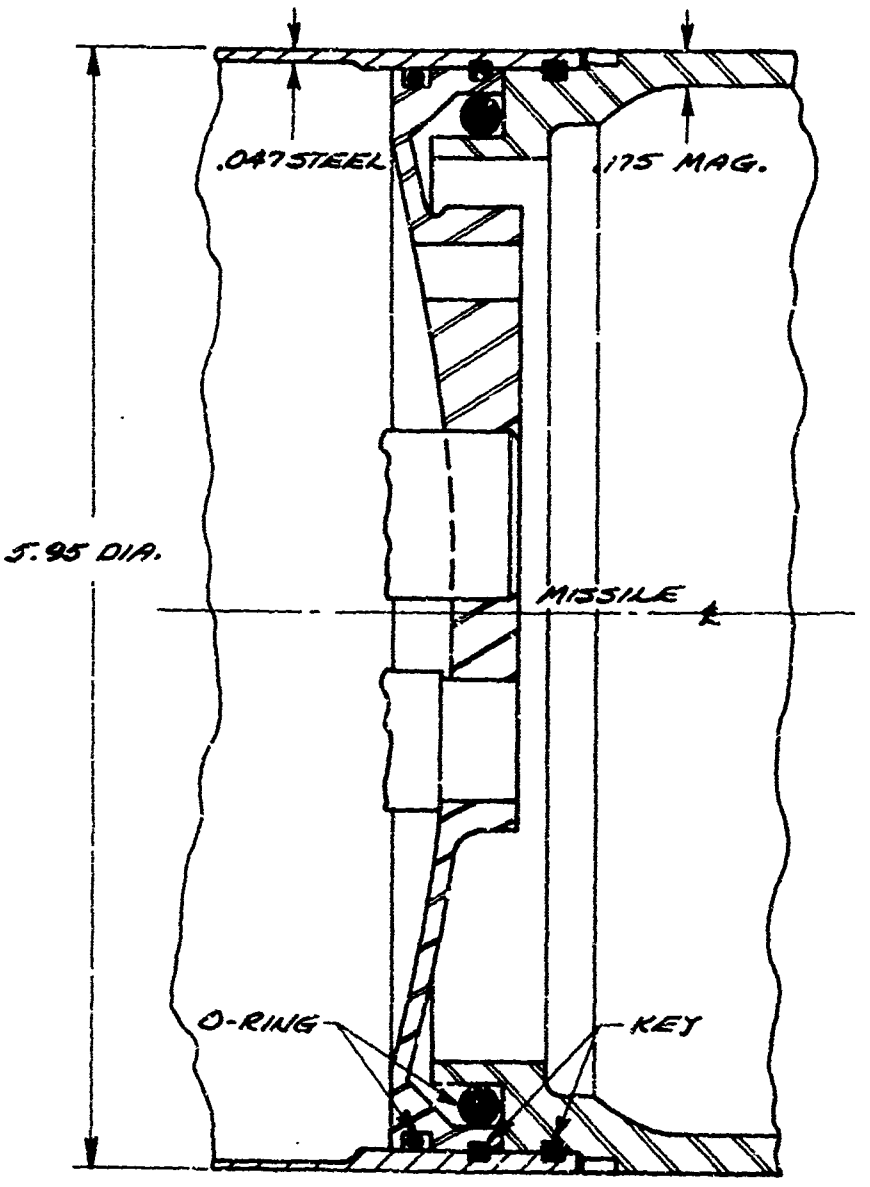

FIGURE I-8

MISSILE : FALCON (GAR-11)
JOINT LOCATION : 30% AIRFRAME LENGTH
JOINT DIAMETER : 9.2 INCHES

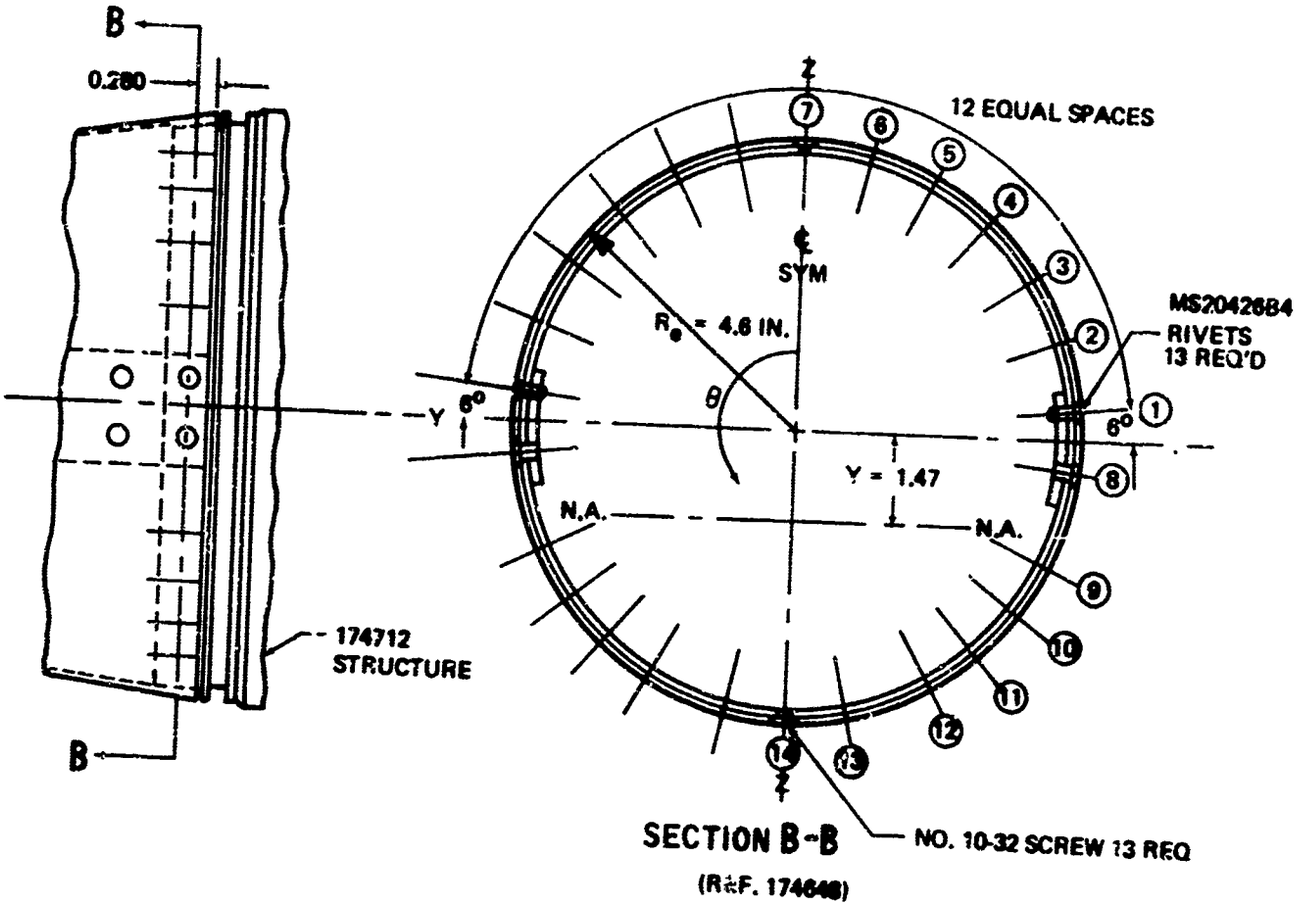

$I_{FWD} = 18.4 \text{ IN.}^4$ $I_{AFT} = 29.0 \text{ IN.}^4$

DESIGN LOADS: 9800 IN.-LB BENDING MOMENT
400 LB SHEAR

FIGURE I-9

MISSILE : FALCON (GAR-11)

JOINT LOCATION : 37% AIRFRAME LENGTH

JOINT DIAMETER : 10.7 INCHES

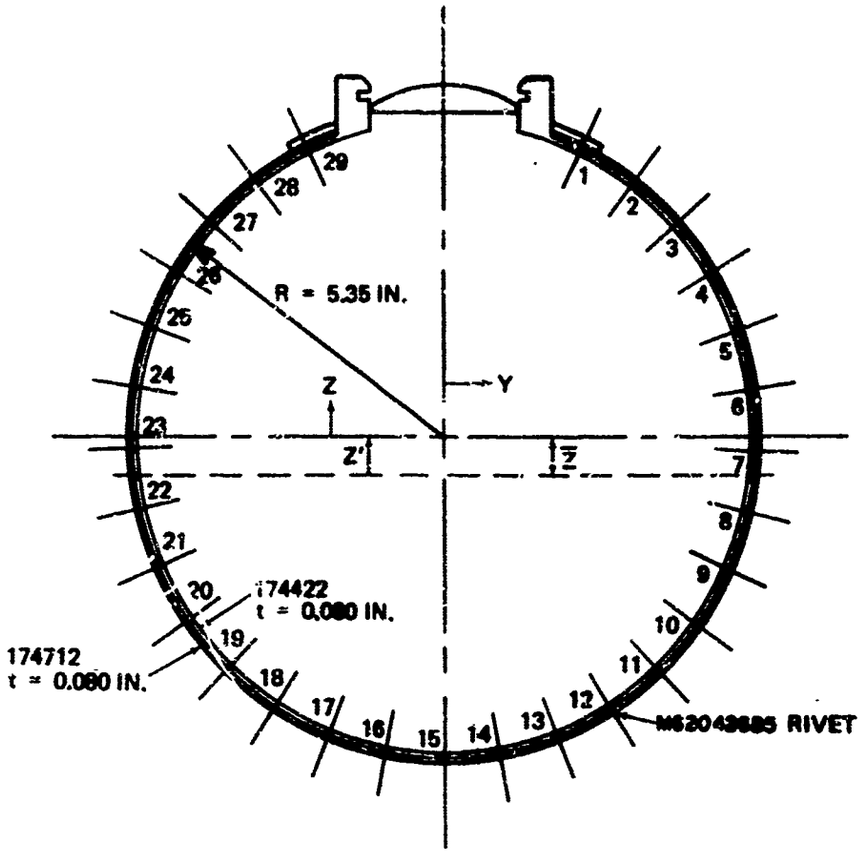

I_{FWD} = 29.8 IN.^{4} I_{AFT} = 30 IN.^{4}

DESIGN LOADS: 12,300 IN.-LB BENDING MOMENT (M_{Y-Y})
AT 258°F

FIGURE I-10

MISSILE: FALCON (GAR-11)
JOINT LOCATION: 57% AIRFRAME LENGTH
JOINT DIAMETER: 11.4 INCHES

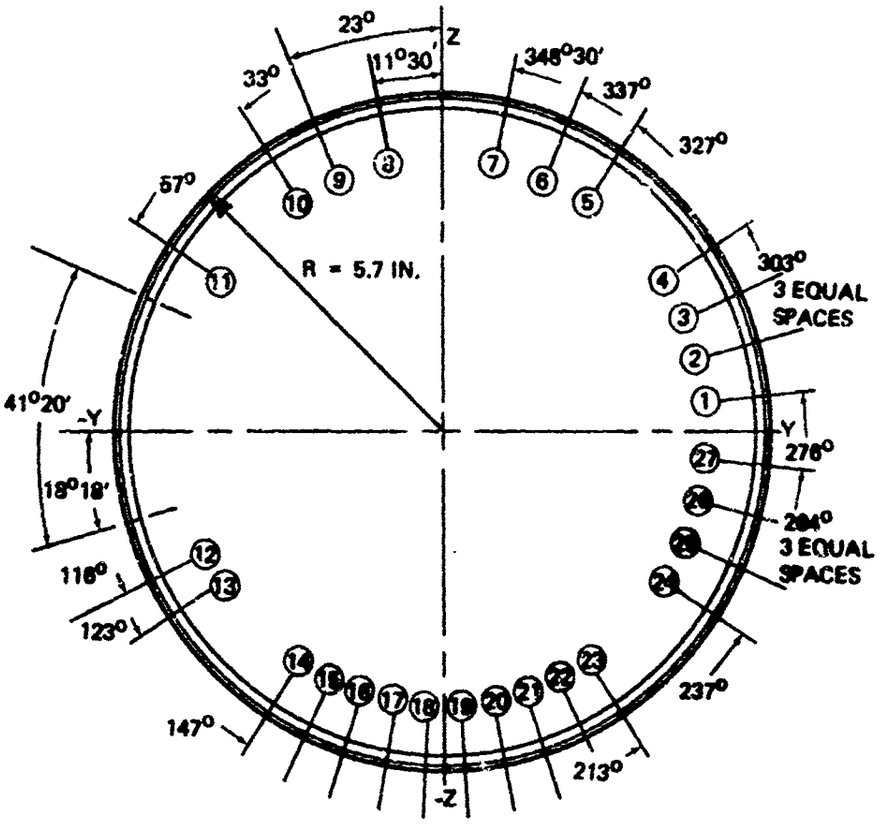

$I_{FWD} = 38.5 \text{ IN.}^4$ $I_{AFT} = 38.7 \text{ IN.}^4$

DESIGN LOADS: 23,300 IN.-LB (M_{Y-Y})
11,600 IN.-LB (M_{Z-Z})

FIGURE I-11

MISSILE: FALCON (GAR-11)
JOINT LOCATION: 60% AIRFRAME LENGTH
JOINT DIAMETER: 11.4 INCHES

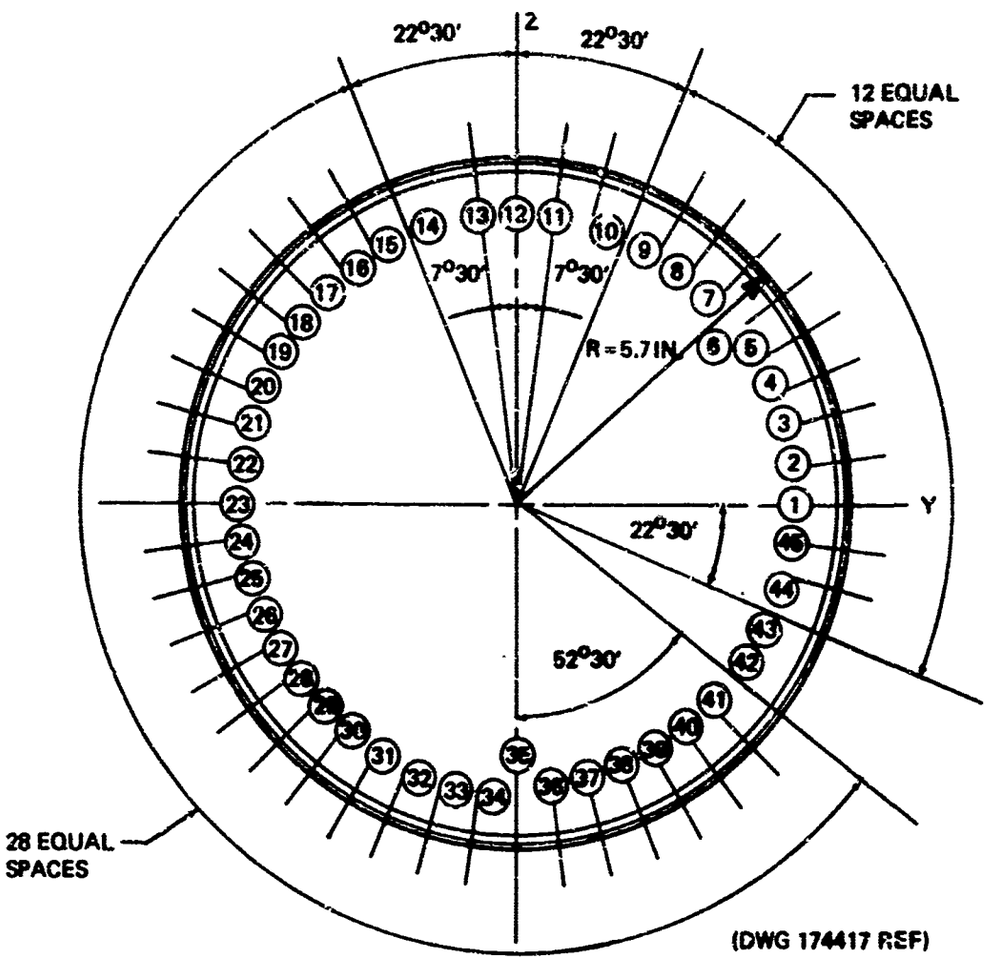

I_{FWD} = 39.2 IN.^{4} I_{AFT} = 39.0 IN.^{4}

DESIGN LOADS: 23,300 IN.-LB (M_{Y-Y})
11,600 IN.-LB (M_{Z-Z})

FIGURE I-12

MISSILE: FALCON (GAR-11)
JOINT LOCATION: 77% AIRFRAME LENGTH
JOINT DIAMETER: 9.8 INCHES

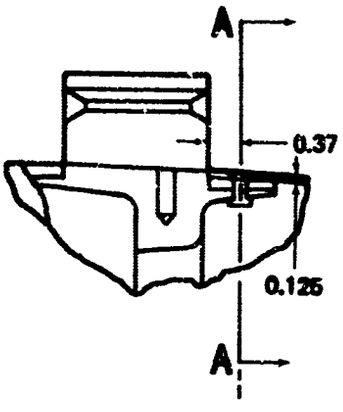

SECTION A A

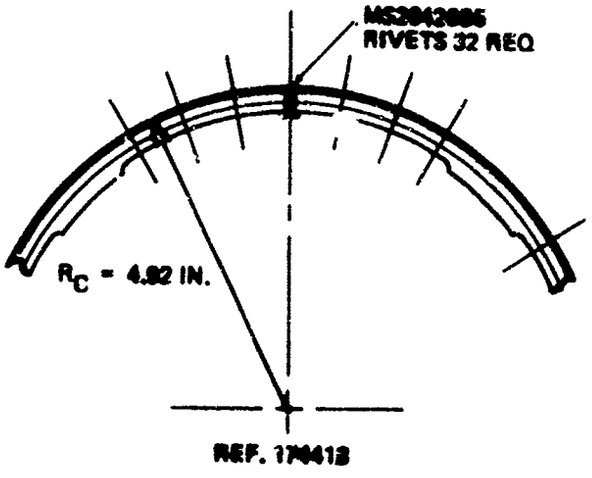

I_{FWD} = 35.5 IN.^{4} I_{AFT} = 34.5 IN.^{4}

DESIGN LOADS: 12,200 IN.-LB BENDING MOMENT
1,200 LB SHEER
9,100 LB THRUST AT 160°F
} AT 230°F

FIGURE I-13

MISSILE: FALCON (GAR-11)
JOINT LOCATION: 85 % AIRFRAME LENGTH
JOINT DIAMETER: 9.3 INCHES

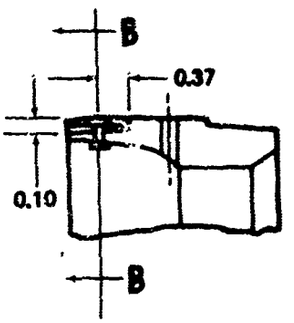

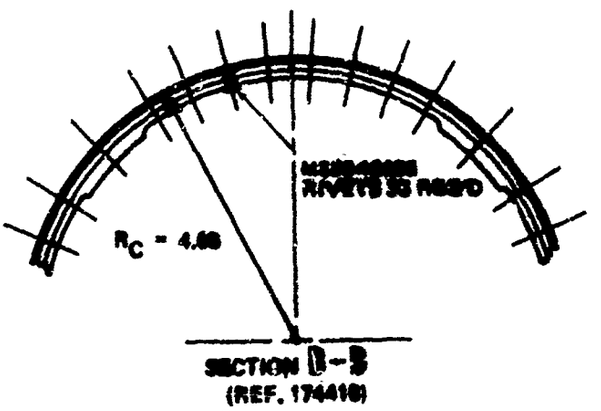

I_{FWD} = 26.2 IN.^{4} I_{AFT} = 25.2 IN.^{4}

DESIGN LOADS: 7500 IN.-LB BENDING MOMENT
AT 380°F.
9100 LB THRUST LOAD

FIGURE I-14

MISSILE: FALCON (GAR-11)
JOINT LOCATION: 86% AIRFRAME LENGTH
JOINT DIAMETER: 9.3 INCHES

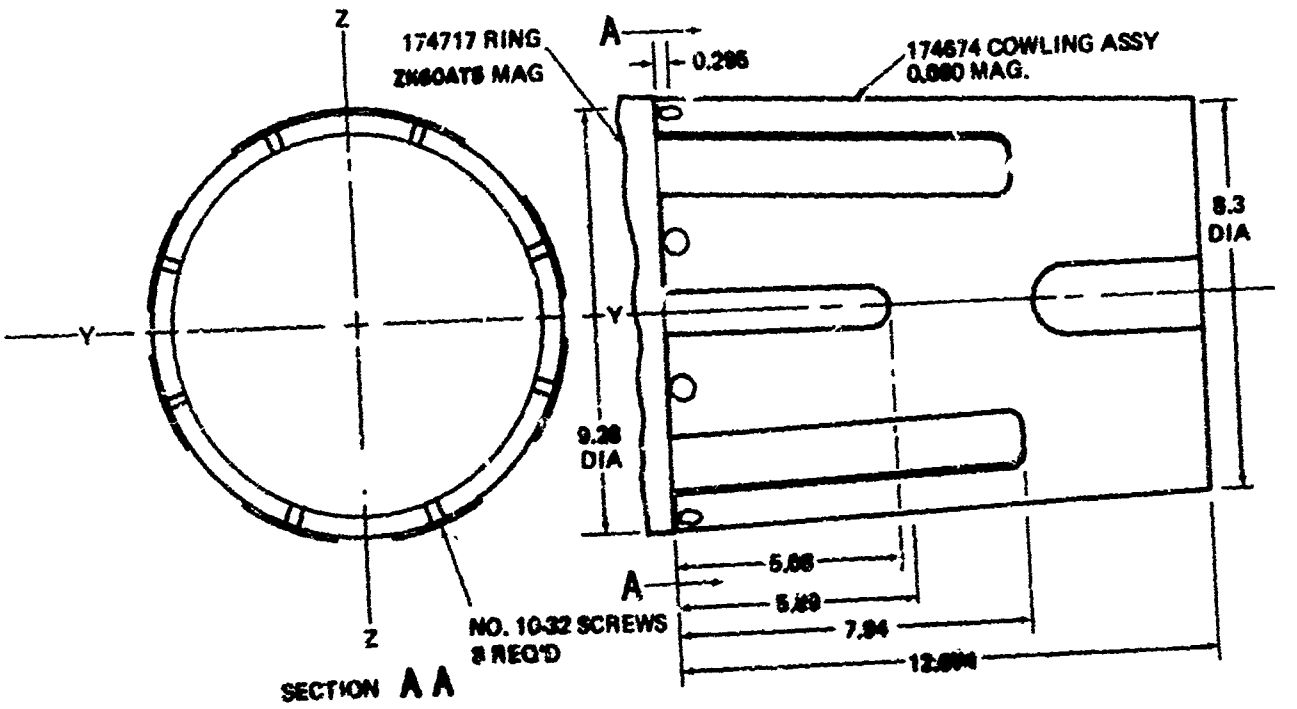

$I_{FWD} = 23.5$ IN.^{4}

DESIGN LOADS: 2500 IN.-LB BENDING MOMENT
600 LB SHEAR

FIGURE I-15

MISSILE : STANDARD MISSILE (RIM-67A)

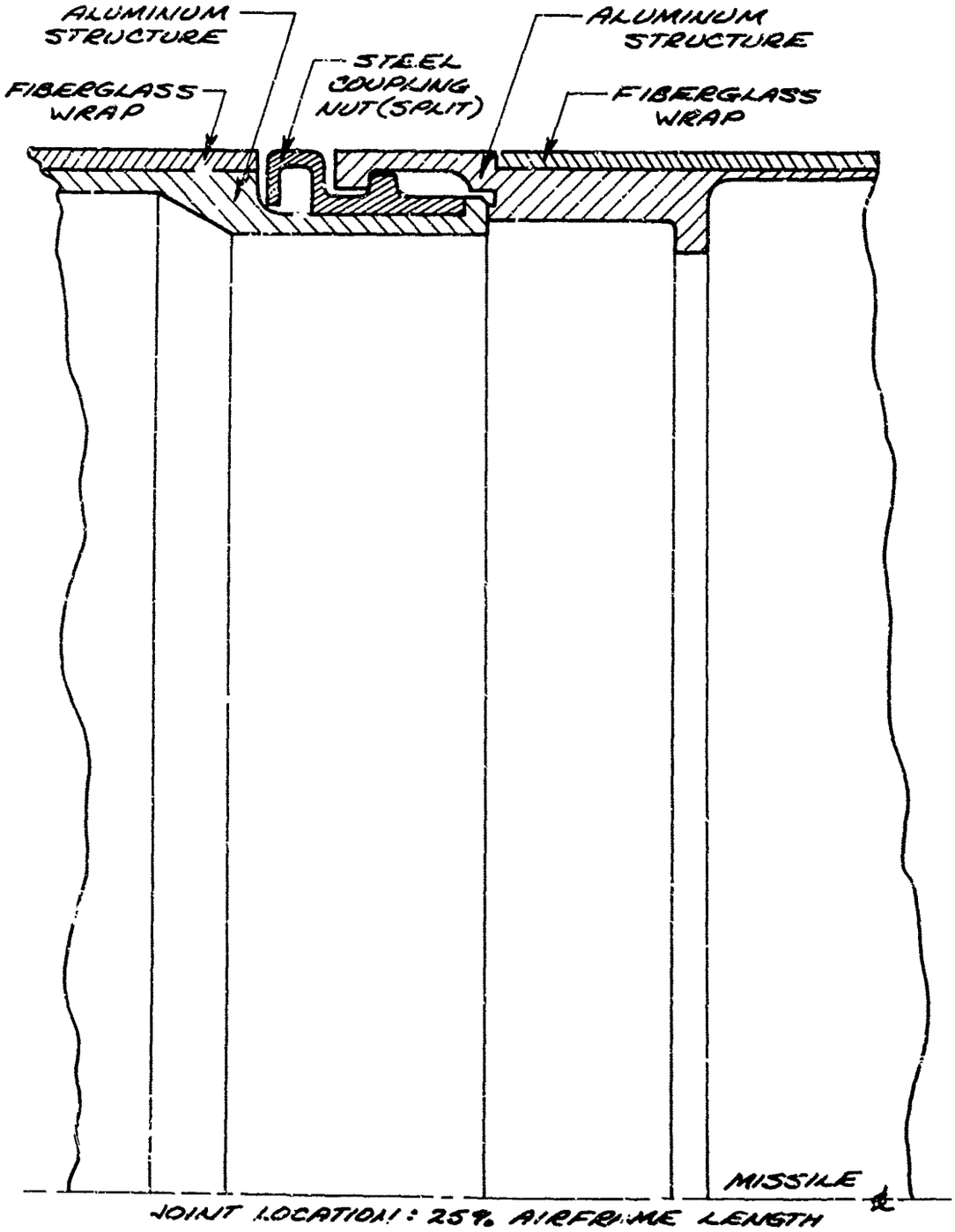

JOINT LOCATION: 25% AIRFRAME LENGTH

JOINT DIAMETER: 13.5 INCHES

SCALE : FULL

FIGURE I-16

MISSILE : STANDARD MISSILE (RIM-67A)

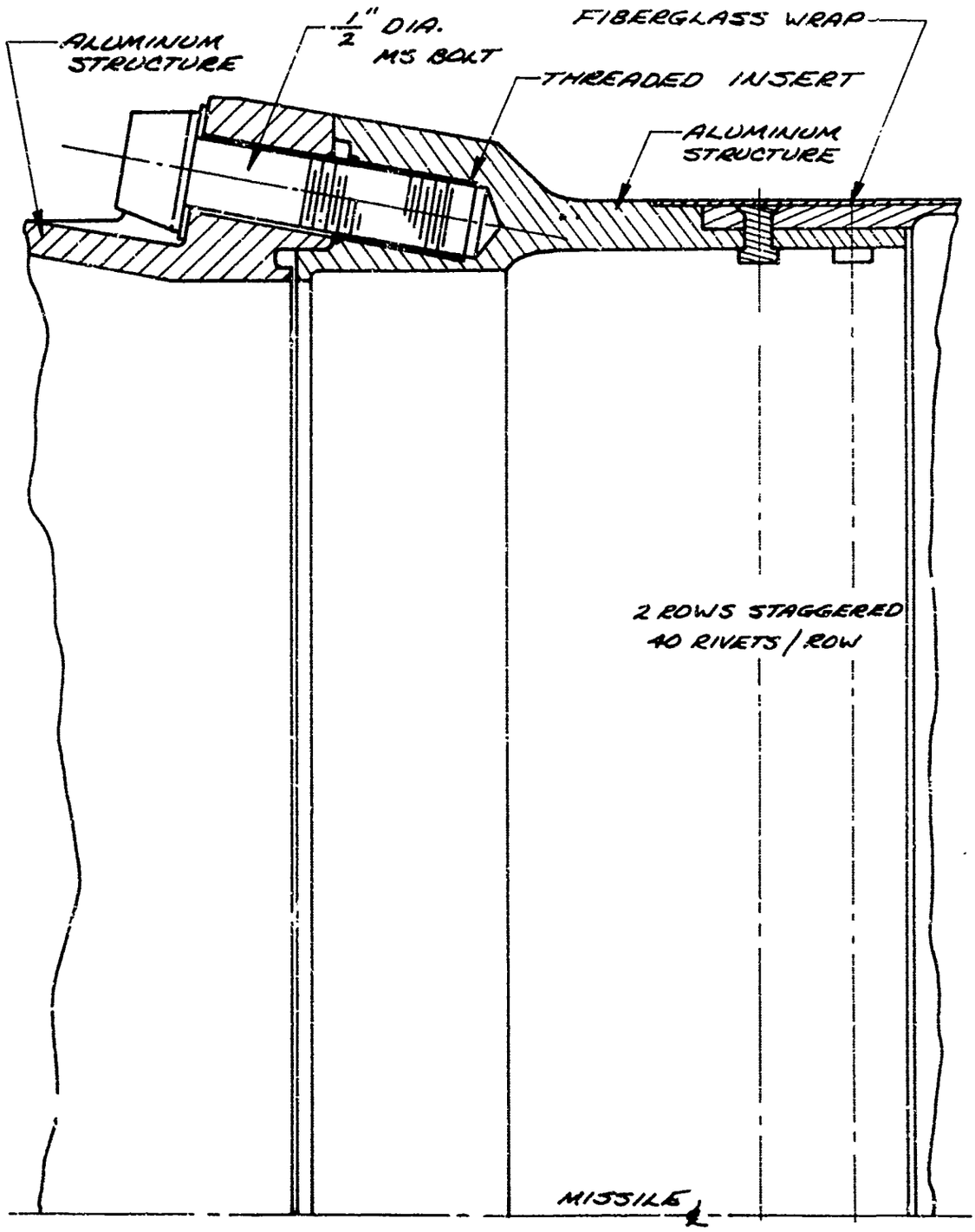

JOINT LOCATION : 39%, 41% AIRFRAME LENGTH

JOINT DIAMETER: 13.5 INCHES

SCALE : FULL

FIGURE I-17

MISSILE: STANDARD MISSILE (RIM-67A)

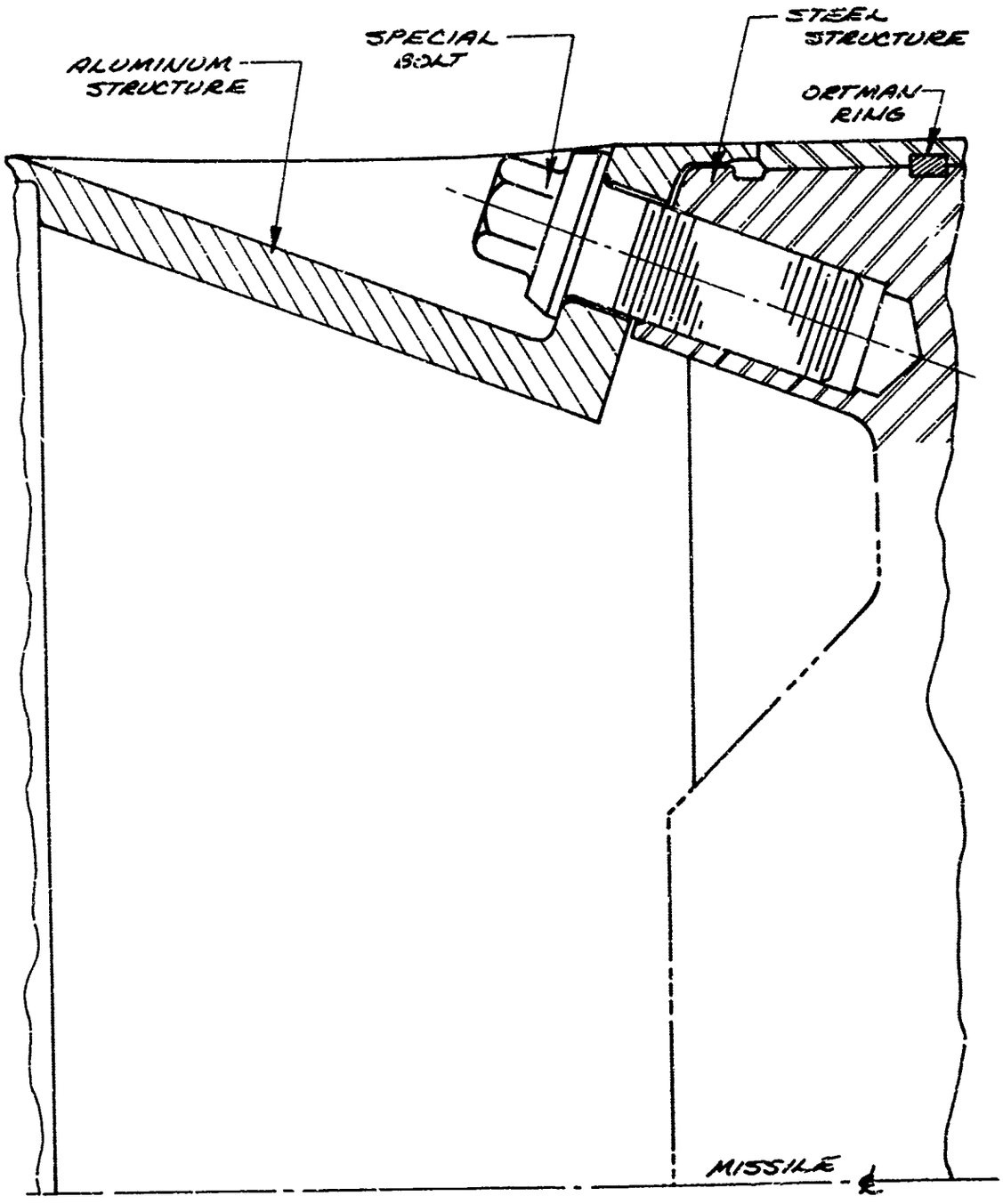

JOINT LOCATION: 49 % AIRFRAME LENGTH

JOINT DIAMETER: 13.5 INCHES

SCALE: FULL

FIGURE I-13

MISSILE : STANDARD MISSILE (RIM-67A)

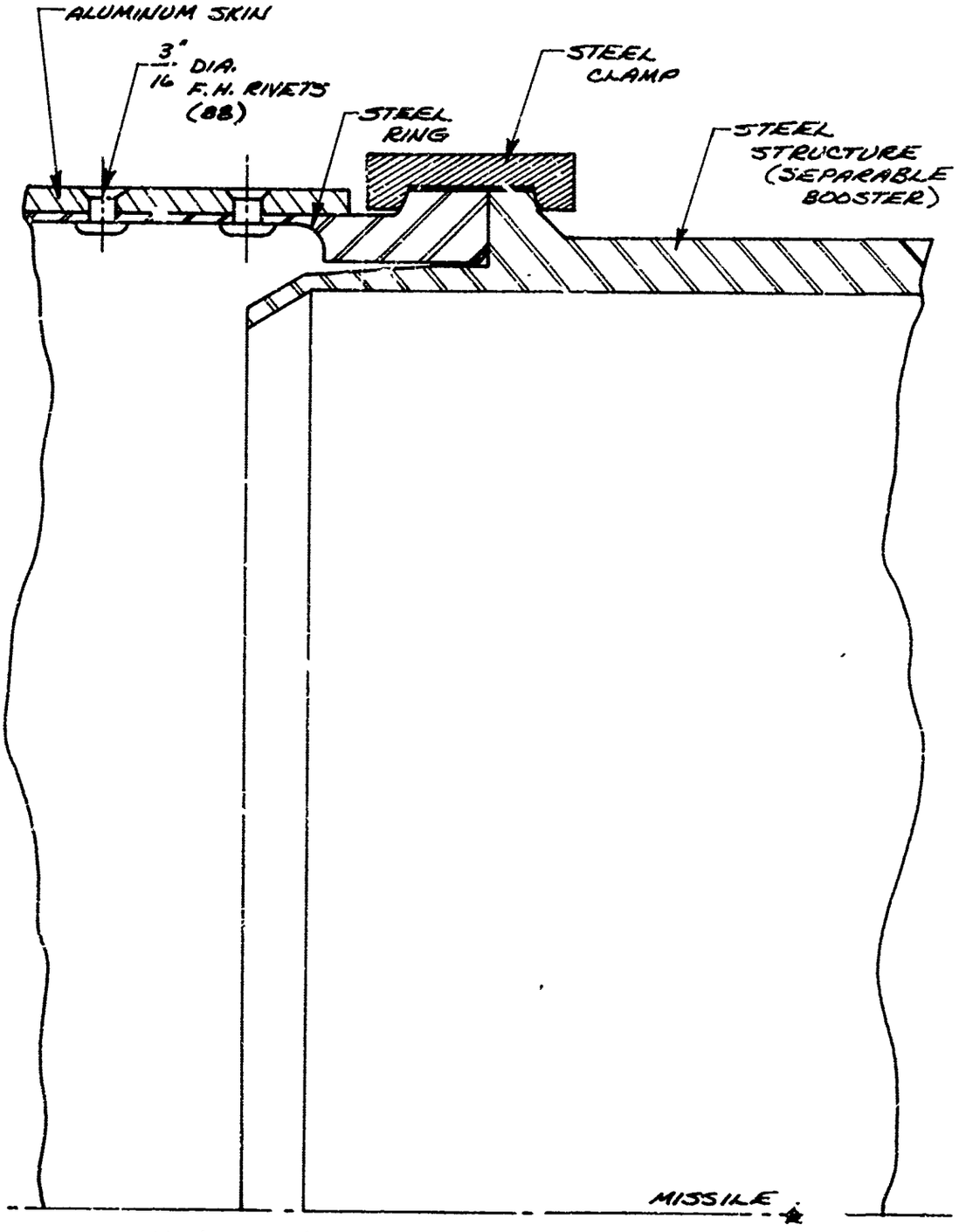

JOINT LOCATION: 100% AIRFRAME LENGTH
JOINT DIAMETER: 13.5 INCHES
SCALE : FULL

FIGURE I-19

MISSILE: STANDARD ARM (AGM-78B)

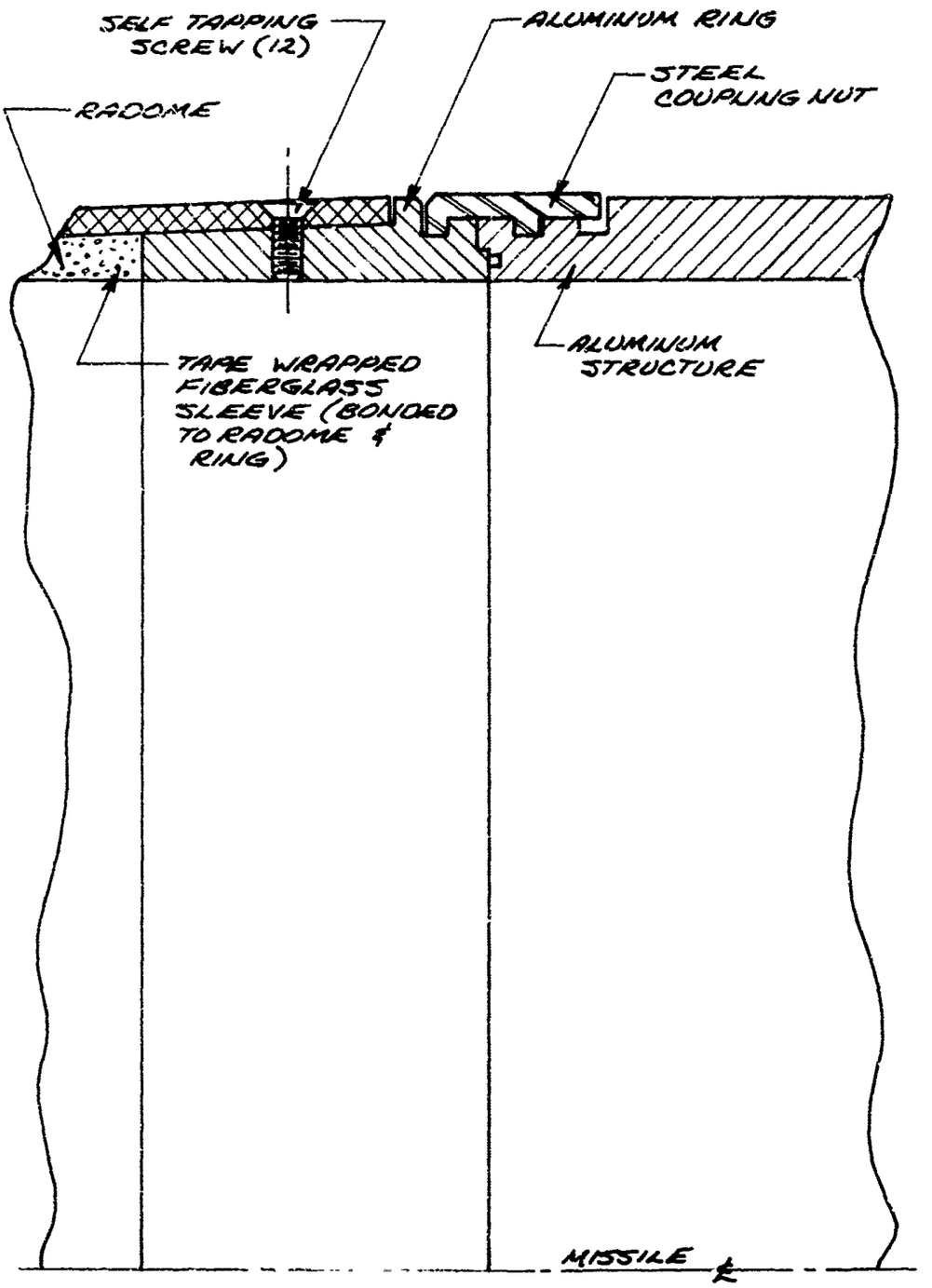

JOINT LOCATION: 189. AIRFRAME LENGTH
JOINT DIAMETER: 13.5 INCHES
SCALE: FULL

FIGURE I- 20

MISSILE : STANDARD 9RM

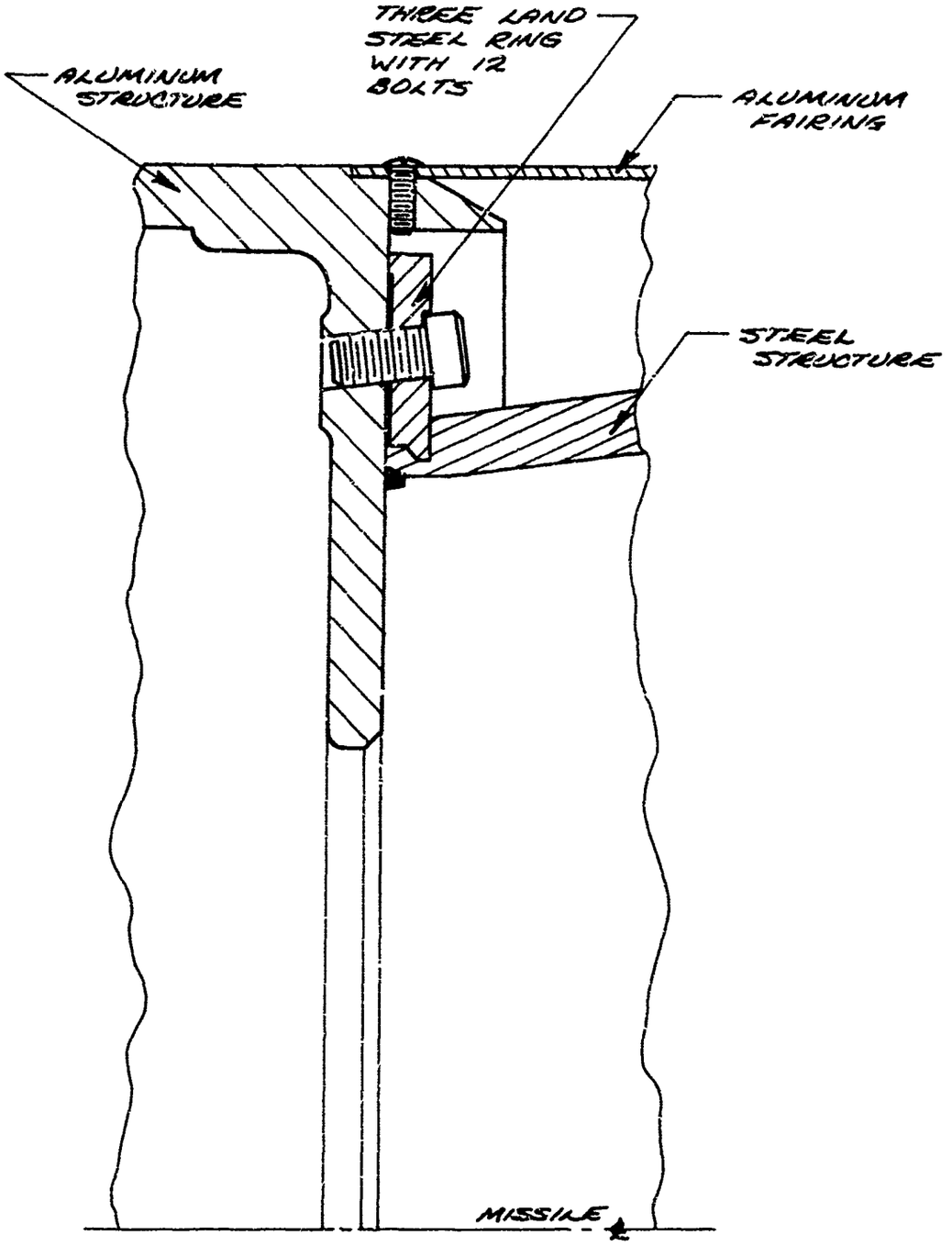

JOINT LOCATION : 23 % AIRFRAME LENGTH

JOINT DIAMETER : 13.5 INCHES

SCALE : FULL

FIGURE I-21

MISSILE: STANDARD ARM (AGM-78B)

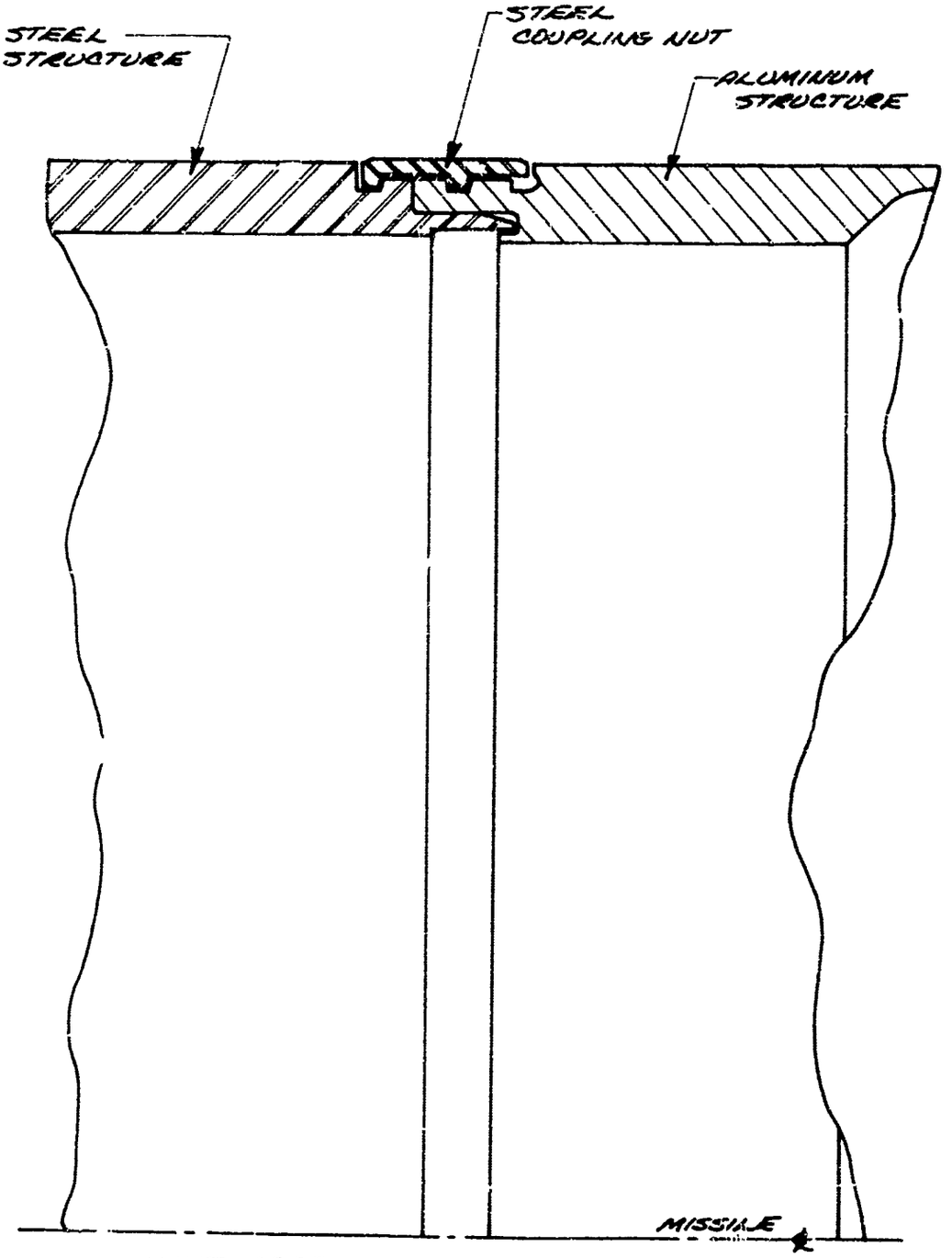

JOINT LOCATION: 35% AIRFRAME LENGTH
JOINT DIAMETER: 13.5 INCHES
SCALE: FULL

FIGURE I-22

MISSILE : STANDARD ARM (AGM-78B)

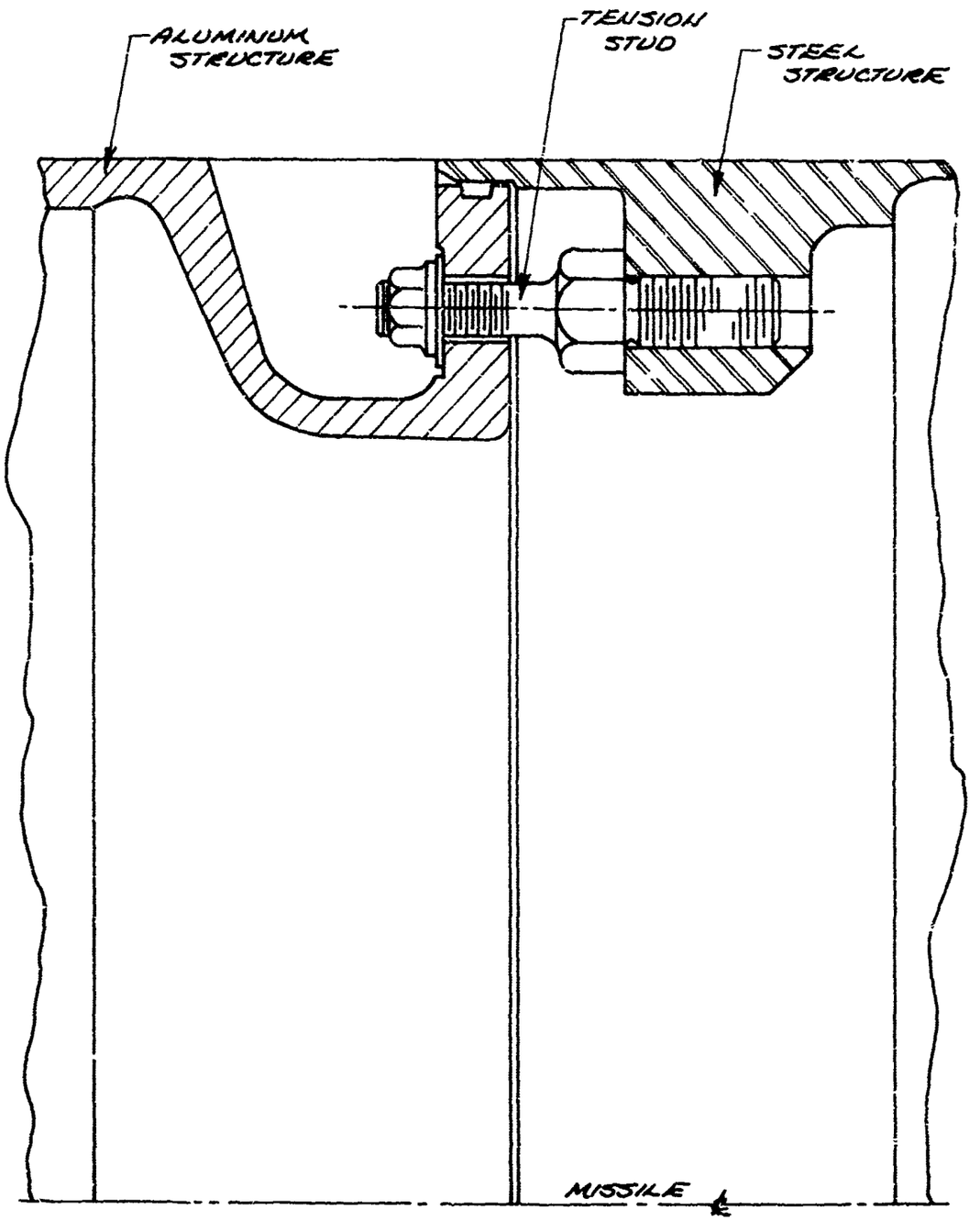

JOINT LOCATION : 43% AIRFRAME LENGTH
JOINT DIAMETER : 13.5 INCHES
SCALE : FULL

FIGURE I-23

MISSILE : STANDARD ARM (AGM-78B)

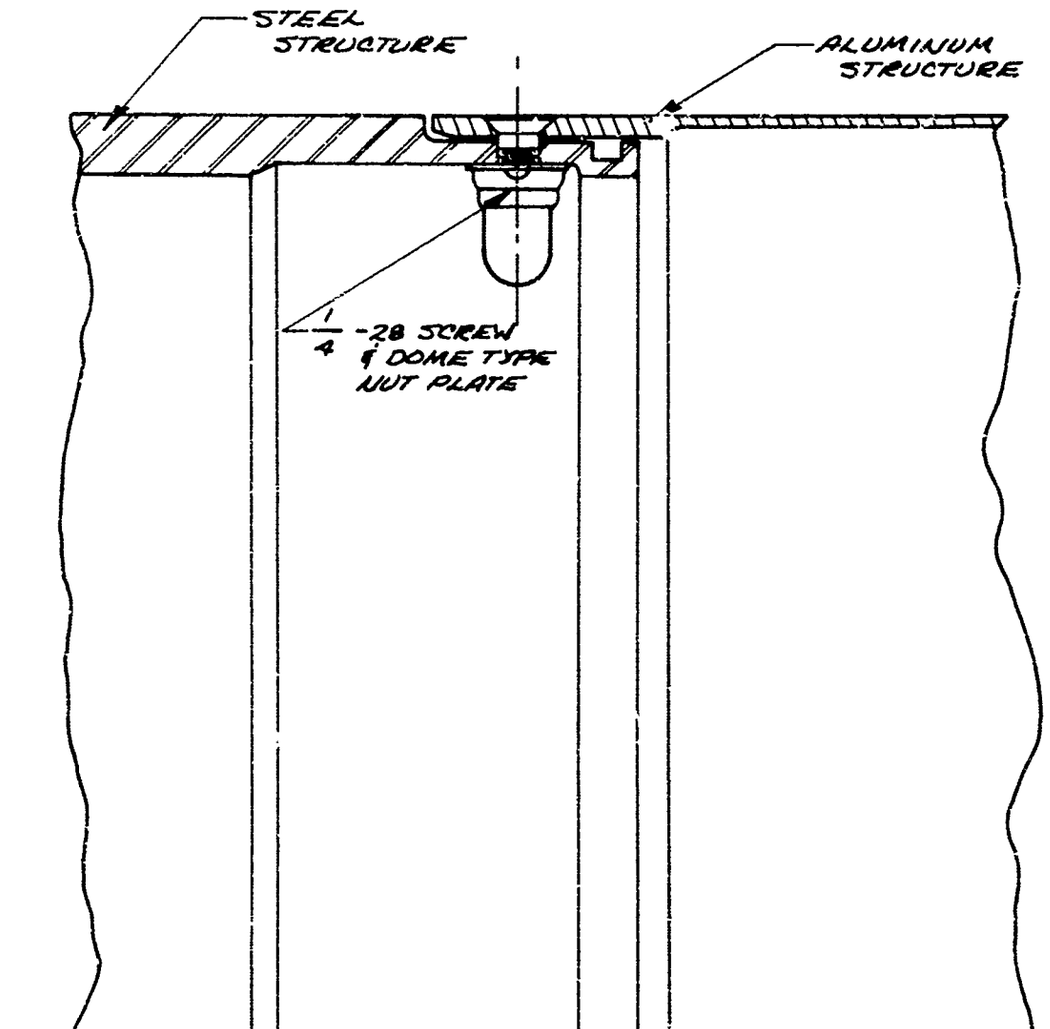

JOINT LOCATION : 88 % AIRFRAME LENGTH

JOINT DIAMETER : 13.5 INCHES

SCALE : FULL

FIGURE I-24

MISSILE: STANDARD ARM (AGM-78B)

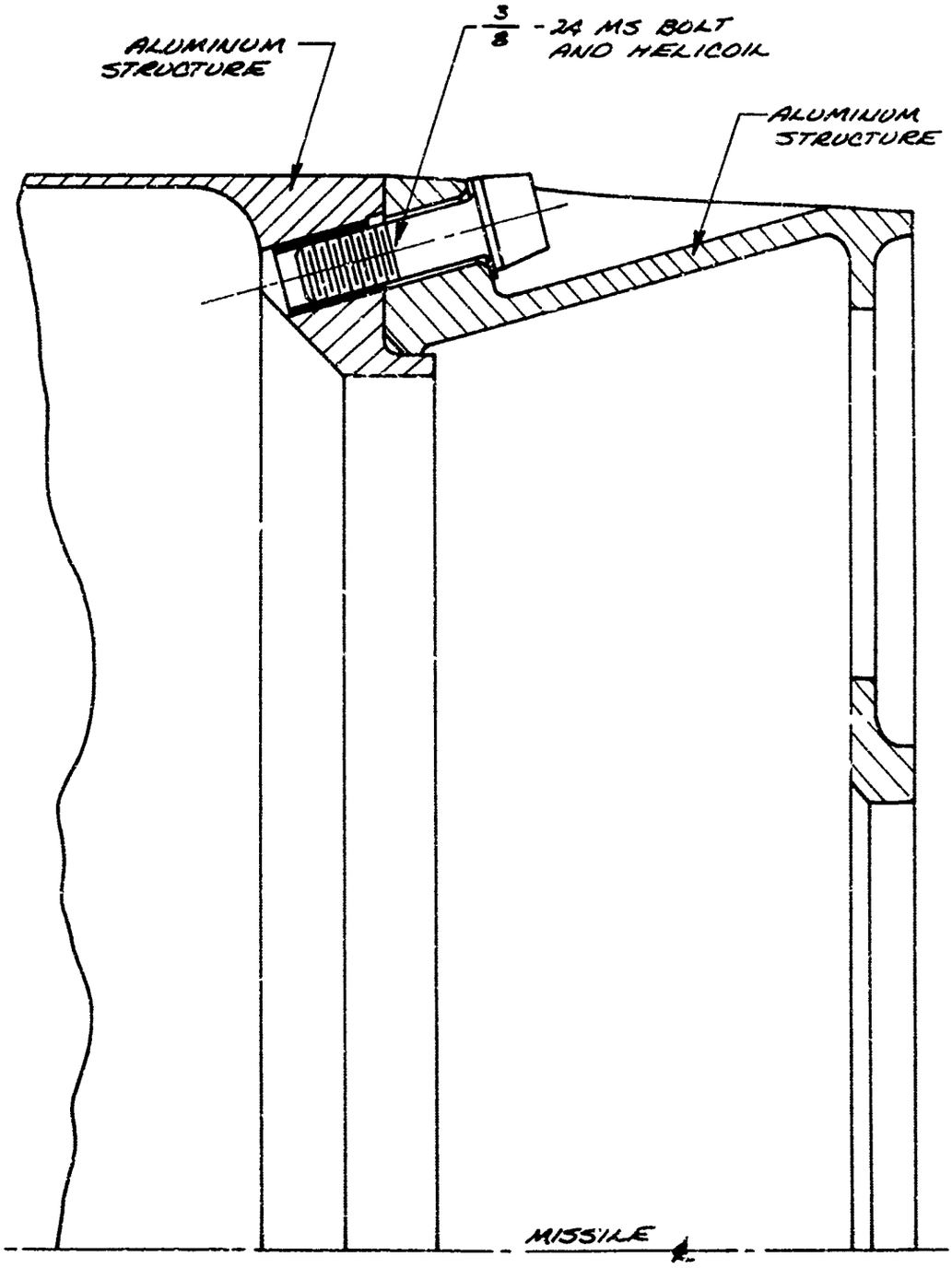

JOINT LOCATION: 93% AIRFRAME LENGTH

JOINT DIAMETER: 13.5 INCHES

SCALE: FULL

FIGURE I-25

MISSILE: PHOENIX (AIM-54A)

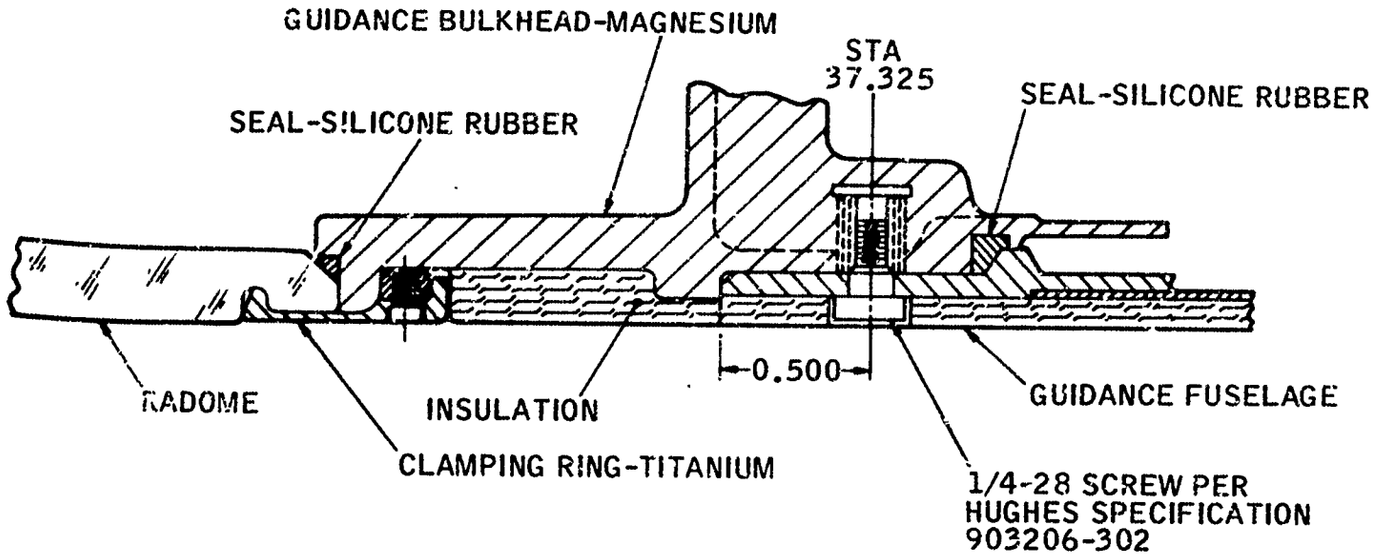

JOINT LOCATION: 23% AIRFRAME LENGTH

JOINT DIAMETER: ≈ 15 INCHES

FIGURE I-26

MISSILE: PHOENIX (AIM-54A)

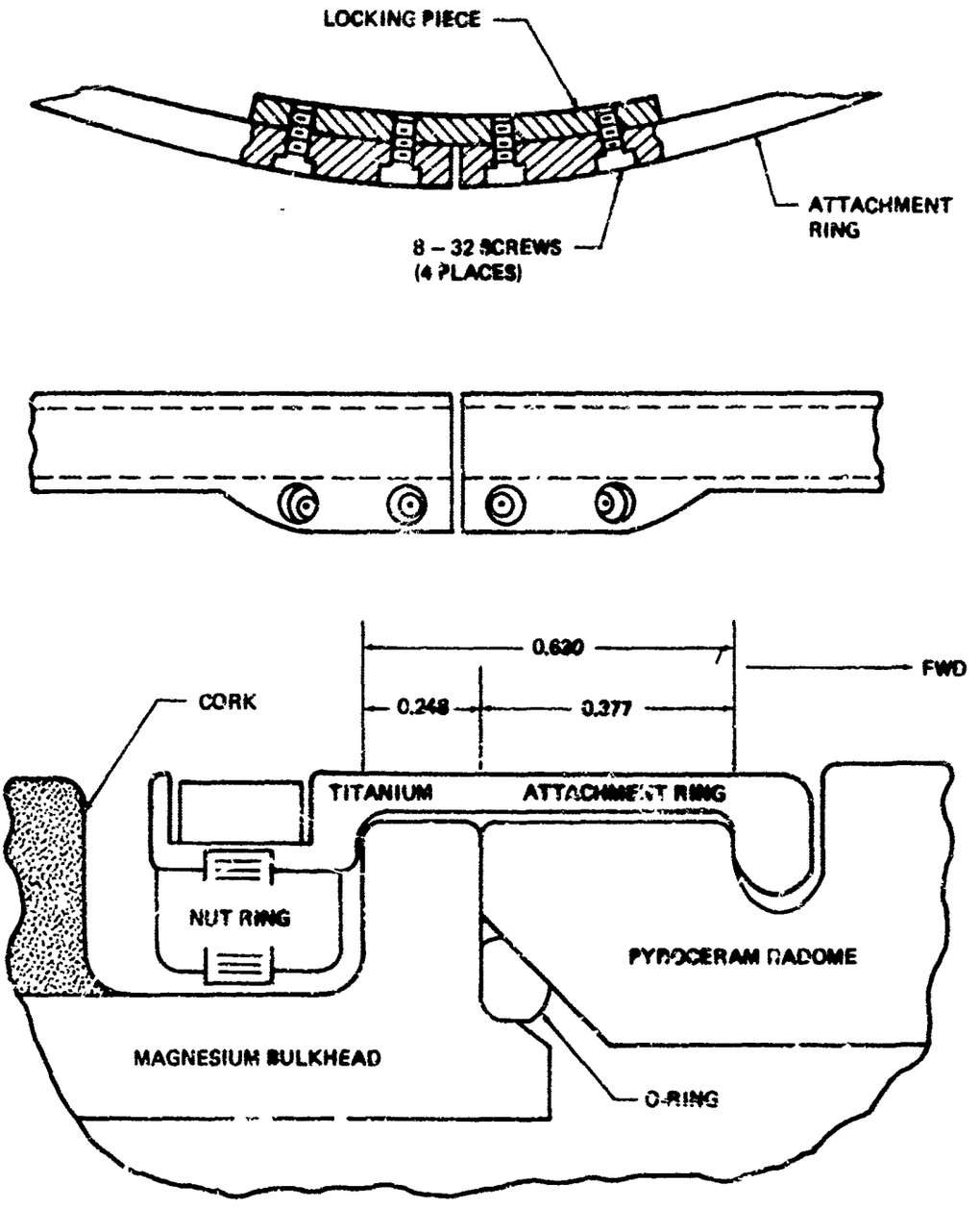

JOINT LOCATION: 22% AIRFRAME LENGTH

JOINT DIAMETER: ≈15 INCHES

FIGURE I-27

MISSILE: PHOENIX (AIM-54A)

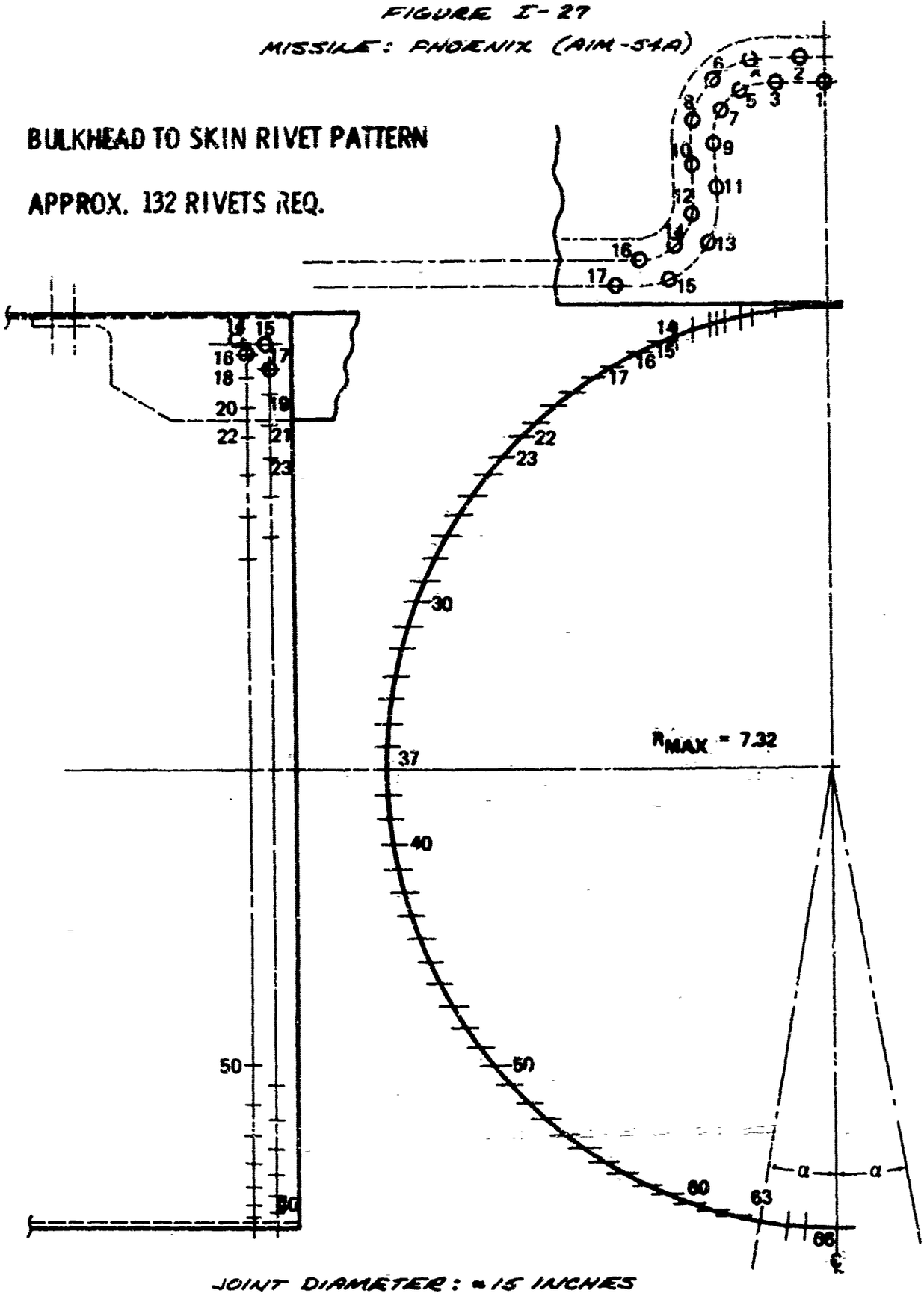

JOINT DIAMETER: ≈ 15 INCHES

FIGURE I-28

MISSILE: PHOENIX (AIM-54A)
JOINT DIAMETER: 21.5 INCHES

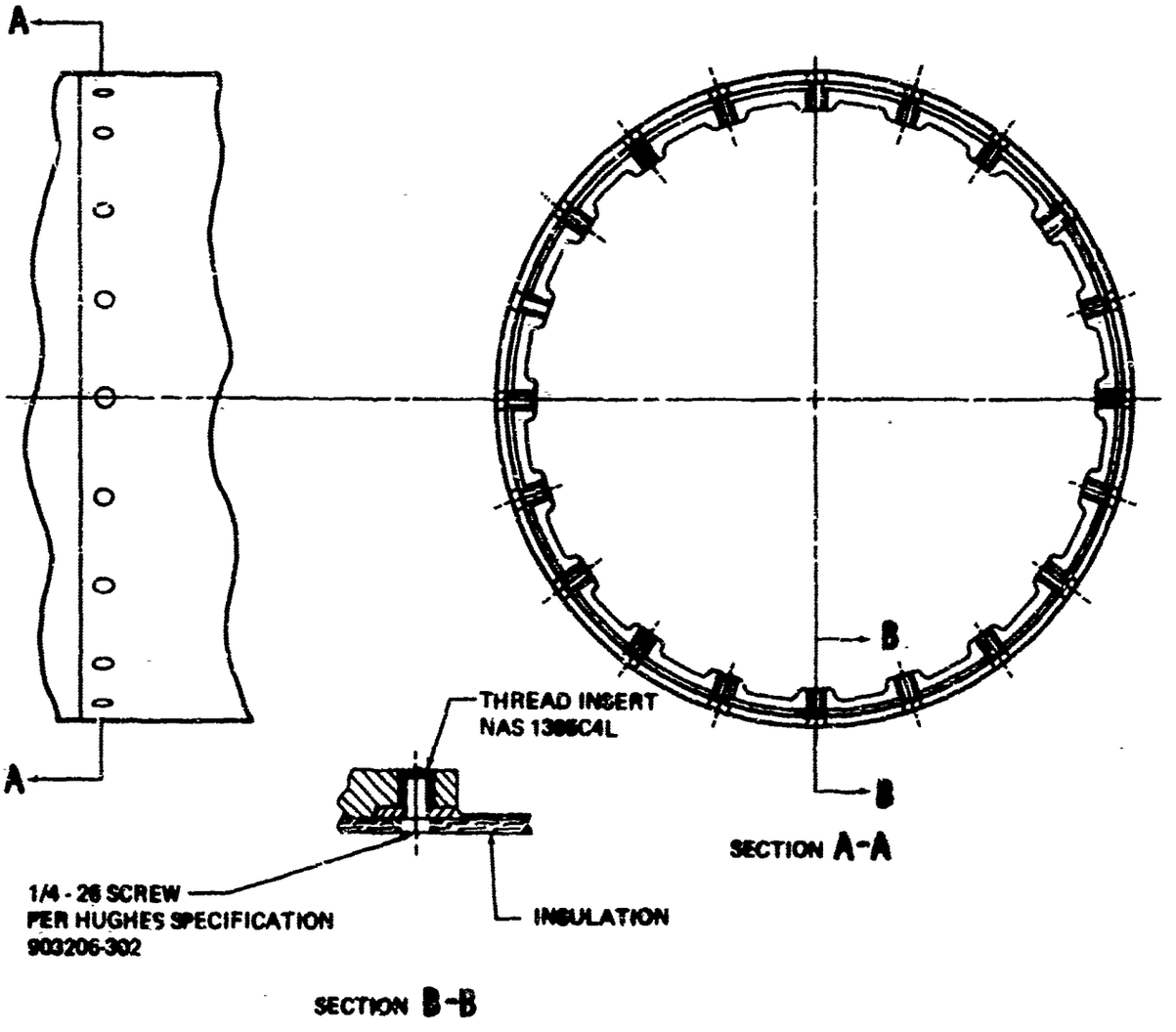

FIGURE I-29

AISSM.E: PHOENIX (AIM-54A)
JOINT DIAMETER: ≈ 15 INCHES

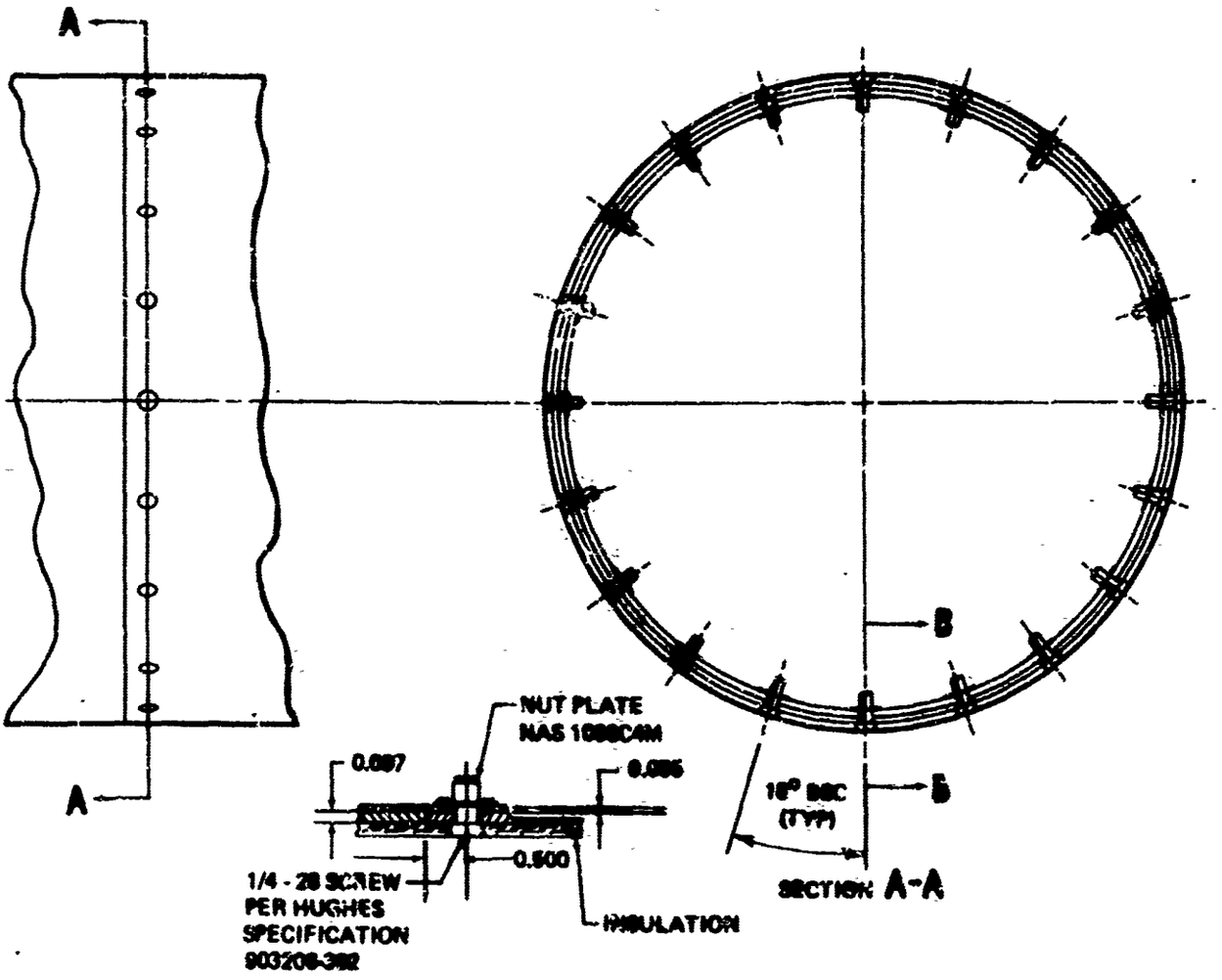

FIGURE I-30

MISSILE: SRAM (AGM-69A)
JOINT LOCATION: 14% AIRFRAME LENGTH
JOINT DIAMETER: 10.3 INCHES

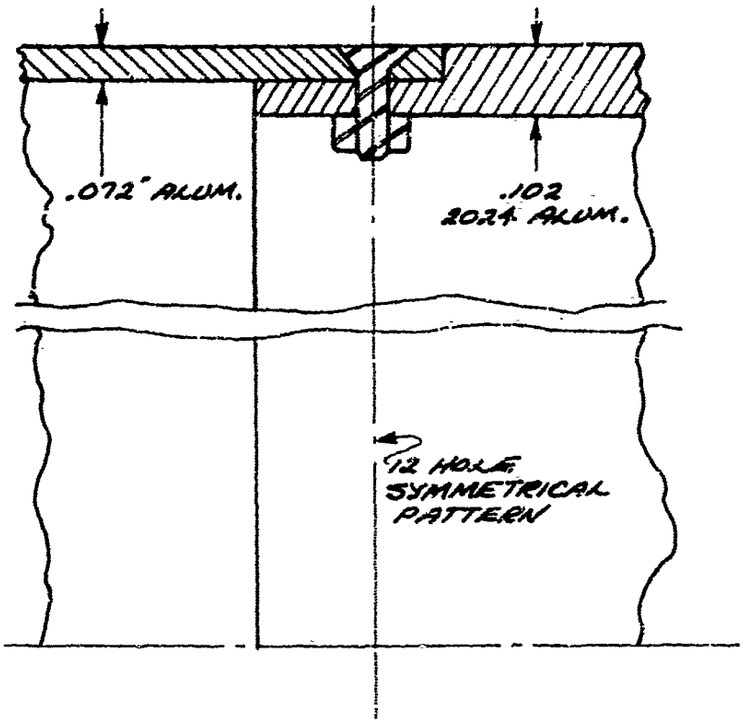

FIGURE E-31

MISSILE : SRAM (AGM-69A)

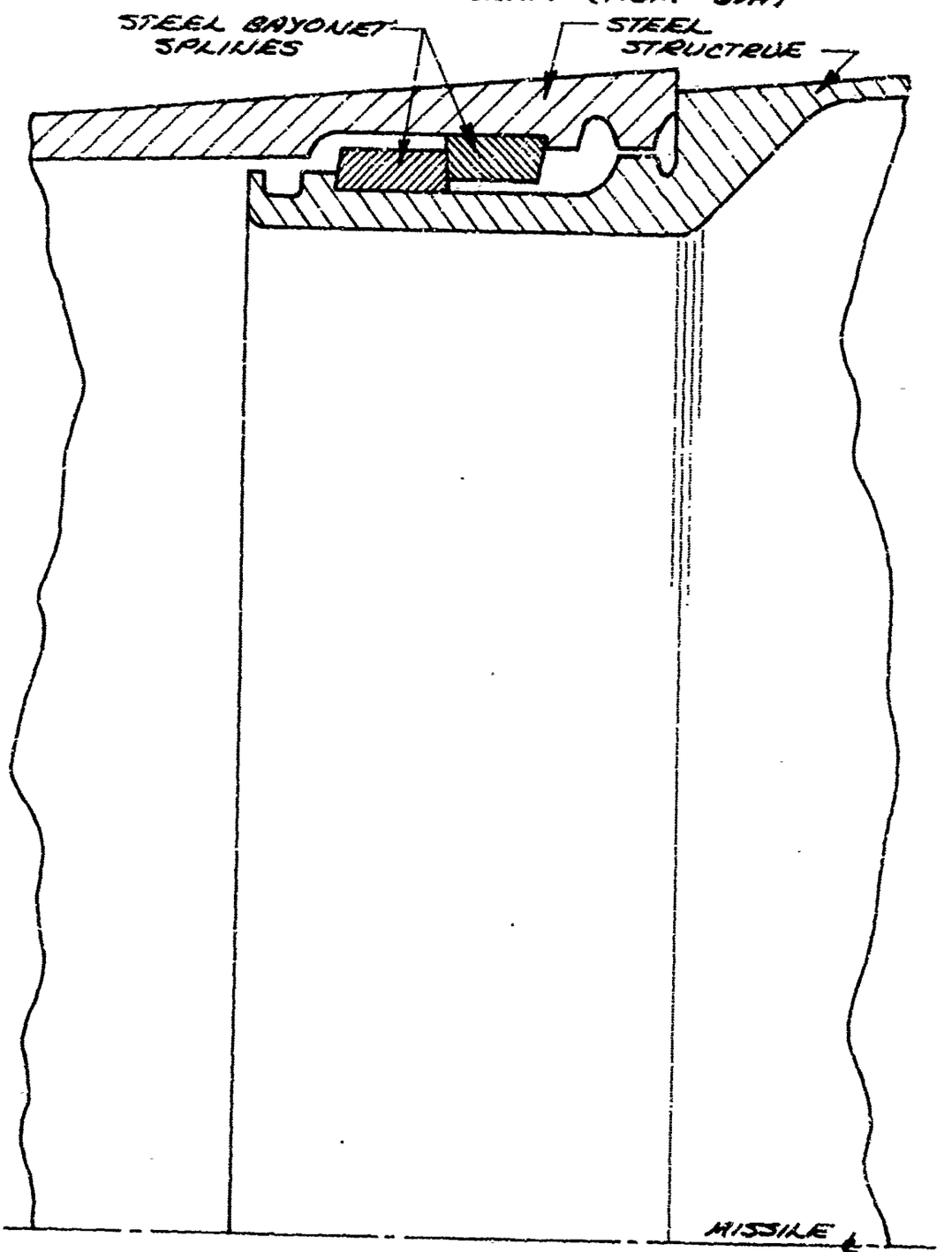

JOINT LOCATION : 31% AIR-FRAME LEAIGTH
JOINT DIAMETER : 15.4 INCHES
SCALE : FULL

APPENDIX II

BIBLIOGRAPHY

A literature search was conducted on the topic of the structural dynamic properties of tactical missile airframe joints. The following literature sources were used.

1. Engineering Index, 1960 to August 1969
2. Scientific and Technical Aerospace Reports, 1960 to 1969
3. Defense Documentation Center search using the following search words: missile joints, joints, mechanical joints, joint stiffness, joint flexibility, and dynamic properties of joints.

A list of publications which contain information relative to the topic follows with a brief summary of each of the articles.

II-1 Alley Jr., V. L. and Leadbetter, S. A., "The Prediction and Measurement of Natural Vibrations on Multistage Launch Vehicles", American Rocket Society Launch Vehicles: Structures and Materials Conference Report April 1962.

Results of an analytical and experimental study to determine natural frequencies of a multistage research rocket are presented. Also studies of the effects of mechanical joint looseness and an empirical treatment of joint flexibility are discussed. Some typical missile joints are illustrated and classified from excellent to loose based on joint compliance and diameter.

II-2 Barton, M. V., "Important Research Problems in Missile and Spacecraft Structural Dynamics", NASA TN D-1296, May 1962.

The author provides a broad overview of structural dynamic problems of missile and space vehicles and attempts to identify those areas in which further research would be fruitful in enhancing the state-of-the-art. Although this report was written nearly 10 years ago and much progress has been made since then, much of what is indicated in this report is pertinent today. He does not explicitly identify missile joints as a problem area although this is implicit in several of the problem areas identified.

II-3 Collins, J. D., and Thomson, W. T., "The Eigenvalue Problem for Structural Systems with Statistical Properties", AIAA Journal, Vol. 7, No. 4, April 1969, pp 642-648.

The treatment of matrix eigenvalue problems for structural systems with statistical properties is presented. Using the techniques described in the paper, Eigenvalues can be determined in a statistical form for a missile which has its joint stiffness properties described in a statistical form. Variations which can occur in serial production can be accounted for and consequently the technique could prove to be very useful.

II-4 DeVries, G., "Design of Joints for Cylindrical Sections", U. S. Naval Ordnance Test Station, China Lake, California, Report No. IDP807, April 1960.

The author classifies the various types of circular joints used in missile applications and presents a set of criterion for evaluating the desirability of the various classes. The criteria used do not include structural dynamic considerations.

II-5 Grambell, R. V., "A Compendium of Structural Joints for Assembly, Field and Flight Separation on Missiles", Boeing Co., Seattle, Report No. D2-125911-1-Rev-Ltr-B, July 68.

The author assembles a cross-section of state-of-the-art designs of missile joints used by the Boeing Company. The merits of the various joints are evaluated, however, structural dynamic response considerations are not examined.

II-6 Hanks, B. R. and Stephens, D. G., "Mechanisms and Scaling of Damping in a Practical Structural Joint", Shock and Vibration Bulletin No. 36 Part 4, pp 1 - 8, January 1967.

The authors report on an investigation directed at determining the effect of geometric scale on the damping of a beam joint assembly. In essence the decay of the fundamental mode of four similar cantilever configurations, varying in scale from 20 to 1, were experimentally determined for various bolt tension loads. It is concluded that damping is inversely proportional to model size.

II-7 Kalinia, N. G., Lebedeve, Y. A., et al., "Structural Damping in Permanent Joints", Translation Division WP-AFB Ohio, FTD-TT-63-755/1 + 2, May 64.

The authors report on various investigations on structural damping and consequently the studies are directed at damping mechanisms associated with structural joints. The authors identify the dominant damping mechanism associated with bolted and riveted joints as coulomb damping associated with interface frictional forces. It should be pointed out that more recent studies put forward evidence indicating that this type of damping is in fact viscous damping associated with the tangential movement of air at the interface.

II-8 Maidanik, G. and Ungar, E. E., "Panel Loss Factors Due to Gas-Pumping at Structural Joints", NASA CR-954, November 1967.

The authors report on a theoretical and experimental study of gas pumping in riveted joints. Results from a mathematical model are compared with experimental results. The results indicate that for the higher frequencies gas pumping is the dominant mechanism. The authors also note that structural damping measurements conducted at an ambient pressure may yield misleading results for structures which operate in a rarefied atmosphere.

II-9 Mead, D. J., and Eaton, D. C. G., "Interface Damping at Riveted Joints, Part I - Theoretical Analysis", Wright-Patterson Air Force Base, Ohio, ASD Technical Report 61-467 Sept. 1961.

A theoretical examination is made of damping in a riveted lap joint having a visco-elastic interfacial layer. Simple design rules are given for maximum interface damping.

II-10 Mentel, T. L., "Joint Interface Layer Damping," Transactions of ASME Vol. 89, Series B, No. 4, Nov. 1967.

An experimental and theoretical study of damping in thin visco-elastic layers is presented. The author notes that the damping mechanism is dominated by the analytically simple shear mechanism.

II-11 Rubenstein, N., Sigillito, V. G., and Stadter, J. T., "Upper and Lower Bounds to Bending Frequencies of Non-uniform Shafts, and Applications to Missiles," The Shock and Vibration Bulletin No. 38, Part 2, Aug. 1968, pp 169 - 176.

The authors present a method for computing upper and lower bounds to bending frequencies of non-uniform shafts which have their EI distribution precisely defined. The authors indicate that this type of determination is important in missile developments and undoubtedly it is, however, precise definition of EI distributions for missiles is difficult to establish due primarily to joint behavior. Consequently the bounds are not necessarily meaningful for many missile applications.

II-12 Smith, F. A., "Acoustic Response Analysis of Large Structures," The Shock and Vibration Bulletin, No. 39, Part 3, Jan. 1969, pp 55 - 64.

The technical approach and results of an acoustic response analysis up to 200 Hz for a large complex structure is presented. An elastic structural model which used 3000 degrees of freedom and based on beam and plate elements together with some one dimensional elements was used. A surprisingly good correlation with measured results was obtained. This type of detailed analysis is desirable because of the quality of the results which can be obtained. An analysis with this degree of complex-

ity (for many missile applications) is often limited due to an inability to describe joint behavior.

II-13 Trotter, W. D., Rauch, G. G. and Muth, D. V., "Missile Dynamic Response Tests," Boeing Company, Seattle, Report No. T2AGM20308-12, 1, -3-69.

Results for the SRAM missile structural dynamic response tests are presented. The effect of the compliance of the airframe joints on the measured bending mode shapes is readily apparent.

II-14 Ungar, E. E. and Carbonell, J. R., "On Panel Vibration Damping Due to Structural Joints," AIAA Journal, August 1966, pp 1385 - 1390.

The author reports on an experimental study of damping mechanisms for bolted joints. He concludes that high frequency damping is primarily due to the pumping of air resulting from surfaces moving away from and toward each other.